

**SPATIAL COHERENCE AND ROUGH BOTTOM
SCATTERING IN SHALLOW WATER**

by
Raden Dwi Susanto

B.S., Bandung Institute of Technology, Indonesia (1986)
M.S.Eng.Sci., Louisiana State University, USA (1992)

Submitted to the Department of Ocean Engineering
in Partial Fulfillment of the Requirements for the
Degree of

MASTER OF SCIENCE
in Ocean Engineering
at the

Massachusetts Institute of Technology
September 1994

© 1994 Raden Dwi Susanto
All rights reserved

The author hereby grants to MIT permission to reproduce and to
distribute publicly paper and electronic copies of this thesis
document in whole or in part

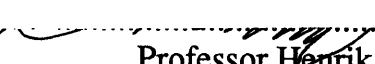
Signature of Author

Department of Ocean Engineering
June 30, 1994



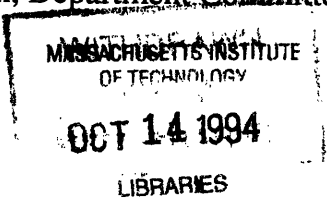
Certified by

Professor Henrik Schmidt
Thesis Supervisor



Accepted by

Professor A. Douglas Carmichael
Chairman, Department Committee on Graduate Students



*Allah who taught (the use of) pen, taught man that which he knew not
Al Qur'an 96:4-5*

*Allah will raise up, to suitable ranks and degrees, those of you who believe
and who have been granted knowledge
Al Qur'an 58:11*

*Verily, with every difficulty. There is relief
Al Qur'an 94:5*

SPATIAL COHERENCE AND ROUGH BOTTOM SCATTERING IN SHALLOW WATER

Raden Dwi Susanto

ABSTRACT

The Mallorca Cruise in the Mediterranean Sea was carried out on March 12-22,1993. The objective of this thesis is to analyze shallow water cruise data for extraction of the spatial coherence and analyze its relation to rough bottom scattering.

Bistatic reverberation measurements were carried out by placing horizontal receiver array with equispaced hydrophones 1 meter above the bottom. A flextentional transducer towed behind the ship was used as a source, generating a 209 dB source level at center frequency 400 Hz, with 5 ms signal length and 10 second interval. The ship made a hexagonal run with the horizontal receiver array inside the track.

Eleven pings have been processed. Since the transducer and the recording system were not synchronized and due to inaccuracy of the positioning system, the source position has been calculated based on an acoustics inversion method. It was found that the receiver array should be moved 150m north and 120m to the east from the position given in the cruise report. Also the receiver array bearing angle was 180° different from the one stated in the cruise report.

A theoretical source model has been designed to approximate the actual source pulse. The modal arrivals are clearly identified in the retarded time series data, therefore, the analysis was performed mode by mode. The total field was decomposed into a mean field (coherent field) and scattered field (incoherent field). Spatial coherence has been calculated using a correlation function and a coherence function. The magnitude square of the complex coherence function (MSC) of the total field was 0.9 while the MSC of the scattered field was 0.1 which suggested that the bottom roughness was very small.

ACKNOWLEDGEMENTS

I would like to gratefully acknowledge every person who has contributed to this thesis. I wish to express sincere gratitude to my supervisor Professor Henrik Schmidt of the Ocean Engineering Department, who patiently guided, advised, and supervised me throughout this study.

I would like to thanks to the Chairman STAID Program and Deputy Chairman for Natural Resources Development of the Agency for Assessment and Application of Technology of the Government of Indonesia, for funding and allowing me to pursue my study at Massachusetts Institute of Technology.

I wish to acknowledge Dr. Jim TenCate and Howard Huang of the Applied Research Laboratories, the University of Texas at Austin, who help me to transfer the cruise data. Sincere thanks to all my office-mates in Room 5-007 MIT, especially Ken Rolt. I would like to thank my friend Margo Black who help me to edit this thesis.

Finally I would like to thank to my lovely wife Ina who always provide me with endless support, love, and encouragement during our honeymoon and study at Boston Massachusetts. I would like to thank my parents, although they are far away, they have provided me support and love during my study here as they have always done throughout my life.

SPATIAL COHERENCE AND ROUGH BOTTOM SCATTERING IN SHALLOW WATER

ABSTRACT	3
ACKNOWLEDGEMENTS	4
TABLE OF CONTENTS	5
LIST OF FIGURES	7
CHAPTER 1 INTRODUCTION	12
1.1. Motivation	13
1.2. Review of Relevant Literature	14
1.3. Outline of Each Chapter	19
CHAPTER 2 EXPERIMENTAL MEASUREMENTS	21
2.1. Environmental Site	22
2.2. Source and Receiver array layout	24
CHAPTER 3 THEORY	28
3.1. Normal Mode Method	28
3.1.1. Normal mode for zeroth order model waveguide	33
3.1.2. Normal mode for Pekeris waveguide	35

3.2. Scattering from rough boundaries	36
3.2.1. Integral formula	37
3.2.2. The Kirchoff Approximation	38
3.2.3. Perturbation Approximation	40
3.3. Spatial Coherence	42
CHAPTER 4 DATA PROCESSING AND RESULTS	48
4.1. Synthetic Source	49
4.2. Receiver array and Source localizations	49
4.3. Spatial Coherence of Scattered Field	53
CHAPTER 5 CONCLUSIONS AND RECOMMENDATIONS	
FOR FUTURE RESEARCH	105
5.1. Conclusions	105
5.2. Recommendations for future research	107
BIBLIOGRAPHY	108

List of Figures

Figure 2.1. Boomer sample at array site	23
Figure 2.2. Shallow water environment, source and array configuration	25
Figure 2.3. Hexagonal measurement track	26
Figure 4.1. Retarded time series data of ping # 1	57
Figure 4.2 Retarded time series data of ping # 1a	58
Figure 4.3 Retarded time series data of ping # 1b	59
Figure 4.4 Retarded time series data of ping # 1c	60
Figure 4.5 Retarded time series data of ping # 2	61
Figure 4.6 Retarded time series data of ping # 3	62
Figure 4.7. Retarded time series data of ping # 4	63
Figure 4.8. Retarded time series data of ping # 5	64
Figure 4.9. Retarded time series data of ping # 6	65
Figure 4.10. Retarded time series data of ping # 7	66
Figure 4.11. Retarded time series data of ping # 8	67
Figure 4.12. Synthetic source pulse	68
Figure 4.13. Receiver array configuration	69
Figure 4.14. The χ^2 values as a function of North-South and East-West shift of receiver array position	70

Figure 4.15. Total field, coherent field, scattered field and its correlation function of mode#1, ping#1	71
Figure 4.16a. Spectral energy of scattered field of mode#1, ping#1	72
Figure 4.16b. Coherence function of total field (solid) and scattered field (dash) of mode#1, ping#1	72
Figure 4.17. Total field, coherent field, scattered field and its correlation function of mode#2, ping#1	73
Figure 4.18a. Spectral energy of scattered field of mode#2, ping#1	74
Figure 4.18b. Coherence function of total field (solid) and scattered field (dash) of mode#2, ping#1	74
Figure 4.19. Total field, coherent field, scattered field and its correlation function of mode#3, ping#1	75
Figure 4.20a. Spectral energy of scattered field of mode#3, ping#1	76
Figure 4.20b. Coherence function of total field (solid) and scattered field (dash) of mode#3, ping#1	76
Figure 4.21. Total field, coherent field, scattered field and its correlation function of mode#1, ping#2	77
Figure 4.22a. Spectral energy of scattered field of mode#1, ping#2	78
Figure 4.22b. Coherence function of total field (solid) and scattered field (dash) of mode#1, ping#2	78
Figure 4.23. Total field, coherent field, scattered field and its correlation function of mode#2, ping#2	79
Figure 4.24a. Spectral energy of scattered field of mode#2, ping#2	80
Figure 4.24b. Coherence function of total field (solid) and scattered field (dash) of mode#2, ping#2	80

Figure 4.25. Total field, coherent field, scattered field and its correlation function of mode#1, ping#3	81
Figure 4.26a. Spectral energy of scattered field of mode#1, ping#3	82
Figure 4.26b. Coherence function of total field (solid) and scattered field (dash) of mode#1, ping#3	82
Figure 4.27. Total field, coherent field, scattered field and its correlation function of mode#2, ping#3	83
Figure 4.28a. Spectral energy of scattered field of mode#2, ping#3	84
Figure 4.28b. Coherence function of total field (solid) and scattered field (dash) of mode#2, ping#3	84
Figure 4.29. Total field, coherent field, scattered field and its correlation function of mode#1, ping#4	85
Figure 4.30a. Spectral energy of scattered field of mode#1, ping#4	86
Figure 4.30b. Coherence function of total field (solid) and scattered field (dash) of mode#1, ping#4	86
Figure 4.31. Total field, coherent field, scattered field and its correlation function of mode#2, ping#4	87
Figure 4.32a. Spectral energy of scattered field of mode#2, ping#4	88
Figure 4.32b. Coherence function of total field (solid) and scattered field (dash) of mode#2, ping#4	88
Figure 4.33. Total field, coherent field, scattered field and its correlation function of mode#1, ping#5	89
Figure 4.34a. Spectral energy of scattered field of mode#1, ping#5	90
Figure 4.34b. Coherence function of total field (solid) and scattered field (dash) of mode#1, ping#5	90

Figure 4.35. Total field, coherent field, scattered field and its correlation function of mode#2, ping#5	91
Figure 4.36a. Spectral energy of scattered field of mode#2, ping#5	92
Figure 4.36b. Coherence function of total field (solid) and scattered field (dash) of mode#2, ping#5	92
Figure 4.37. Total field, coherent field, scattered field and its correlation function of mode#1, ping#6	93
Figure 4.38a. Spectral energy of scattered field of mode#1, ping#6	94
Figure 4.38b. Coherence function of total field (solid) and scattered field (dash) of mode#1, ping#6	94
Figure 4.39. Total field, coherent field, scattered field and its correlation function of mode#2, ping#6	95
Figure 4.40a. Spectral energy of scattered field of mode#2, ping#6	96
Figure 4.40b. Coherence function of total field (solid) and scattered field (dash) of mode#2, ping#6	96
Figure 4.41. Total field, coherent field, scattered field and its correlation function of mode#1, ping#7	97
Figure 4.42a. Spectral energy of scattered field of mode#1, ping#7	98
Figure 4.42b. Coherence function of total field (solid) and scattered field (dash) of mode#1, ping#7	98
Figure 4.43. Total field, coherent field, scattered field and its correlation function of mode#2, ping#7	99
Figure 4.44a. Spectral energy of scattered field of mode#2, ping#7	100

Figure 4.44b. Coherence function of total field (solid) and scattered field (dash) of mode#2, ping#7 100

Figure 4.45. Total field, coherent field, scattered field and its correlation function of mode#1, ping#8 101

Figure 4.46a. Spectral energy of scattered field of mode#1, ping#8102

Figure 4.46b. Coherence function of total field (solid) and scattered field (dash) of mode#1, ping#8 102

Figure 4.47. Total field, coherent field, scattered field and its correlation function of mode#2, ping#8 103

Figure 4.48a. Spectral energy of scattered field of mode#2, ping#8104

Figure 4.48b. Coherence function of total field (solid) and scattered field (dash) of mode#2, ping#8 104

CHAPTER 1

INTRODUCTION

Sound propagation in the sea has been thoroughly studied since the beginning of the World War II [58]. Since then considerable effort has been put into understanding the mechanism that causes scattering of wave propagation in the ocean. Scattering is a mechanism of loss, interference and fluctuation which can happen almost anywhere in the ocean and cover a wide band of frequencies [49].

Acoustics scattering in the sea can be categorized into [68] :

- a. surface scattering, which is caused by the rough ocean surface and a thin bubble layer beneath the sea surface.
- b. Volume scattering, which is caused by organic species or temperature and density fluctuations.
- c. Bottom scattering, which is caused by bottom characteristics (roughness and composition), layers of densities and sound speeds, and inhomogeneities within the bottom.

This research evaluates scattering in the shallow water environment of the Mallorca Cruise data taken in the Mediterranean Sea in March 1993. During the cruise the sea surface condition was calm, and this thesis will therefore concentrate on rough bottom scattering. Usually the seafloor is a lossy boundary, which means that the propagation is dominated by bottom reflection loss at low and intermediate frequencies ($<1\text{kHz}$) and scattering losses at high frequencies[49].

The ocean bottom is frequently extremely complicated and its properties vary, often randomly, in space (and time) on many scales. Therefore, interactive investigations of experiment, theoretical modeling, and numerical modeling are essential in constructing new analytical models and understanding physical processes for acoustic scattering from the sea floor.

1.1. Motivations

My interest in shallow water acoustic propagation is motivated by the following :

- a. I work for the government of Indonesia, the Ocean Division of the Agency for Assessment and Application of Technology. Seventy percent (70%) of the total area of Indonesia is ocean, and mostly shallow water.

- b. The acoustics of shallow water has been thoroughly investigated both theoretically and experimentally, but both have failed to give us quantitative understanding required for prediction of long range propagation in the shallow water [49]. In shallow water the surface, volume and bottom properties are all important, spatially varying, and the parameters are generally not known in sufficient detail.
- c. There has been a lot of research in scattering problems but mostly in deep water which studies rough scattering as a separate problem i.e., rough surface scattering and rough bottom scattering.
- d. A few studies in scattering problems have calculated spatial coherence via correlation and coherence functions.

1.2. Review of Relevant Literature

Because underwater acoustics has been intensively studied since World War II this section will not cover all the existing literature but only that highly correlated to sound propagation and scattering in a shallow water environment.

There are a lot of books which describe sound propagation in ocean. The most recent one published in 1994 is an excellent book by Jensen *et*

al.[49] covers fundamentals of ocean acoustics, wave propagation theory and all methods on sound propagation models. The sound propagation models which include ray method, wavenumber integration technique, normal mode, parabolic equation and finite element and finite different methods are discussed. The second book on sound propagation in the sea is by George Frisk[50]. In this book covers in more detail Green functions, boundary conditions, normal modes, Hankel transform and WKB approximations.

Probably the first reported work on scattering from rough surfaces was by Rayleigh (1877), whose work led to the development of the Rayleigh scattering criterion for determining of roughness a surface [59]. The scattered field from the seafloor can consist of contributions of two general types: scattering from interface roughness and scattering from volume heterogeneities. The most intensive literature on rough bottom scattering, mainly a theoretical approach, is given by Ogilvie [41,59].

Most of the scattering theories are based on idealized boundary conditions, i.e., assume pressure release surface (Dirichlet boundary condition) or an ideally rigid body surface (Neumann boundary condition), both of which are not appropriate for scattering from the seafloor. Realistic boundary conditions, i.e., continuity of pressure and the normal component of particle velocity, may be described by two well known theories: perturbation and Kirchoff approximations.

The perturbation approximation[33,36] is based on small roughness, also known as Rayleigh-Ritz approximation, is valid for small radii of curvature (roughness height is every much smaller compared to the acoustic wavelength). Meanwhile the Kirchoff theory is an approximation for the scattered field on the scattering surface in terms of incident field and plane wave reflection coefficients. Its physical basis is that any point on the rough surface is assumed to behave as if the surface were locally flat. This approach requires no rapid changes in the gradient, but it has no explicit restrictions on the magnitude of the height or gradient[37,41,59].

Due to lack of overlap between the perturbation and Kirchoff approximations a composite roughness model combining those approaches has been successfully applied to ocean surface scattering. This model treats the topography as the sum of small and large scale surfaces. The large surfaces must have radii of curvature comparable to or larger than the acoustic wavelength, and the small scale surfaces must have relief smaller than the wavelength[39,73]. McDaniel[1] used small-slope theory applied to scattering from pressure release surface by expansion of the kernel of an integral equation of the first kind. This approach included a treatment of multiple scattering and shadowing.

Kuperman and Ingenito[80] have used a boundary perturbation method based on a small waveheight assumption to determine normal mode

attenuation coefficients due to scattering from rough boundaries. McDaniel[79] has derived coupled power equations for calculating the energy transfer between modes due to scattering from rough seafloor modeled as a stationary Gaussian process. She also derived the mode coupling due to lateral seabed inhomogeneities on propagation loss and transverse horizontal spatial coherence[71]. Bellis[77] and McDaniel[75] have studied coupled mode approach on rough surface scattering. The mode coupling theory applied on the range dependent environment has been studied by some authors [69,72-75,78].

Assuming that a seafloor is an elastic layer which supports a shear, the rough bottom scattering becomes more realistic and more complicated. Dacol and Berman[35], Kuperman and Schmidt [32] and recently Essen[2] have applied the perturbation theory to scattering from a rough shear supporting seafloor. Dacol and Berman presented numerical results for a solid seafloor with shear velocity exceeding the sound velocity of water and using the Gaussian-shaped roughness spectrum. Kuperman and Schmidt derived a self-consistent perturbation approach which they applied to simulate the scattering loss of the coherent sound field in a stratified waveguide. Essen presented a simplified perturbation approach which directly determined the scattered acoustic field based on the Born approximation.

The problem of modeling fully three-dimensional ocean acoustic scattering is a computationally intensive one, nevertheless, is of great practical interest. Milder [19,24] described that operator expansion formalism can accurately compute wave scattering from arbitrarily rough surface as long as the Fresnel number (the Rayleigh height times the surface slope) is small at all roughness scales. Meanwhile, Dawson[20,27] developed a boundary integral equation method (BIEM) theory for the computation of scattering of underwater sound from compact deformation of an oceanic waveguide's surfaces.

There are two approaches to describe spatial coherence between separated hydrophones, i.e. correlation function and coherence function. Urick[63] discusses the spatial coherence using correlation function, while Bendat [57] defines spatial coherence using coherence function. An experimental and theoretical analysis of coherence function of scattered field from the ice has been studied by LePage[15] who used Carter's [46] frequency averaging.

Carter[44] computed the bias of magnitude squared of the complex coherence (MSC) between two jointly stationary random processes. He concluded that even with a large number of FFT segments estimates of MSC can be significantly biased downward giving an erroneous indication of the value of the coherence. Smith[45] studied the theoretical coherence function of pure tone sound fields hypothesizing that the component fields

of individual paths or modes are locally plane waves and mutually incoherent in the average.

1.3. Outline of Each Chapter

Chapter 2 is a brief description of the Mallorca Cruise in the Mediterranean Sea taken in March 1993. Sea surface conditions, bathymetry and sediment compositions in the site area are described. It also defines the layout and characteristic of flextentional transducer as a source and horizontal hydrophone line array as receivers.

Chapter 3 explains the basic theory of the research which includes the Normal Mode Method to model the sound propagation in the shallow water wave guide. This chapter covers the theory of rough bottom scattering based on the integral equation, the Kirchoff approximation and perturbation approach and basic theory of spatial coherence between separated hydrophone using correlation and coherence functions.

Data processing and analysis of the results are described in Chapter 4. A theoretical source mode has been designed to approximate the actual source pulse and an acoustic inversion method was used to localize the source and receiver array position and orientation. Eleven pings have been processed, three pings as additional data to find the source and receiver positions while the other eight pings have been processed to obtain the

spatial coherence using correlation and coherence functions between separated hydrophones. The magnitude square complex coherence function (MSC) of the total field and scattered field are determined.

Chapter 5 is the conclusion and addresses future research works related to this thesis.

CHAPTER 2.

EXPERIMENTAL MEASUREMENTS

The Mallorca Cruise was carried out on March 7-22, 1993, in the Mediterranean Sea off the Balearic Islands, Italy. This cruise was a joint research project between scientists from SACLANT Undersea Research Center, La Spezia, Italy and scientists from the US Naval Research Laboratory, Applied Research Laboratory of University of Austin in Texas, and MIT.

The objective of the research was to examine and develop a better understanding of the bottom seismo-acoustic effect on low frequency sonar in a shallow water environment. This objective included topics such as frequency dependence of seismo acoustic propagation, matched field inversion and localization of seafloor characterization, seismo acoustic sensing, and seafloor reverberations.

The cruise gathered complete data by measuring the sea water characteristics (salinity, temperature, sound speed), sea

floor bathymetry using Side-scan sonar, Boomer and Sparker, and sea floor properties by coring and seismic profiling.

2.1. Environmental site

Preliminary measurements suggested that the water depth was about 108 m; the sound speed profile was approximately constant at 1508 m/s; and the sea surface condition was calm.

Based on the report by Max and Michelozzi[66], the seafloor along the northwestern part of the Mallorca Plateau was generally flat and smooth, except for some small scale roughness in the acoustics basement south the sedimentary basin and isolated rocks a little over 3 m in the southern part of the area. Based on the side scan sonar the relief was less than 1 m. Recent sediment layer was present only as a thin veneer less than 4 m thick except near the shelf edges where in some areas it became 20 m thick. The recent sediments were dominated by shell fragments, calcareous algae, rugose coral which were strongly reflective. The basement was interbedded between limestone and shale. A Boomer sampling of the site is shown in Figure 2.1.

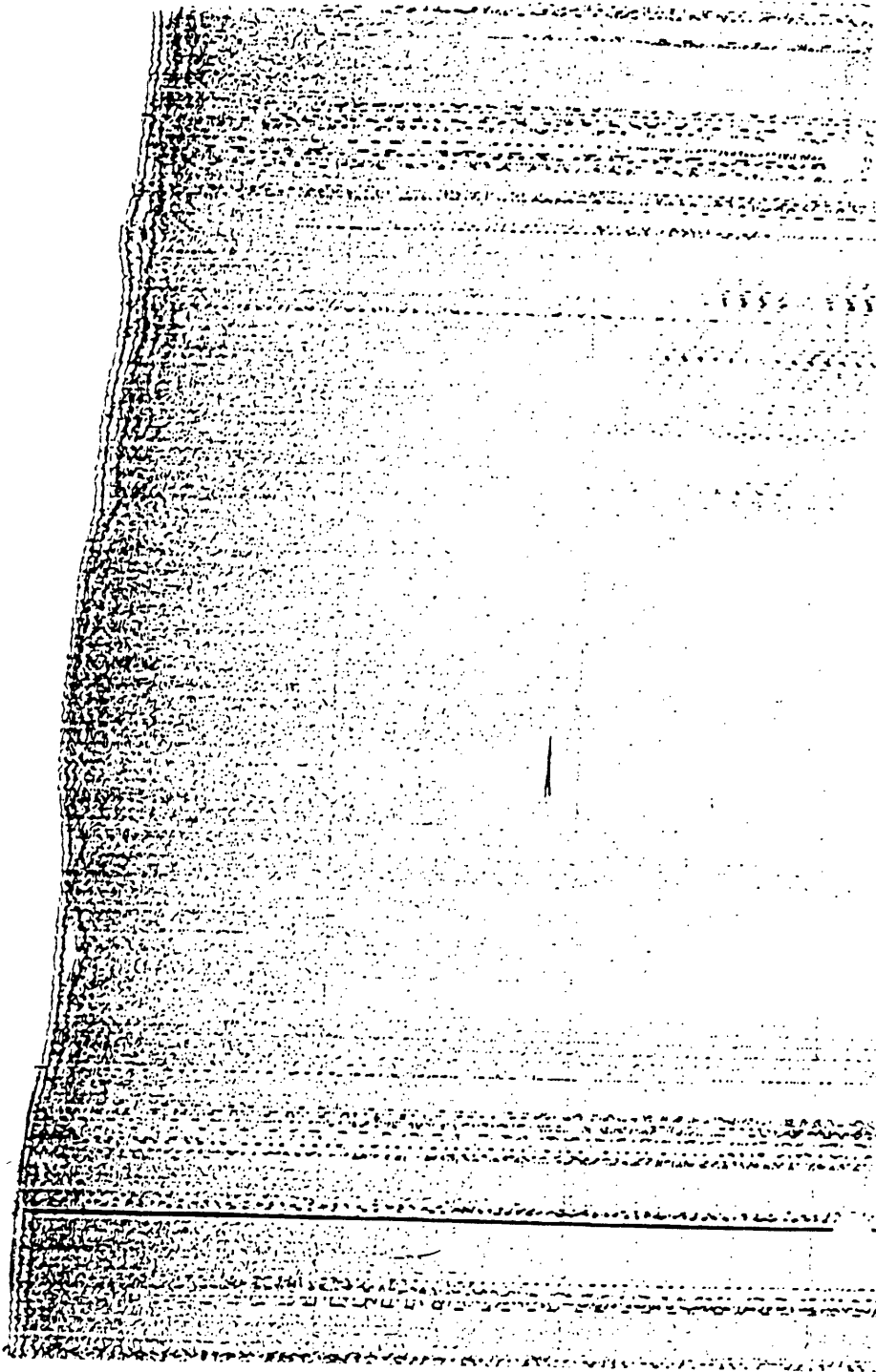


Figure 2.1. Boomer sample at array site

2.2. Source and receiver layout

There were several source types used during the cruise: SUS charge, TNT and flextentional transducers. Meanwhile, the receiver arrays were a hydrophone (DARPA) array in vertical and horizontal as well as seismic (OBS) arrays.

This thesis focuses on the data taken on March 20, 1994, with the flextentional transducer as a source and DARPA horizontal line array as a receiver array. The flextentional transducer had frequency resonance near 400Hz at source level 209dB/uPa/m.

The 50m length of receiver array was laid out 1m above the seafloor containing 24 hydrophones with 2m equispaced separation (see Figure 2.2.). Meanwhile, the source mounted behind the R/V Alliance making a hexagonal track with the receiver array was in the middle of the track at a distance between 1-1.5nmiles (see Figure 2.3.). The approximate source depth is 20m below the mean sea surface. The source pulse signal was 5ms length and released every 10seconds.

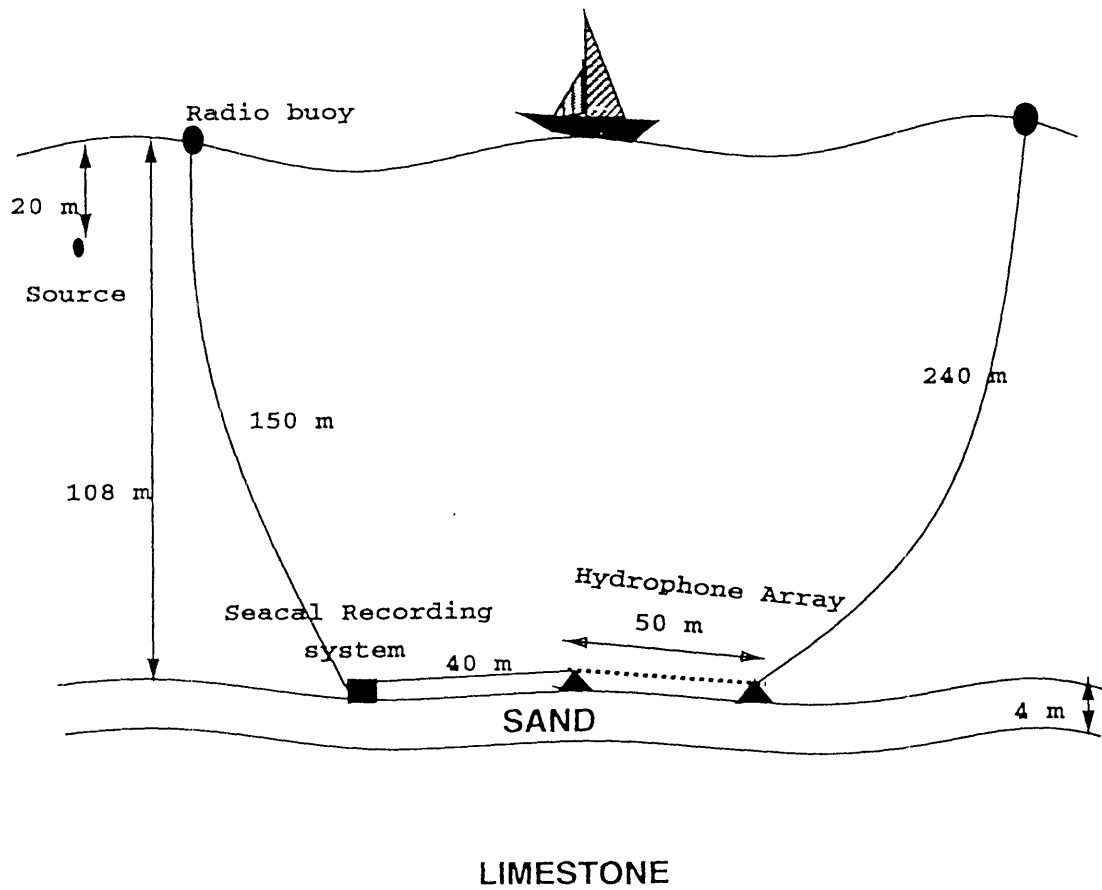


Figure 2.2. Shallow water environment, source and array configuration

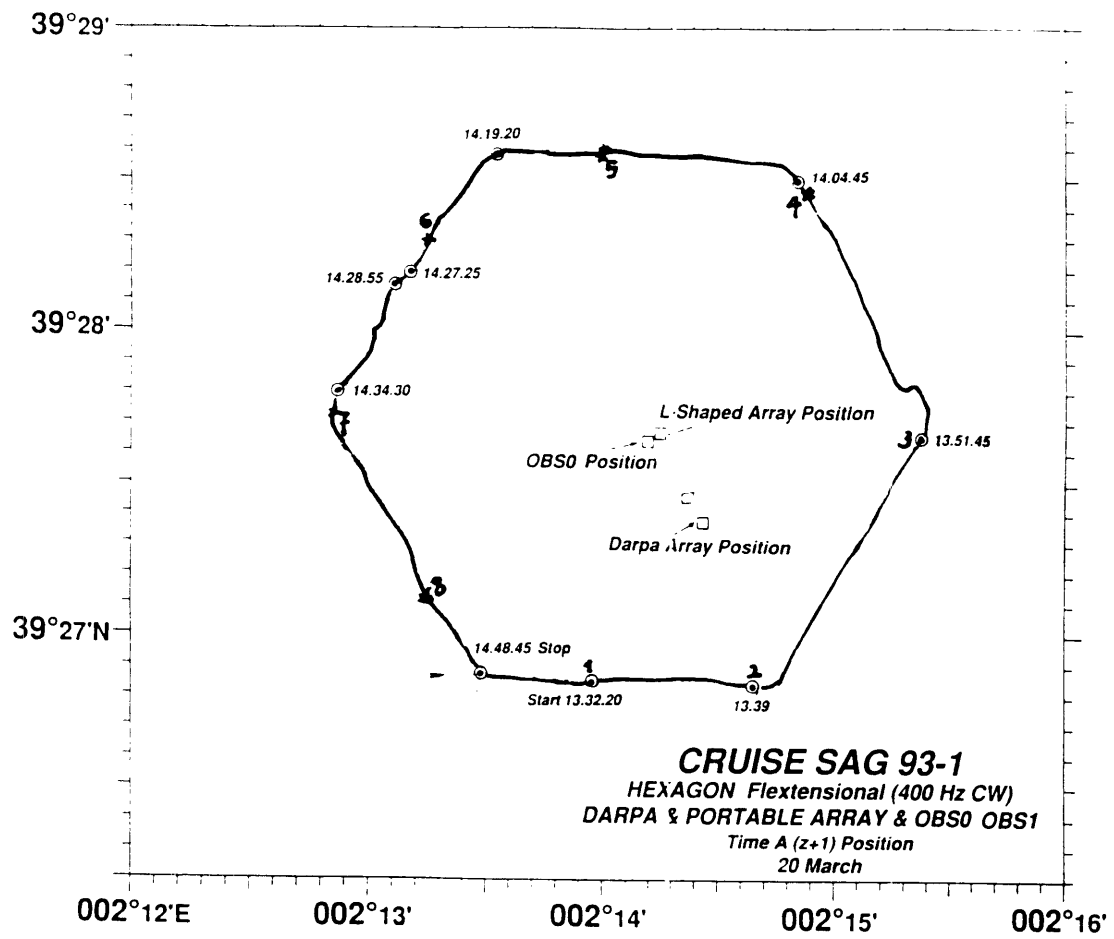


Figure 2.3. Hexagonal measurement track

The horizontal line array (HLA) settings are :

Sensitivity: Hydrophone#1 and #24 = -205.5 dBVolt re 1 μ Pa

Hydrophone#1 thru #23 = -170 dBVolt.

Gain : Hydrophone#1 = 0 dB

Hydrophone#2 thru #23 = 42 dB

Hydrophone#24 = 24 dB

Pre-emphasis : Hydrophone#1 thru #11, OFF

Hydrophone#13-24, OFF

Hydrophone#12, ON (-6 dB/octave from 1 kHz).

Due to inaccurate GPS (Global Positioning System) during the experiments and the unsynchronized source-receiver time, the source and receiver positions will be calculated using the inversion method to be discussed in Chapter 4.

CHAPTER 3.

THEORY

3.1. Normal Mode Method

There is much literature about the normal mode theory which has been applied to the underwater acoustic, however, in this thesis I would like to paraphrase the theory from the book published by Jensen *et al.*[49] and Frisk[50] in 1994.

Starting from two-dimension Helmholtz equation, we consider a point source with cylindrical coordinates (assuming cylindrical symmetry about z axis) in a horizontally stratified fluid medium with density and velocity depending only on depth z :

$$\frac{1}{r} \frac{\partial}{\partial r} r \left[\frac{\partial p}{\partial r} \right] + \frac{\partial^2 p}{\partial z^2} + \rho(z) \frac{\partial}{\partial z} \left[\frac{1}{\rho(z)} \right] \frac{\partial p}{\partial z} + k^2(z) p = -\frac{\delta(r) \delta(z-z_s)}{2\pi r} \quad (3.1)$$

Using a separation variable, we seek a solution in the following form $p(r,z)=\Phi(r)\Psi(z)$ with an assumption that $\Psi(z)$ satisfies the eigenvalue equation :

$$\frac{1}{\rho(r)} \frac{d^2 \Psi_n}{dz^2} + \frac{d}{dz} \left[\frac{1}{\rho(z)} \right] \frac{d \Psi_n}{dz} + \frac{k_{zn}^2}{\rho(z)} \Psi_n = 0 \quad (3.2)$$

where $k_{zn}^2 = k^2(z) - k_n^2$ and k_n and k_{zn} are the discrete values of the horizontal and vertical wavenumbers, respectively, associated with the eigenfunction $\Psi_n(z)$. By adding and subtracting the term ω^2/c_m^2 in above equation, where c_m is the minimum value of $c(z)$, we obtain the modal equation :

$$\frac{1}{\rho(z)} \frac{d^2 \Psi_n}{dz^2} + \frac{d}{dz} \left[\frac{1}{\rho(z)} \right] \frac{d \Psi_n}{dz} + \left[\frac{k^2(z) - \omega^2/c_m^2}{\rho(z)} + \frac{\omega^2/c_m^2 - k_n^2}{\rho(z)} \right] \Psi_n = 0 \quad (3.3)$$

This equation is an eigenvalue equation of Sturm-Liouville Problem (SLP) which has some following properties :

- a. The eigenfunctions $\Psi_n(z)$ satisfy boundary conditions on the interval $a \leq z \leq b$ which are (1) Dirichlet, (2) Neumann, (3) periodic, or (4) mixed boundary conditions.

b. The eigenfunctions $\Psi_n(z)$ are orthonormal.

$$\int_a^b \frac{\Psi_n(z)\Psi_m(z)}{\rho(z)} = \delta_{nm} \quad (3.4)$$

c. The eigenfunctions $\Psi_n(z)$ satisfy the closure or completeness relation:

$$\sum_n \frac{\Psi_n(z_s)\Psi_m(z_s)}{\rho(z_s)} = \delta(z-z_s) \quad (3.5)$$

Finally, the modes form a complete set which means we can represent an arbitrary function as a sum of the normal modes. Therefore, we can write the pressure field as :

$$p(r, z) = \sum_{n=1}^{\infty} \Phi_n(r) \Psi_n(z) \quad (3.6)$$

Substituting Equation (3.6) to Equation (3.1), we obtain :

$$\begin{aligned} & \sum_{n=1}^{\infty} \left\{ \frac{1}{r} \frac{d}{dr} \left(r \frac{d\Phi_n(r)}{dr} \right) \Psi_n(z) + \Phi_n(r) \left[\rho(z) \frac{d}{dz} \left(\frac{1}{\rho(z)} \frac{d\Psi_n(z)}{dz} \right) + \frac{\omega^2}{c^2(z)} \Psi_n(z) \right] \right\} \\ & = -\frac{\delta(r)\delta(z-z_s)}{2\pi r} \end{aligned} \quad (3.7)$$

The term in [] can be simplified using the modal equation (Eq.3.3). This yields,

$$\sum_{n=1}^{\infty} \left\{ \frac{1}{r} \frac{d}{dr} \left(r \frac{d\Phi_n(r)}{dr} \right) \Psi_n(z) + k_n^2 \Phi_n(r) \Psi_n(z) \right\} = -\frac{\delta(r)\delta(z-z_s)}{2\pi r} \quad (3.8)$$

Using the orthonormality (Eq.5.4), we can simplify Equation (3.8) to obtain :

$$\frac{1}{r} \frac{d}{dr} \left[r \frac{d\Phi_n(r)}{dr} \right] + k_n^2 \Phi_n(r) = -\frac{\delta(r)\Psi_n(z_s)}{2\pi \rho(z_s)} \quad (3.9)$$

This is a simply Bessel equation whose solution is given in terms of a Hankel function of the first kind (assuming that the solution must satisfy the Sommerfield radiation condition).

$$\Phi_n(r) = \frac{i}{4\rho(z_s)} \sum_{n=1}^{\infty} \Psi_n(z_s) H_0^1(k_n r) \quad (3.10)$$

The pressure field can be written as

$$p(r, z) = \frac{i}{4\rho(z_s)} \sum_{n=1}^{\infty} \Psi_n(z_s) \Psi_n(z) H_0^1(k_n r) \quad (3.11)$$

In the far field ($k_n r \gg 1$), we can substitute the asymptotic form for the Hankel function into Eq.(3.11) to obtain

$$p(r, z) \cong \frac{i}{\rho(z_s) \sqrt{8\pi r}} e^{-i\pi/4} \sum_{n=1}^{\infty} \Psi_n(z_s) \Psi_n(z) \frac{e^{ik_n r}}{\sqrt{k_n}} \quad (3.12)$$

Normally we define the transmission loss rather than the pressure field. The transmission loss is defined by

$$TL(r, z) = -20 \log \left| \frac{p(r, z)}{p_0(r=1)} \right|, \quad (3.13)$$

where $p_0(r) = \frac{e^{ik_0 r}}{4\pi r}$ is the pressure for point source in free space. Therefore, we may write

$$TL(r, z) \cong -20 \log \left| \frac{1}{\rho(z_s)} \sqrt{\frac{2\pi}{r}} \sum_{n=1}^{\infty} \Psi_n(z_s) \Psi_n(z) \frac{e^{ik_n r}}{\sqrt{k_n}} \right| \quad (3.14)$$

In the shallow water environment, it is useful to define the incoherent transmission loss due to bottom-interacting

$$TL_{inc}(r, z) \cong -20 \log \frac{1}{\rho(z_s)} \sqrt{\frac{2\pi}{r}} \sqrt{\sum_{n=1}^{\infty} \left| \Psi_n(z_s) \Psi_n(z) \frac{e^{ik_n r}}{\sqrt{k_n}} \right|^2} \quad (3.15)$$

3.1.1. Normal mode for a homogeneous fluid layer with a soft top and hard bottom(zeroth order waveguide)

The normal mode theory applies to an oceanic waveguide with a pressure release surface and hard bottom. For the case of constant density, the eigenvalue equation in Eq. (3.2) becomes

$$\frac{d^2 \Psi_n(z)}{dz^2} + k_{zn}^2 \Psi_n(z) = 0 \quad (3.16)$$

and the solution is

$$\Psi_n(z) = \sqrt{\frac{2\rho}{h}} \sin k_{zn} z, \quad k_{zn} = \frac{(n - \frac{1}{2})\pi}{h}, \quad n = 1, 2, 3, \dots \quad (3.17)$$

So the pressure field (Eq.3.6) is as

$$p(r, z) = \frac{i}{2h} \sum_{n=1}^{\infty} \sin k_{zn} z_0 \sin k_{zn} z H_0^1(k_n r) \quad (3.18)$$

Each mode propagates with a phase speed C_n which defines as

$$C_n = \frac{\omega}{k_n} = \frac{\omega}{\sqrt{k^2 - k_{zn}^2}} = \frac{c}{\sqrt{1 - \frac{\omega_n^2}{\omega^2}}} \quad (3.19)$$

There are three possible values of C_n , depending on the root term in the denominator :

- a. $k > k_{zn}$, both C_n and k_n are real, this regime is radially propagating modes with phase speed $C_n > c$
- b. $k = k_{zn}$, only pure standing waves in depth occur.
- c. $k < k_{zn}$, both C_n and k_n are imaginary, and the modes are exponentially decaying (evanescent) with range.

Based on the criterion above, only n th modes will propagate when the frequency is less than the modal cutoff frequency ω_n which is given by

$$\omega_n = k_{zn} z = \frac{(n - \frac{1}{2}) \pi c}{h} \quad (3.20)$$

where h is water depth and c is sound speed of wave propagating in the water.

The group velocity is a measure of the rate of energy transport which defines as

$$V_n = \frac{d\omega}{dk_n} = C_n + k_n \frac{dC_n}{dk_n} = c \sqrt{1 - \frac{\omega_n^2}{\omega^2}} \quad (3.21)$$

3.1.2. Normal mode for Pekeris waveguide

When the waveguide has impenetrable boundaries, the solution consists totally of a sum of discrete modes; on the other hand, when one of the boundaries is penetrable, the solution is composed by discrete modes and continuum modes. So the total pressure field $p(r,z)$ as

$$p(r,z) = p_d(r,z) + p_c(r,z) \quad (3.22)$$

where :

$$p_d(r,z) = \frac{i}{4\rho} \sum_{n=1}^{\infty} A_n^2 \sin k_{zn} z_0 \sin k_{zn} z H_0^1(k_n r) \quad (3.23)$$

$$p_c(r,z) = \frac{ip_1}{2\pi\rho} \int_{c_s} \frac{k_z}{k_{1z}} \frac{\sin k_z k_0 \sin k_z z}{\left[\sin^2 k_z h + \frac{\rho_1^2 k_z^2}{\rho^2 k_{1z}^2} \cos^2 k_z h \right]} H_0^1(k, r) dk_z \quad (3.24)$$

For far field approximations, using the asymptotic behavior of Hankel function, the solution becomes :

$$p_d(r,z) \approx \frac{e^{i\pi/4}}{\rho\sqrt{2\pi}} \sum_{n=1}^{n_{\max}} A_n^2 \sin k_{zn} z_0 \sin k_{zn} z \frac{e^{ik_n r}}{\sqrt{k_n^0 r}} \quad (3.25)$$

$$p_c(r, z) \approx \frac{e^{i\pi/4}}{2h\sqrt{2\pi}} \sum_{n=n_{\max}+1}^{\infty} \sin k_{zn}^2 z_0 \sin k_{zn}^0 z e^{-\frac{\rho_1^0 k_n^0 r}{\rho_1 h k_n^0}} \frac{e^{ik_n^0 r}}{\sqrt{k_n^0 r}} \quad (3.26)$$

Maximum number of propagating discrete modes is

$$n_{\max} = \frac{2h}{\lambda} \sqrt{1 - \frac{c^2}{c_1^2}} + \frac{1}{2} \quad (3.27)$$

and the cutoff frequency is

$$\omega_n' = \frac{\pi c}{h} \frac{(n - \frac{1}{2})}{\sqrt{1 - \frac{c^2}{c_1^2}}} = \frac{\omega_n}{\sqrt{1 - \frac{c^2}{c_1^2}}} \quad (3.28)$$

where c is the sound speed in the water and c_1 is sound speed in the lower medium and ω_n is the cut-off frequency if the bottom boundary is rigid bottom.

3.2. Scattering from rough boundaries

The derivation in Section 3.1. we have assumed that the boundaries are perfectly smooth, but in the real ocean environment there is no perfectly smooth surface. Therefore, when waves hit the rough surfaces, scattering will occur. In this section we will discuss about scattering from rough

bottom boundaries starting from the exact integral equation then discuss two approximate methods, Kirchoff and perturbation theories.

3.2.1. Integral formula for scattered field

Randomly rough boundary acts as a scatterer and the total field $T(r)$ may be taken to be composed of the incident field $I(r)$ and a scattered field $S(r)$:

$$T(r) = I(r) + S(r) \quad (3.29)$$

The total field at any point r is given exactly by the Helmholtz equation scattering formula (see, for example Ogilvy[41]) :

$$T(r) = I(r) + \int_{P_0} \left[S(r_0) \frac{\partial G(r, r_0)}{\partial n_0} - G(r, r_0) \frac{\partial S(r_0)}{\partial n_0} \right] dP_0 \quad (3.30)$$

with an assumption that there is no source within the closed integration area P_0 , and

$$G(r, r_0) = \frac{\exp(ik|r - r_0|)}{4\pi|r - r_0|} \quad (3.31)$$

The n_0 is unit surface normal pointing towards the source.

When the surface P_0 is closed the scattered field $S(r_0)$, appearing in the integrand in equation (3.30), is interchangeable with the total field, $T(r_0)$ since :

$$\int_{P_0} \left[I(r_0) \frac{\partial G(r, r_0)}{\partial n_0} - G(r, r_0) \frac{\partial I(r, r_0)}{\partial n_0} \right] dP_0 = 0 \quad (3.32)$$

if there are no sources of I within P_0 . Therefore the scattered field can be written as :

$$\begin{aligned} S(r) &= T(r) - I(r) \\ &= \int_{P_0} \left[T(r_0) \frac{\partial G(r, r_0)}{\partial n_0} - G(r, r_0) \frac{\partial T(r, r_0)}{\partial n_0} \right] dP_0 \end{aligned} \quad (3.33)$$

3.2.2. The Kirchoff Approximation

The physical basis of the Kirchoff approximation is that any surface on the rough surface is assumed to behave as if the surface were locally flat. The total pressure field on the surface is given by

$$T(r_0) = [1 + R_0(r_0)]I(r_0) \quad (3.34)$$

and the gradient of the pressure is

$$\frac{\partial T(r_0)}{\partial n_0} = i[1 - R_0(r_0)](k_{inc} \cdot n_0)I(r_0) \quad (3.35)$$

General far-field approximation is defined as [59] :

$$S(r) = \frac{ike^{ikr}}{4\pi r} \int_{r_s} (a \partial h / \partial x_0 + b \partial h / \partial y_0 - c) \exp\{ik[Ax_0 + By_0 + Ch(x_0, y_0)]\} dx_0 dy_0 \quad (3.36)$$

where

$$\begin{aligned} A &= \hat{k}_x^- = \sin \theta_1 - \sin \theta_2 \cos \theta_3 \\ B &= \hat{k}_y^- = -\sin \theta_2 \sin \theta_3 \\ C &= \hat{k}_z^- = -(\cos \theta_1 + \cos \theta_2) \end{aligned} \quad (3.37)$$

$$\begin{aligned} a &= (\hat{k}^+ - R_0 \hat{k}^-)_x = \sin \theta_1 (1 - R_0) + \sin \theta_2 \cos \theta_3 (1 + R_0) \\ b &= (\hat{k}^+ - R_0 \hat{k}^-)_y = -\sin \theta_2 \sin \theta_3 \\ c &= (\hat{k}^+ - R_0 \hat{k}^-)_z = \cos \theta_1 (1 + R_0) - \cos \theta_1 (1 - R_0) \end{aligned} \quad (3.38)$$

Limitation of Kirchoff Approximation is that the deviation of the surface from flat (over a distance comparable to the projection of the incoming wavelength onto the surface) must be small compared to the wavelength of the incoming waves.

$$kr_c \cos^3 \theta \gg 1 \quad (3.39)$$

where r_c is local curvature of surface, θ is global angle of incident measured from the mean plane normal and k is the bulk wavenumber of media.

3.2.3. Perturbation Approximation

The perturbation approach to wave scattering from rough surfaces necessitates restrictions on the height h and gradient ∇h of the surface :

$$\begin{aligned} kh(x, y) &\ll 1 \\ |\nabla h(x, y)| &\ll 1 \end{aligned} \quad (3.40)$$

The total pressure field (Eq.3.29) can be written as

$$T(r) = I(r) + \sum_{n=0}^{\infty} S_n(r) \quad (3.41)$$

So perturbation theory assumes that the scattered field can be expanded in an infinite series. If the boundary conditions on the rough surface are

$$f(x, y, z) \Big|_{z=h(x, y)} = 0 \quad (3.42)$$

and it can be expanded using the Taylor series as

$$f(x, y, h) = f(x, y, 0) + h \frac{\partial f(x, y, 0)}{\partial z} + \frac{h^2}{2} \frac{\partial^2 f(x, y, 0)}{\partial z^2} + \dots \quad (3.43)$$

By expanding the scattered field in Equation (3.41) and equating the term of the same order of h with Equation (3.43) it will get the scattered field. Therefore, we will have zeroth, first, second and higher order approximations.

The first perturbation theory applies to the boundary conditions[59] :

a. Dirichlet boundary condition

The pressure release surface boundary condition can be written as :

$$S_1|_{z=0} = -h\left(\frac{\partial I}{\partial z} + \frac{\partial S_0}{\partial z}\right) \quad (3.44)$$

and the scattered field is

$$S_1 = -\int_{P_M} h(r_0)\left(\frac{\partial I}{\partial z} + \frac{\partial S_0}{\partial z}\right)\frac{\partial G^*(r, r_0)}{\partial z_0} dP_M(r_0) \quad (3.45)$$

b Neumann boundary condition

The rigid boundary can be written as

$$\begin{aligned} \left. \frac{\partial S_1}{\partial z} \right|_{z=0} &= \frac{\partial h}{\partial x} \left[\frac{\partial}{\partial x} (I + S_0) \right]_{z=0} + \frac{\partial h}{\partial y} \left[\frac{\partial}{\partial y} (I + S_0) \right]_{z=0} + \\ &+ h \left[\frac{\partial^2}{\partial x^2} (I + S_0) \right]_{z=0} \end{aligned} \quad (3.46)$$

and the scattered field as

$$\begin{aligned} S_1 = - \int_{P_M} \left\{ \frac{\partial h}{\partial x} \left[\frac{\partial I(r_0)}{\partial x} + \frac{\partial S_0(r_0)}{\partial x} \right] + \frac{\partial h}{\partial y} \left[\frac{\partial I(r_0)}{\partial y} + \frac{\partial S_0(r_0)}{\partial y} \right] - \right. \\ \left. h \left[\frac{\partial^2 I(r_0)}{\partial z^2} + \frac{\partial^2 S_0(r_0)}{\partial z^2} \right] \right\} G^*(r, r_0) dP_M(r_0) \end{aligned} \quad (3.47)$$

The first order perturbation approach is usually accurate when $kh_{\text{rms}} \ll 1$. The additional requirement $k\lambda \leq 1$ is needed for scattering angle away from specular angle[59].

3.3. Spatial Coherence

Two functions representing spatial coherence are correlation function and coherence function. The correlation function of signals is defined by comparing the amplitude and/or phase of a signal received on one hydrophone with a signal received on another which is separated from the first

by a certain directional distance relative to the propagation[63]. The magnitude of their correlation function is their cross correlation coefficient.

For example, let the output of the first hydrophone be $x(t)$ and the second hydrophone $y(t)$; the correlation coefficient is defined by [51] as:

$$R_{xx}(\tau) = \lim_{T \rightarrow \infty} \frac{1}{T} \int_0^T x(t)x(t+\tau) dt \quad (3.48)$$

$$R_{yy}(\tau) = \lim_{T \rightarrow \infty} \frac{1}{T} \int_0^T y(t)y(t+\tau) dt \quad (3.49)$$

$$R_{xy}(\tau) = \lim_{T \rightarrow \infty} \frac{1}{T} \int_0^T x(t)y(t+\tau) dt \quad (3.50)$$

where R_{xx} and R_{yy} are the auto correlation functions, while R_{xy} is the cross-correlation function. The normalized R_{xy} (at zero lag the correlation equals to 1), is defined as[63]:

$$R_{xy}(t) = \frac{\frac{1}{T} \int_0^T x(t)y(t)dt}{\left[\frac{1}{T} \int_0^T x^2(t)dt \right]^{1/2} \left[\frac{1}{T} \int_0^T y^2(t)dt \right]^{1/2}} \quad (3.51)$$

The coherence function is defined as :

$$C_{xy}^2(f) = \frac{|D_{xy}(f)|^2}{D_{xx}(f)D_{yy}(f)} = \frac{|S_{xy}(f)|^2}{S_{xx}(f)S_{yy}(f)} \quad 0 \leq C_{xy}^2(f) \leq 1 \quad (3.52)$$

where:

D_{xx} and D_{yy} are the double-sided auto spectra density function, while D_{xy} is double-sided cross spectra density function since there are defined for all frequencies positive and negative frequencies. $S(f)$ is the single-sided spectra density function.

There are three methods to find the spectral density functions[51], but only two of these will be derived:

a. Spectra via correlation functions

The spectral cross correlation functions are defined as their Fourier Transforms:

$$D_{xx}(f) = \int_{-\infty}^{\infty} R_{xx}(\tau) e^{-j2\pi f\tau} d\tau \quad (3.53)$$

$$D_{yy}(f) = \int_{-\infty}^{\infty} R_{yy}(\tau) e^{-j2\pi f\tau} d\tau \quad (3.54)$$

$$D_{xy}(f) = \int_{-\infty}^{\infty} R_{xy}(\tau) e^{-j2\pi f\tau} d\tau \quad (3.55)$$

The single-sided spectral density functions are :

$$\begin{aligned} S_{xy}(f) &= 2D_{xy}(f) = 2 \int_{-\infty}^{\infty} R_{xy}(\tau) e^{-j2\pi f\tau} d\tau & f > 0 \\ &= D_{xy}(f) & f = 0 \\ &= 0 & f < 0 \end{aligned} \quad (3.56)$$

$$\begin{aligned} S_{xx}(f) &= 2D_{xx}(f) = 2 \int_{-\infty}^{\infty} R_{xx}(\tau) e^{-j2\pi f\tau} d\tau & f > 0 \\ &= D_{xx}(f) & f = 0 \\ &= 0 & f < 0 \end{aligned} \quad (3.57)$$

Since the auto correlation functions are always even functions of τ it follows that the spectra are given by only the real part of the Fourier transform :

$$S_{xx}(f) = 2 \int_{-\infty}^{\infty} R_{xx}(\tau) e^{-j2\pi f\tau} d\tau = 4 \int_0^{\infty} R_{xx}(\tau) \cos(2\pi f\tau) d\tau \quad (3.58)$$

b. Spectra via Fourier Transform

The second method to develop spectra density functions is in terms of the direct Fourier transform of the original data records $x(t)$, and $y(t)$, where the finite Fourier transforms over k th record of length T , which is define as:

$$X_k(f, T) = \int_0^T x_k(t) e^{-j2\pi f t} dt \quad (3.59)$$

$$Y_k(f, T) = \int_0^T y_k(t) e^{-j2\pi f t} dt \quad (3.60)$$

The double-sided cross spectral density function between $x(t)$ and $y(t)$ is defined using X^*Y and not XY^* as:

$$D_{xy}(f) = \lim_{T \rightarrow \infty} \frac{1}{T} E[X_k^*(f, T) Y_k(f, T)] \quad (3.61)$$

The single-sided auto and cross spectral density functions are :

$$S_{xy}(f) = \lim_{T \rightarrow \infty} \frac{2}{T} E[X_k^*(f, T) Y_k(f, T)] \quad f > 0 \quad (3.62)$$

$$S_{xx}(f) = \lim_{T \rightarrow \infty} \frac{2}{T} E[|X_k^*(f, T)|^2] \quad f > 0 \quad (3.63)$$

$$S_{yy}(f) = \lim_{T \rightarrow \infty} \frac{2}{T} E[|Y_k^*(f, T)|^2] \quad f > 0 \quad (3.64)$$

where the expected-value operator E denotes an averaging operation over the index k.

CHAPTER 4

DATA PROCESSING AND RESULTS

The original data came from Dr. Jim TenCate (Applied Research Laboratory, the University of Texas at Austin) transferred via binary files. After applying a gain correction and unit conversion to pressure units (μPa), the results are as shown in Figures 4.1. through 4.11.(at the end of this Chapter). The modal arrivals are clearly identified in the retarded time series of those figures. I should clarify that the zero position in time-axis does not correspond to the ping's time.

Given the environment (see Chapter 2), 108m water depth(h) and 400Hz source frequency(f), we can calculate the number of propagating modes using Equation 3.20 (assuming zeroth order wave guide). The result is 58 modes. Also we can calculate the phase and group speed of each mode using Equation 3.19 and 3.21, respectively. If we use Pekeris wave guide with 1650m/s sandy bottom speed, we can calculate the maximum number of propagating discrete modes using

Equation 3.27, which equals to 23 modes. We can see that the more lossy bottom the lesser number of discrete propagating modes.

4.1. Synthetic Source

The acoustics source was the flextentional transducer with frequency near 400Hz and 5ms continuous wave signal length or 2cycles, driven electronically to the transducers. Since the tone burst of the signal generated by the transducer was unknown a synthetic source pulse was built based on a theoretical flextentional characteristic. The flextentional transducer usually has Q equal to 4 or 5 [69], where Q represents the number of cycles to reach the steady state condition. During the cruise the source was shut off before reaching the steady state condition (see Figure 4.12.).

4.2. Receiver Array and Source Localizations

As mentioned in Chapter 2 the old generation GPS systems gave significant errors during the cruise, consequently we do not have good estimate of the position of the receiver array and source. Also, the time pings and the

receiver were not synchronized. The inversion method based on the time series data was used to find the source and receiver positions and orientations assuming the following :

- a. Ping#1 is the reference position (2°13.95'E, 39°26.85'N).
- b. The hydrophone#1 position (as starting zero position) is 2°14.42'E, 39°27.39'N.
- c. The ship had constant speed(26.5m/s) and direction between ping#1 and ping#1c with 30 second intervals.
- d. The receiver array is a straight line.
- e. The sound speed is constant, 1508 m/s.

The time series data of ping#1 has been processed to check the validity of an assumption (c) using the inversion method. The receiver array was not an exactly straight line as shown in Figure 4.13.

The source and receiver array localization formula is:

$$t_{\text{arrival}} = t_{\text{shot}} + t_{\text{S-R}} \quad (4.1)$$

$$\hat{t}_{\text{shot}} = \frac{1}{N} \sum_{i=1}^N (\hat{t}_{\text{arrival}} - t_{\text{S-R}}) \quad (4.2)$$

$$\hat{t}_{\text{arrival}} = \hat{t}_{\text{shot}} + t_{\text{S-R}} \quad (4.3)$$

$$\chi^2 = \sum_{i=1}^N (t_{\text{arrival}} - \hat{t}_{\text{arrival}})^2 \quad (4.4)$$

where :

t_{arrival} = arrival time

$t_{\text{S-R}}$ = travel time from source to receiver

t_{shot} = shot time

\hat{t} = time estimate

First, set a position of receiver array (x,y,θ) , then calculate $t_{\text{S-R}}$ and set a t_{shot} . Using Equations 4.1 through 4.4 and the time series data of ping#1, ping#1a, ping#1b, ping#1c and ping#2 as inputs, the value of χ^2 can be minimized by setting (x,y,θ) as variables.

The results show that the array position should be moved 120m to the east and 150m to the north from the position given in the cruise report (see Figure 4.14). Meanwhile, the receiver array bearing should be 158° instead of 338° or 292° as stated on the cruise report. The other source positions (ping#2 through ping#8) were determined using these corrected receiver array position and orientation.

The distances between the pings(source) and receiver array (hydrophone#1) are :

Ping#	Distance (m)
1	1374.6
2	1183.9
3	2086.3
4	1972.3
5	2383.0
6	2418.1
7	2741.4
8	2432.8

The source-receiver distances based on these above results were used to generate time series data using the following image method with pressure released surface at the top (Dirichlet boundary condition) and hard bottom at the seafloor (Neumann boundary condition)[49,50]:

$$p(r) = \sum_{n=0}^{\infty} (-1)^n \left[\frac{e^{R_{n1}}}{R_{n1}} + \frac{e^{R_{n2}}}{R_{n2}} - \frac{e^{R_{n3}}}{R_{n3}} - \frac{e^{R_{n4}}}{R_{n4}} \right] \quad (4.5)$$

and

$$\begin{aligned} R_{n1} &= \sqrt{r^2 + (z - z_0 - 2nh)^2}; & R_{n2} &= \sqrt{r^2 + [z + z_0 - 2(n+1)h]^2}; \\ R_{n3} &= \sqrt{r^2 + (z + z_0 + 2nh)^2}; & R_{n4} &= \sqrt{r^2 + [z - z_0 - 2(n+1)h]^2}; \end{aligned} \quad (4.6)$$

where :

$p(r)$ = pressure

z_0 = source depth; z = receiver depth,

r = horizontal distance from source to receiver,
 h = water depth.

The time series of ping#1 through ping#8 are compared to synthetic time series data generated using the image method to check the validity of source and receiver positions. The results show an excellent agreement.

4.3. Spatial Coherence of Scattered Field

The total field, $T(r,t)$ can be written as a composite of mean field, $M(r,t)$, or coherent field and residual field or scattered field, $S(r,t)$, (incoherent field).

$$T(r,t) = M(r,t) + S(r,t) \quad (4.7)$$

The procedure to find the scattered field every mode for every ping and its correlation function is :

- a. Beamform/time delay the time series data.
- b. Add coherently for whole hydrophones
- c. Take an average for the whole hydrophones

- d. Get the residual field or scattered field by subtracting the average value from the total field for every hydrophone.
- e. Take cross correlations between hydrophones.

The correlation function is calculated using the Equation (3.51) as

$$R_{xy}(s,t) = \frac{1}{N-s} \sum_{s=0}^{N-s} \max \left[\frac{\frac{1}{T} \sum_{t=0}^T H_i(t) H_{i+s}(t)}{\left[\frac{1}{T} \sum_{t=0}^T H_i(t) \right] \left[\frac{1}{T} \sum_{t=0}^T H_{i+s}(t) \right]} \right], \quad s=0,1,2,\dots,21 \quad (4.8)$$

where i is hydrophone number and s is hydrophone separation distance; $s=0,1,2,\dots$ are 2,4,6... meter separation distances. $H(t)$ is a hydrophone time series data of each mode with length T . Figure 4.15 shows the result of all procedures above for the ping#1.

The spectral energy of the scattered field is determined by taking the Fourier Transform of the scattered field as shown in Figure 4.16a. It can be clearly seen that the scattered field energy at frequency around $\pm 400\text{Hz}$ and the magnitude varies with hydrophone arrays.

The magnitude square coherence function (MSC) of total field, T(r,t), and scattered field, S(r,t), are calculated using the formula in Eq.(3.52) as:

$$C_{xy}^2(s, f) = \frac{|G_{xy}(f)|^2}{G_{xx}(f)G_{yy}(f)} = \frac{\left[\frac{2}{N-s} \sum_{i=1}^{N-s} G_i^*(f)G_{i+s}(f) \right]^* \left[\frac{2}{N-s} \sum_{i=1}^{N-s} G_i^*(f)G_{i+s}(f) \right]}{\left[\frac{2}{N-s} \sum_{i=1}^{N-s} G_i^*(f)G_i(f) \right] \left[\frac{2}{N-s} \sum_{i=1}^{N-s} G_{i+s}^*(f)G_{i+s}(f) \right]} \quad (4.9)$$

where i is hydrophone number and s is hydrophone separation distance; s=0,1,2... are 2,4,6... meter separation distances. G(f) is a single sided spectral density function of the total field or the scattered field of each mode for every hydrophone. Figure 4.16b. shows the coherence function for the total field and the scattered field. These procedures are repeatedly applied for mode#2 and mode#3 of ping#1 and other pings (see Figures 4.17 through 4.48)

From Figure 4.17 through 4.48, the correlation function of the scattered field is very high (0.9 to 0.65). The magnitude square complex coherence function (MSC) of the total field is high (about 0.9), on the other hand, the MSC of

the scattered field varies from 0.15 to 0.0 for 2m to 42m hydrophone separation. Based on this result we can conclude that the bottom roughness was very small.

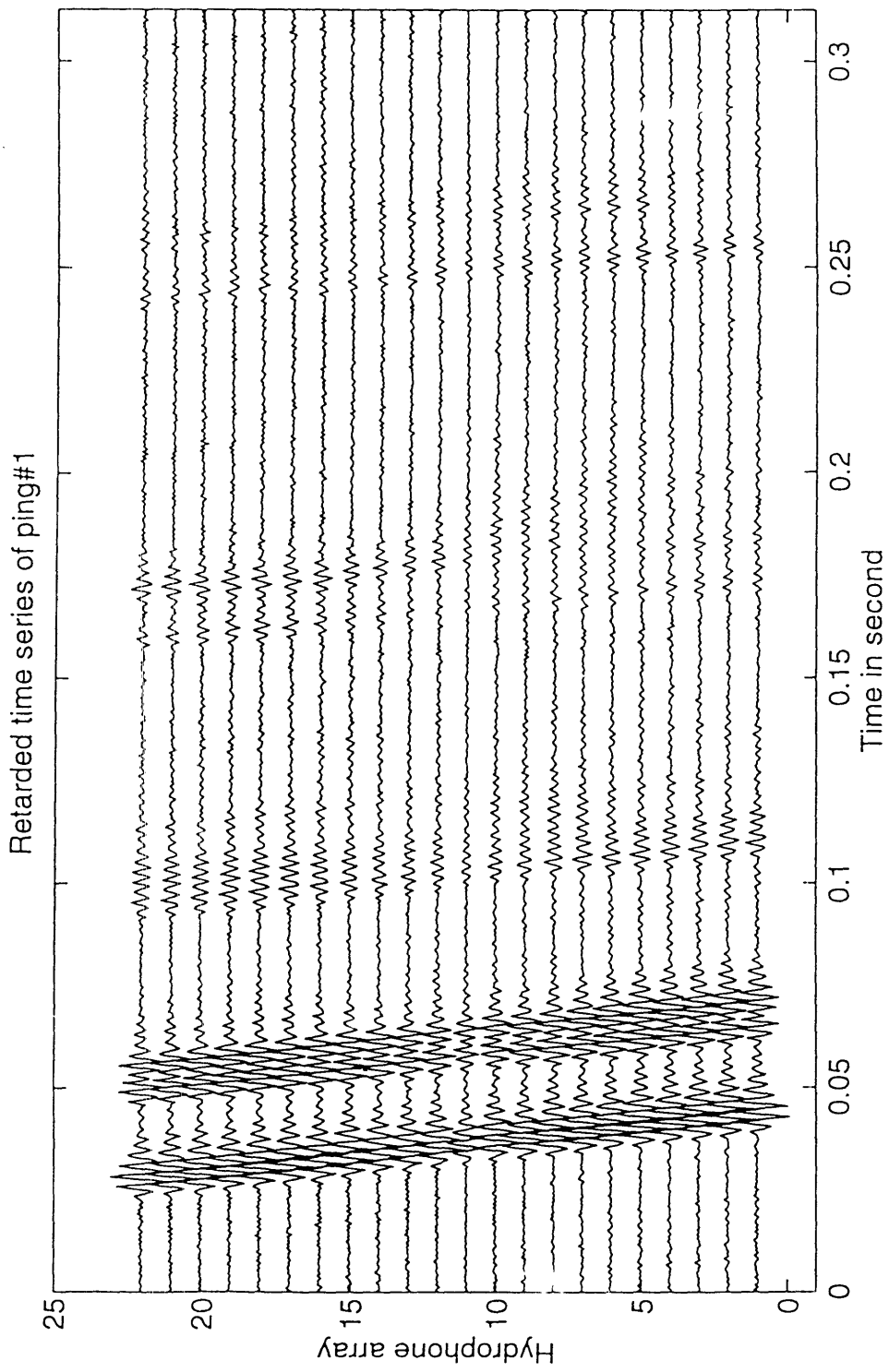


Figure 4.1. Retarded time series data of ping # 1

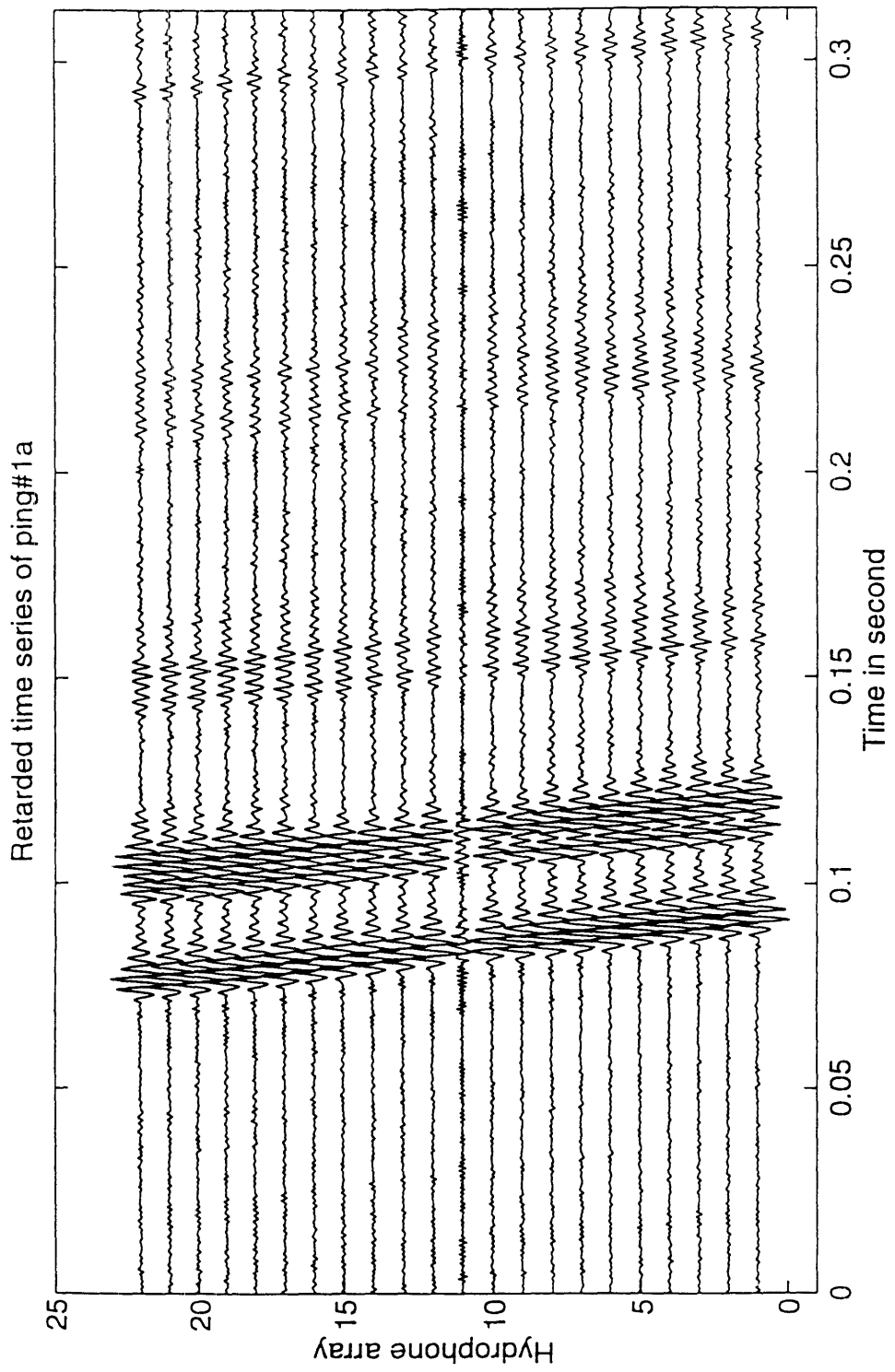


Figure 4.2 Retarded time series data of ping # 1a

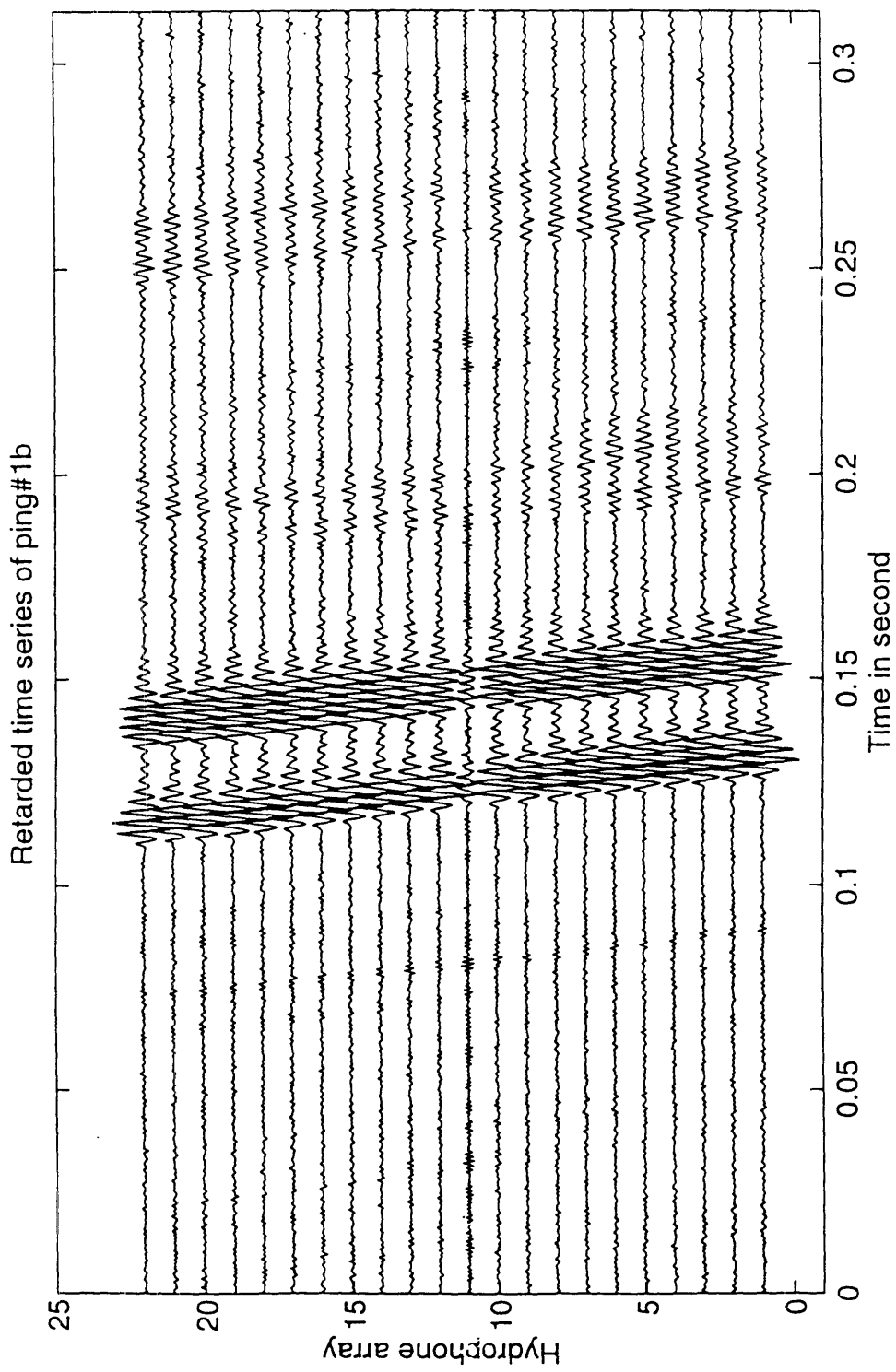


Figure 4.3 Retarded time series data of ping # 1b

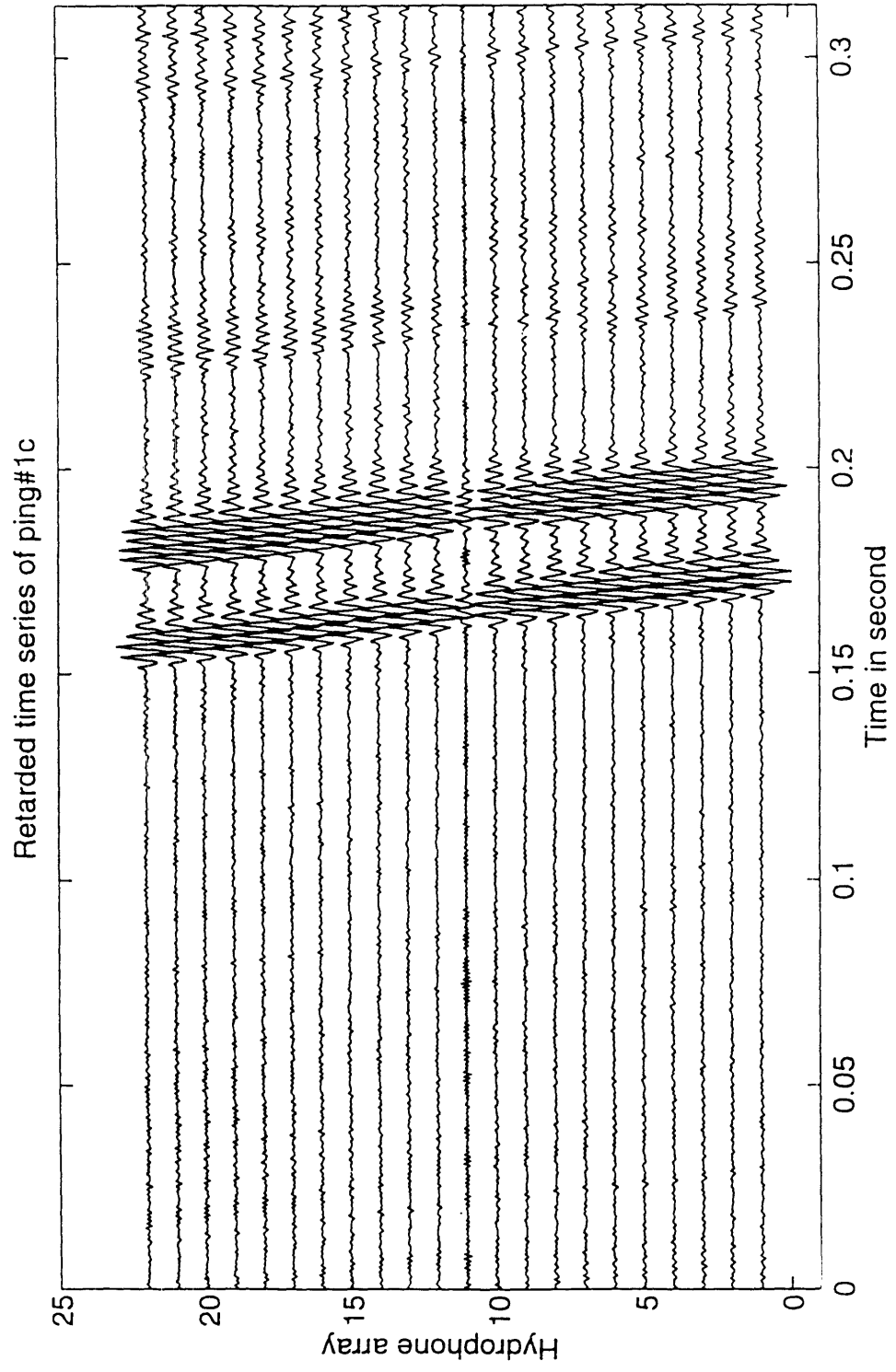


Figure 4.4 Retarded time series data of ping # 1c

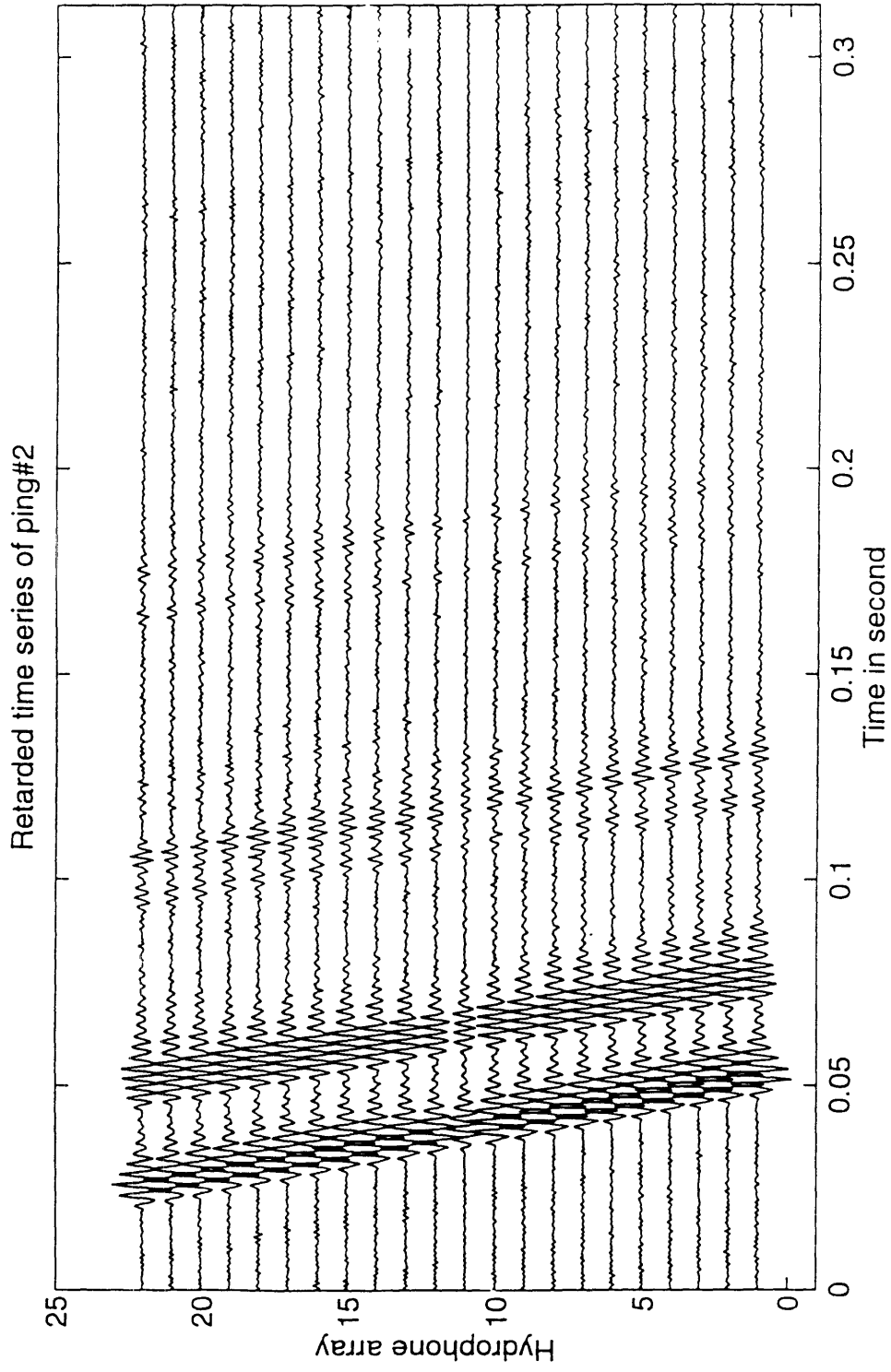


Figure 4.5 Retarded time series data of ping # 2

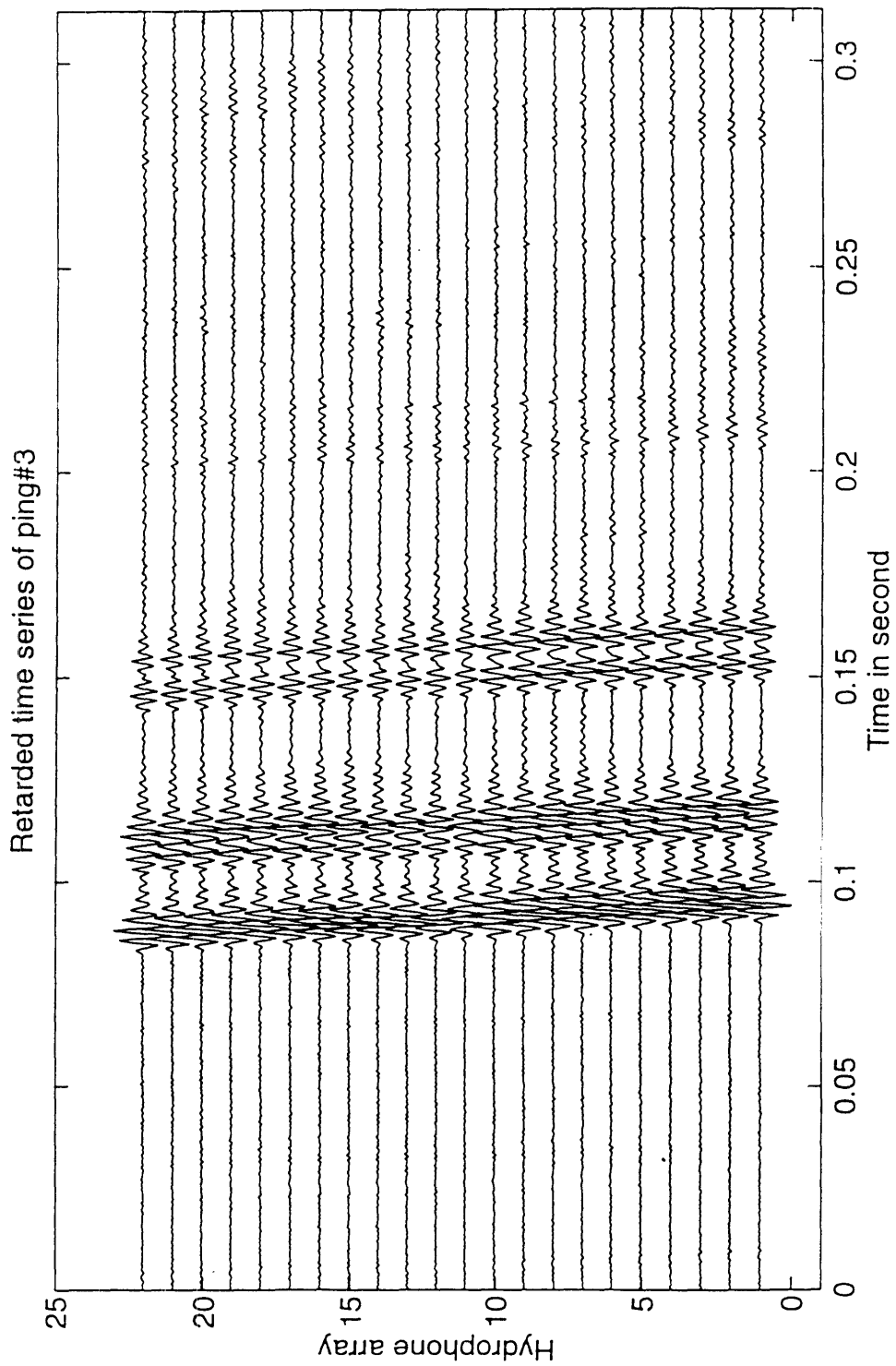


Figure 4.6 Retarded time series data of ping # 3

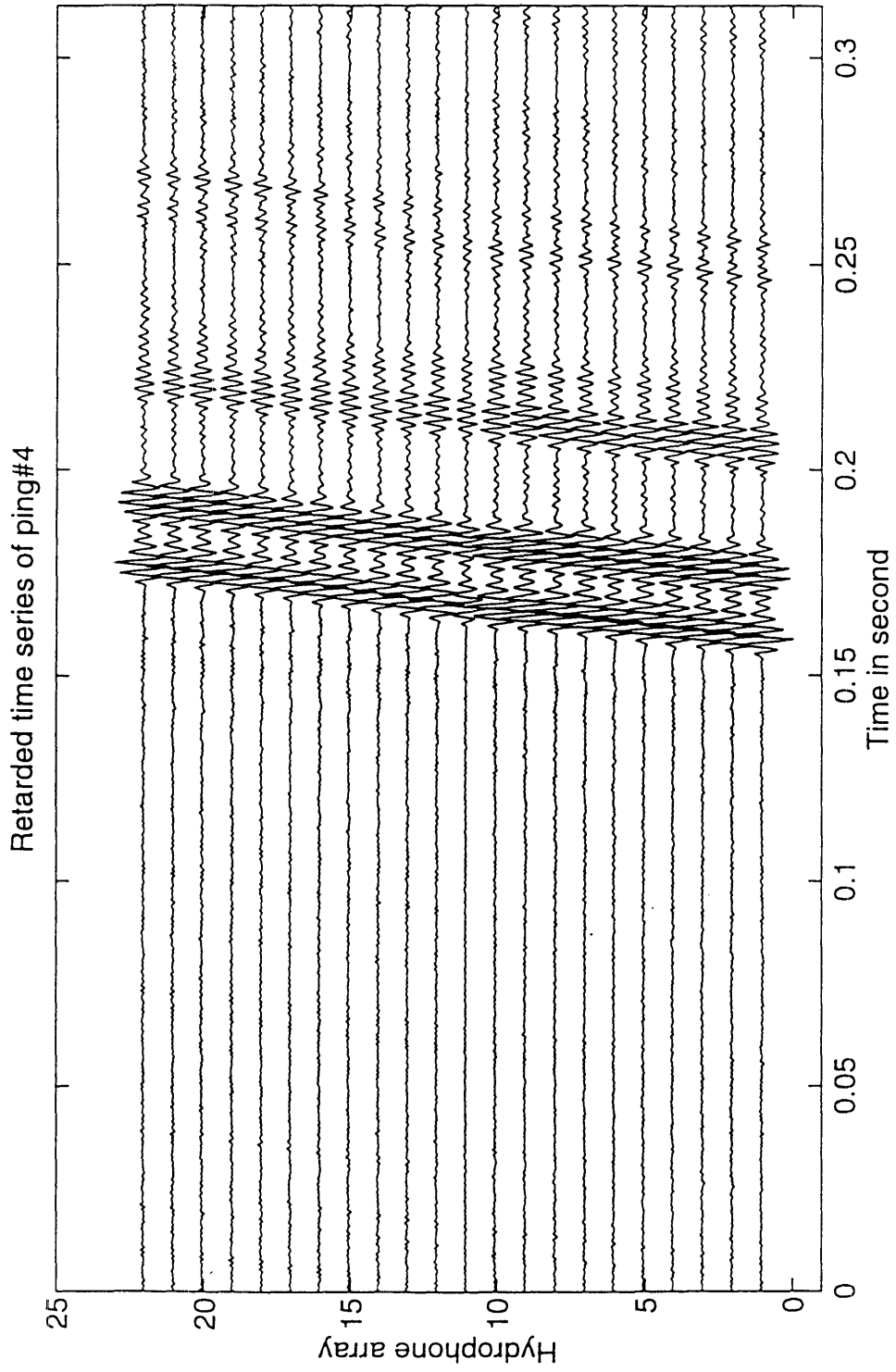


Figure 4.7. Retarded time series data of ping # 4

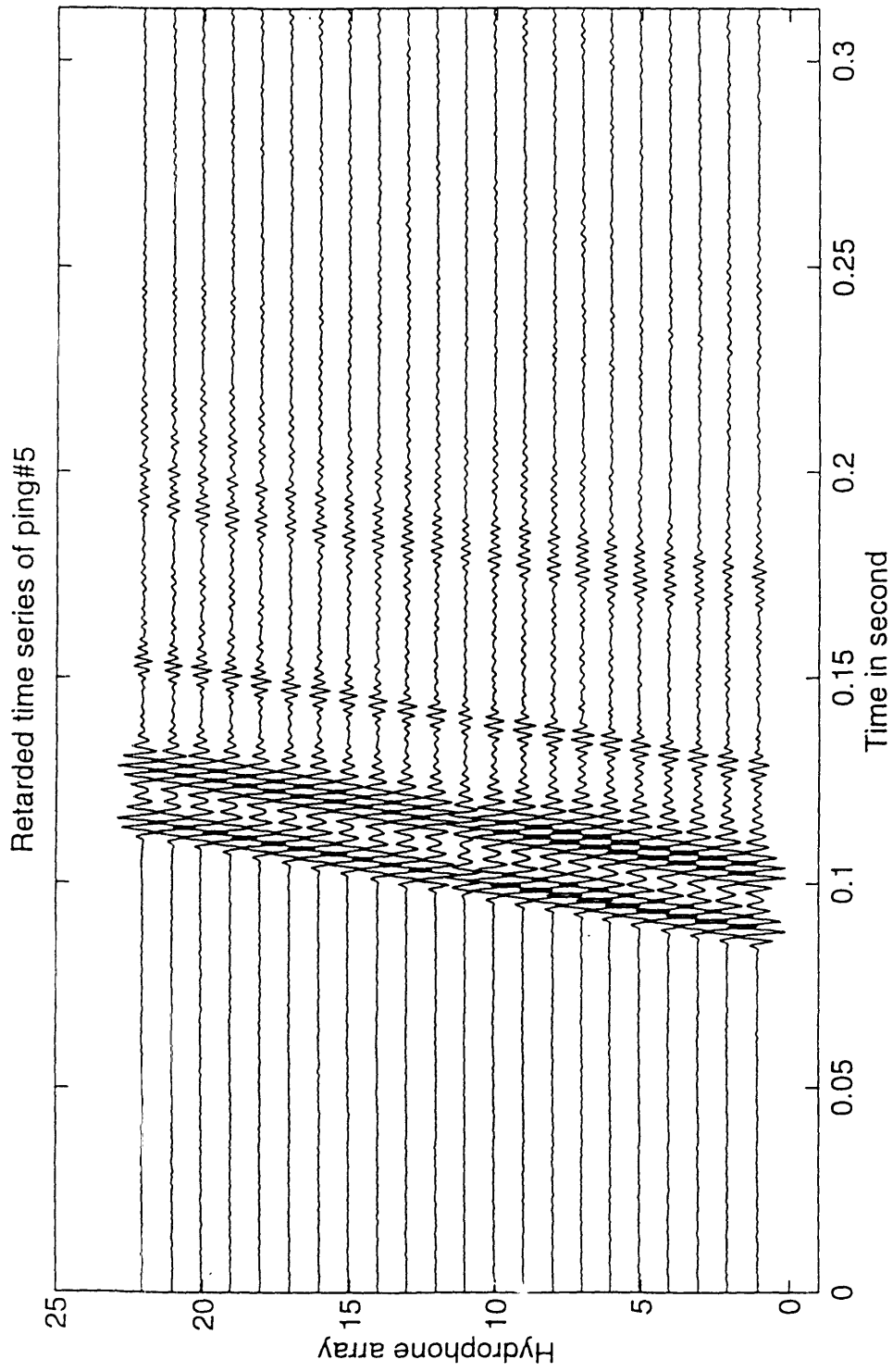


Figure 4.8. Retarded time series data of ping # 5

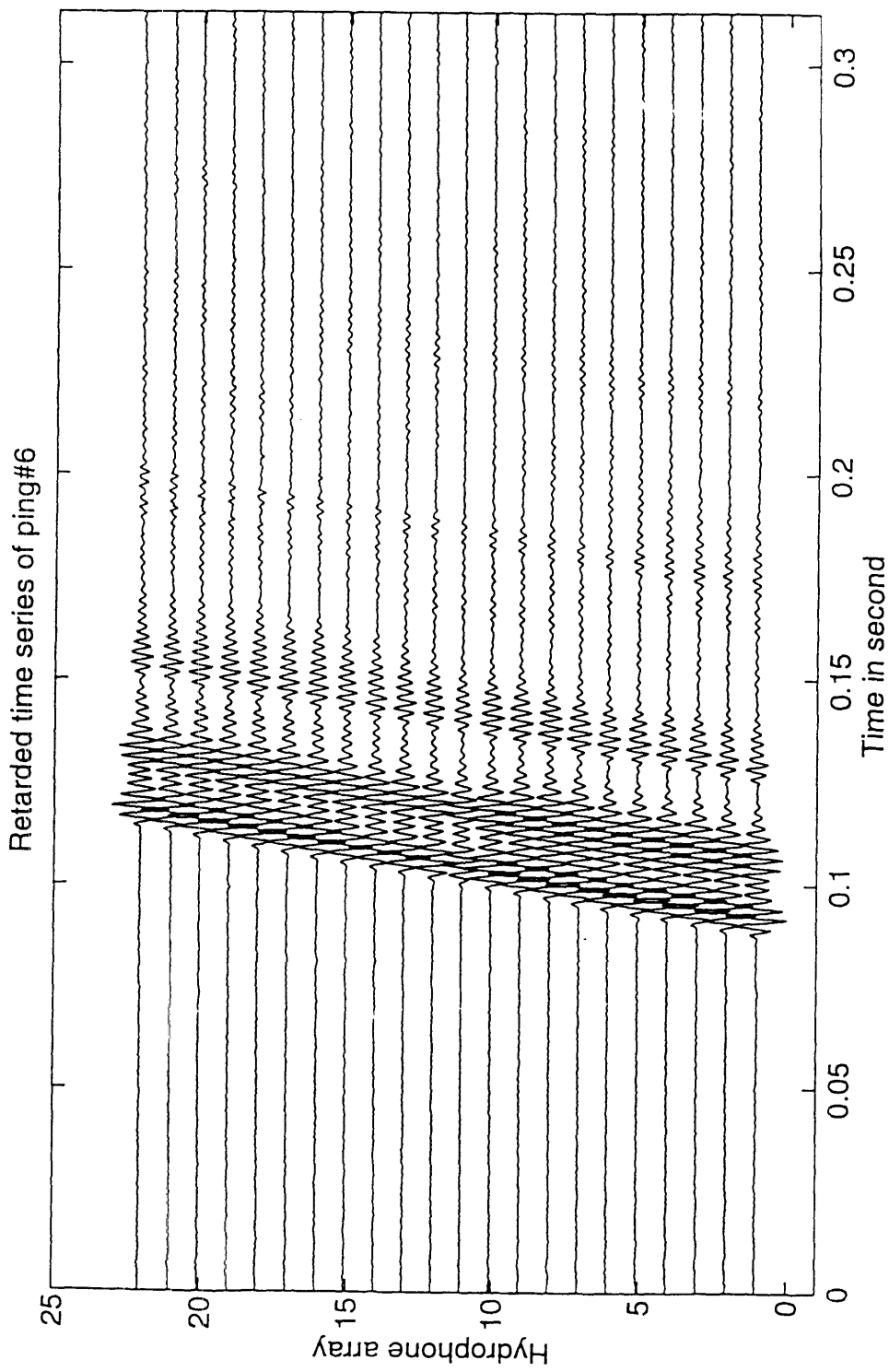


Figure 4.9. Retarded time series data of ping # 6

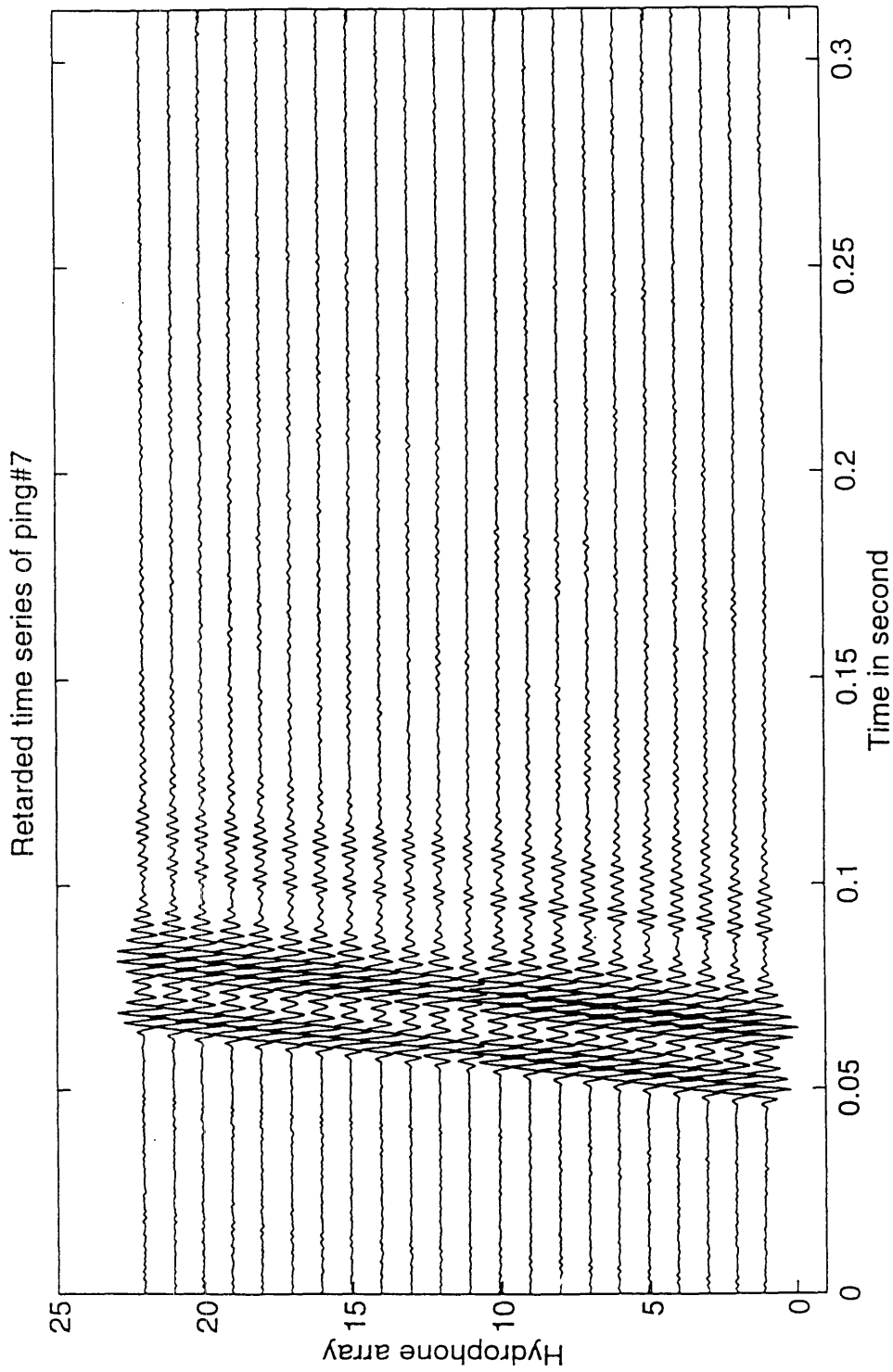


Figure 4.10. Retarded time series data of ping # 7

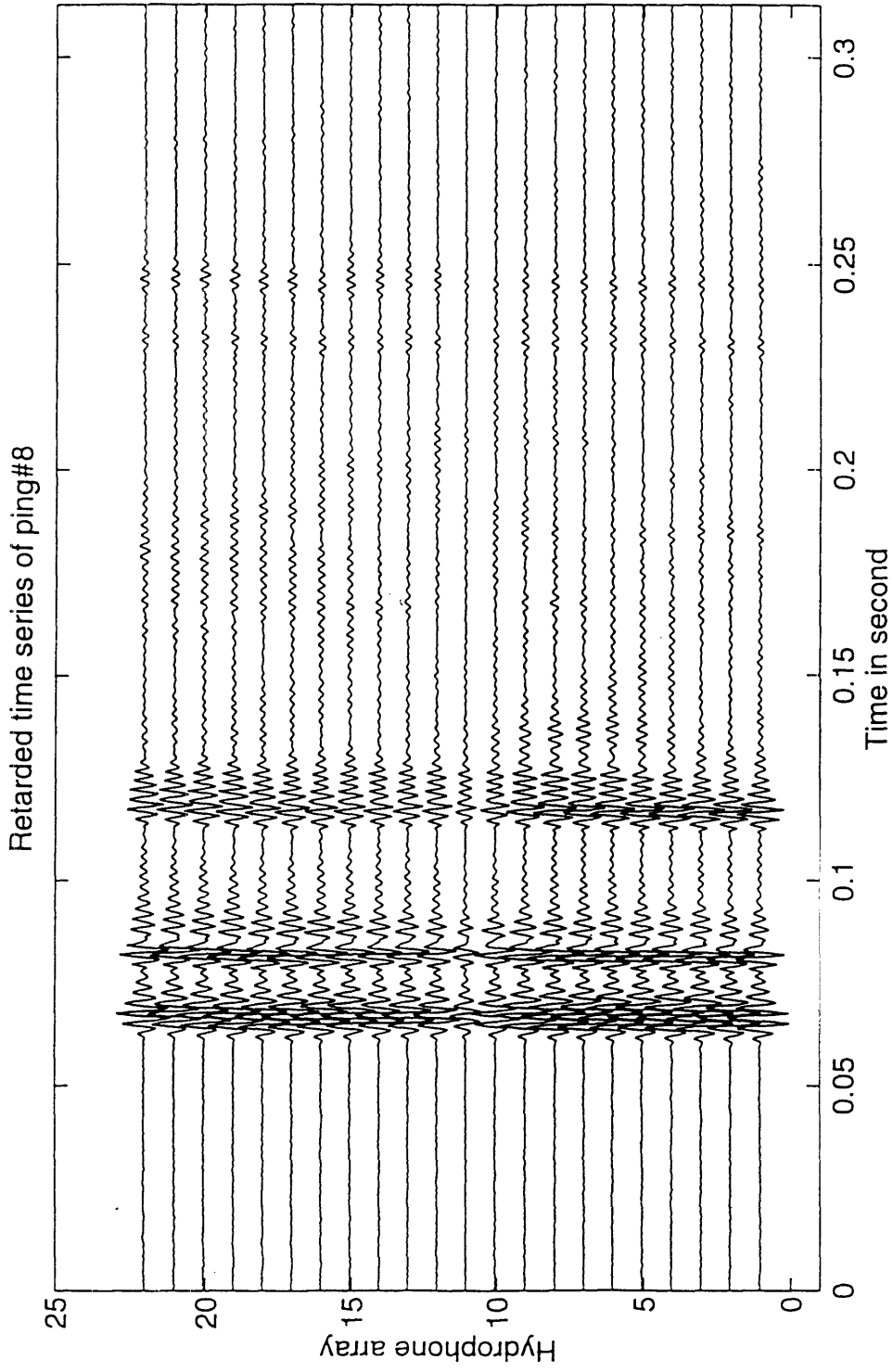


Figure 4.11. Retarded time series data of ping # 8

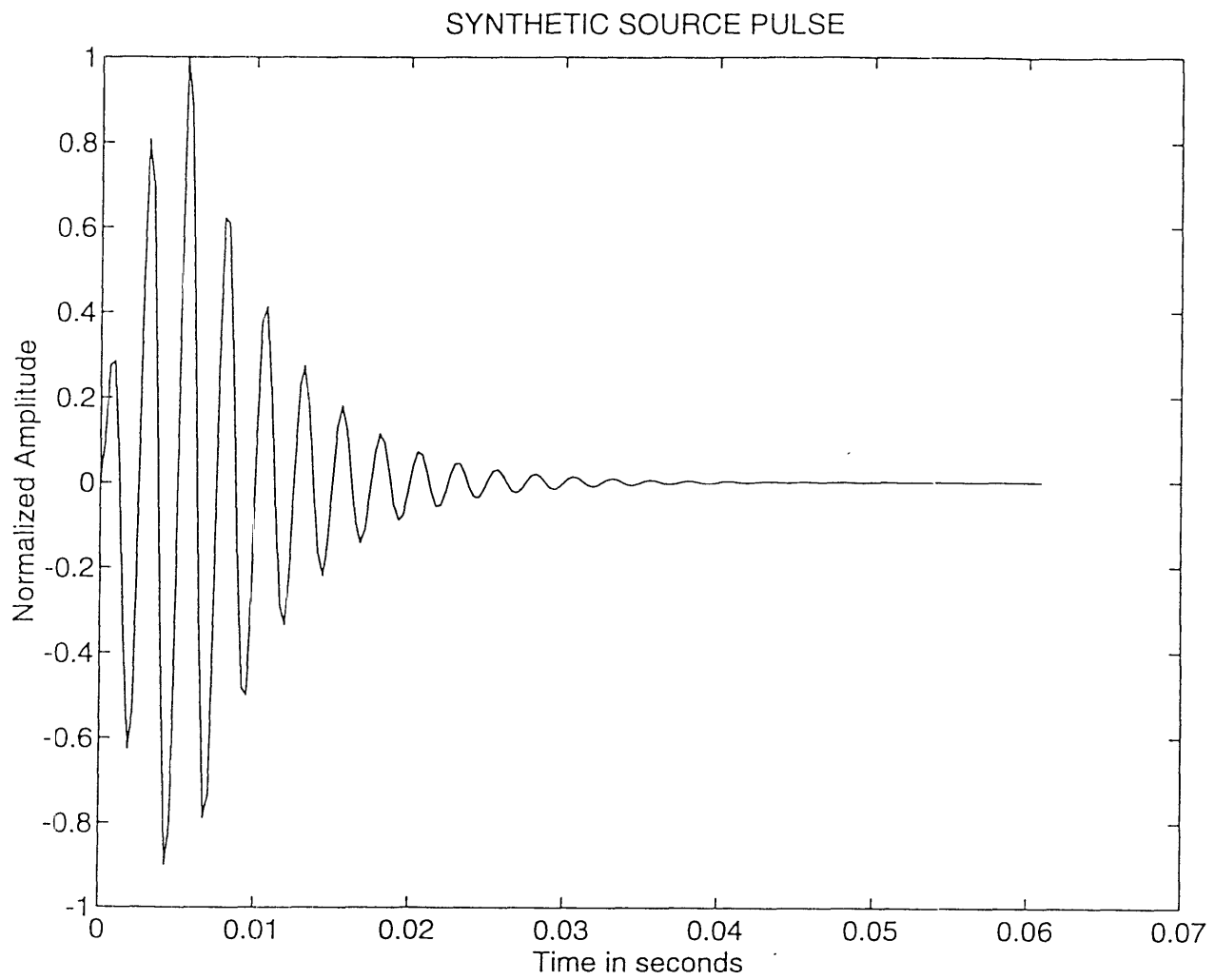


Figure 4.12. Synthetic source pulse

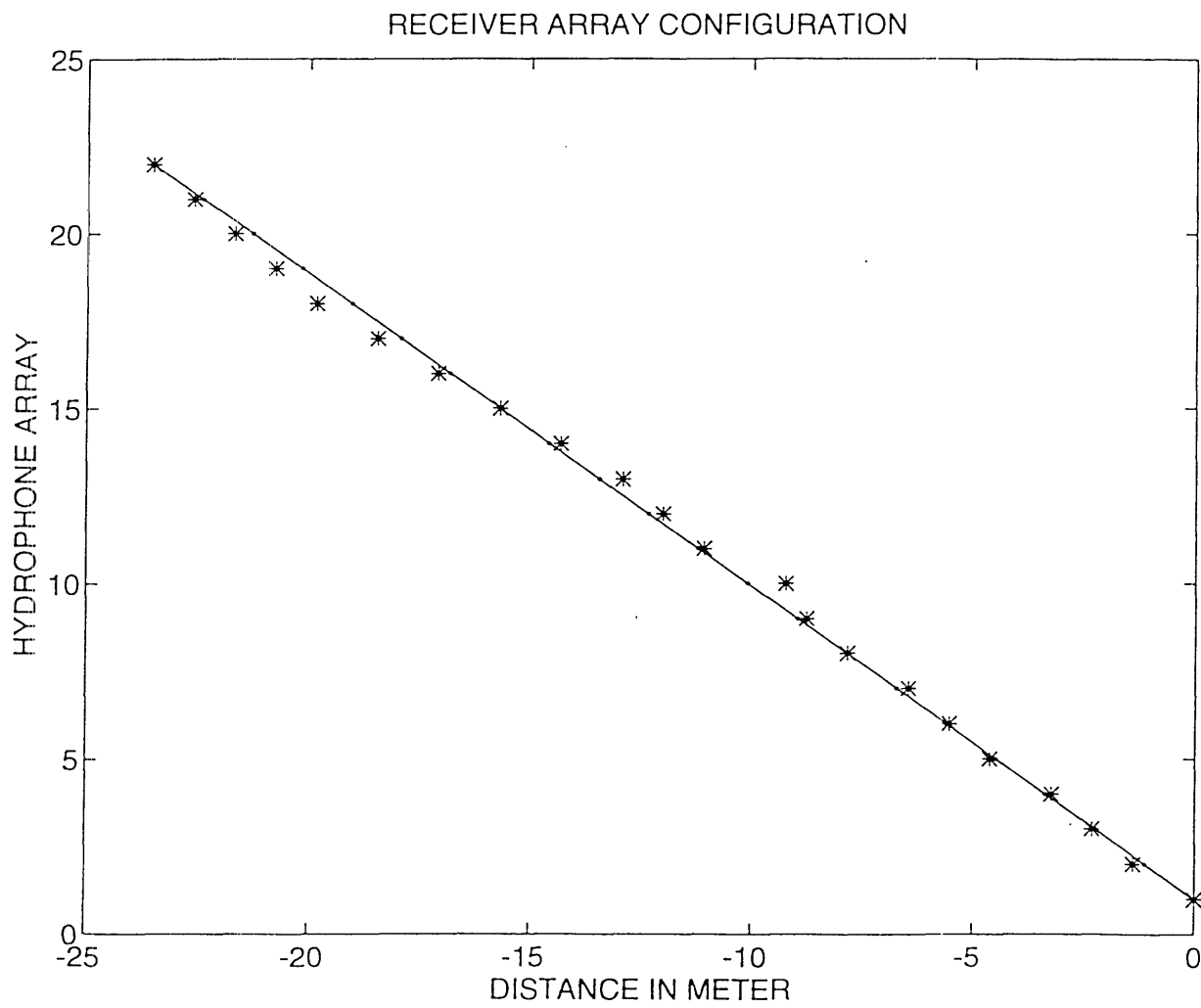


Figure 4.13. Receiver array configuration

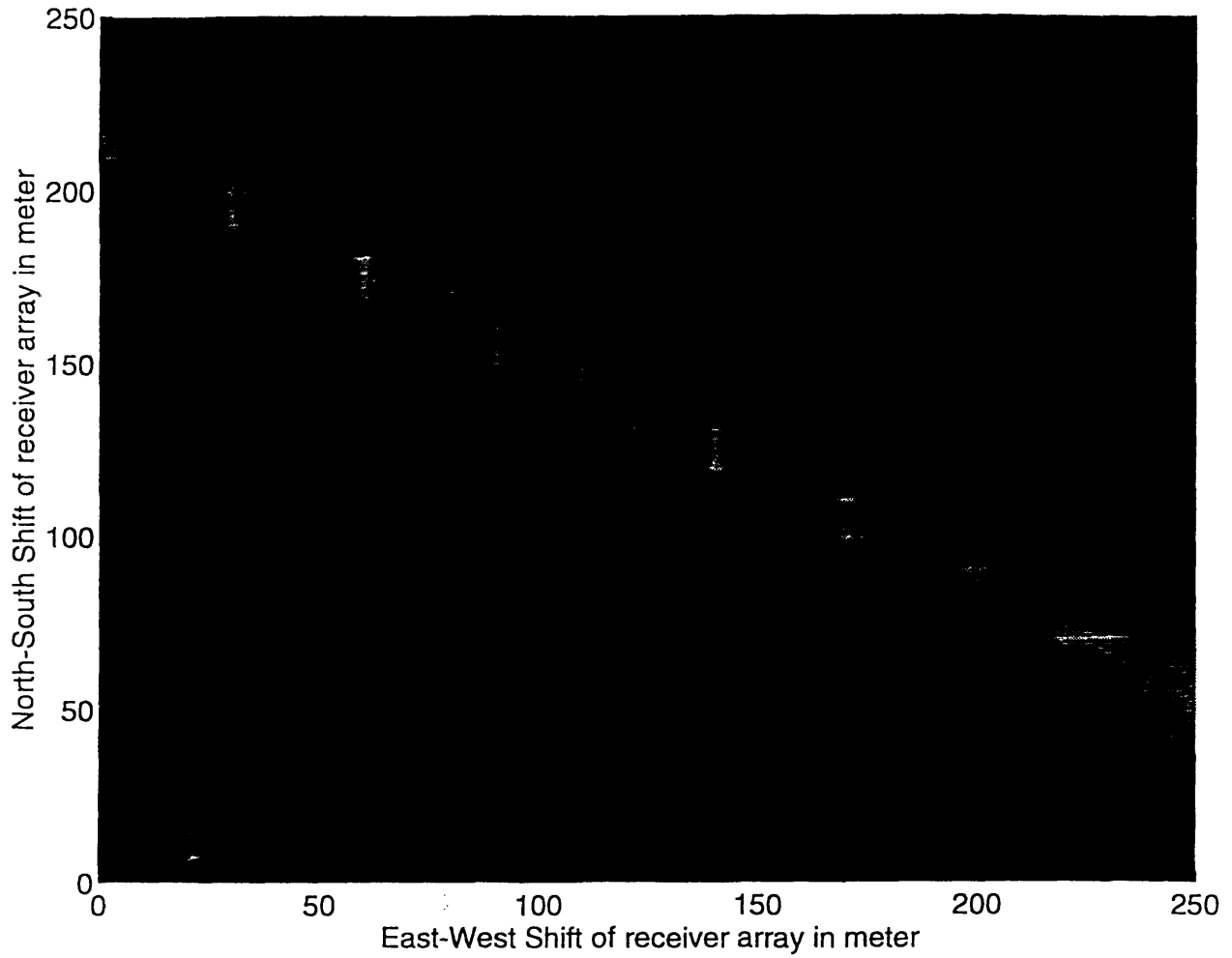


Figure 4.14. The χ^2 values as a function of North-South and East-West shift of receiver array position.

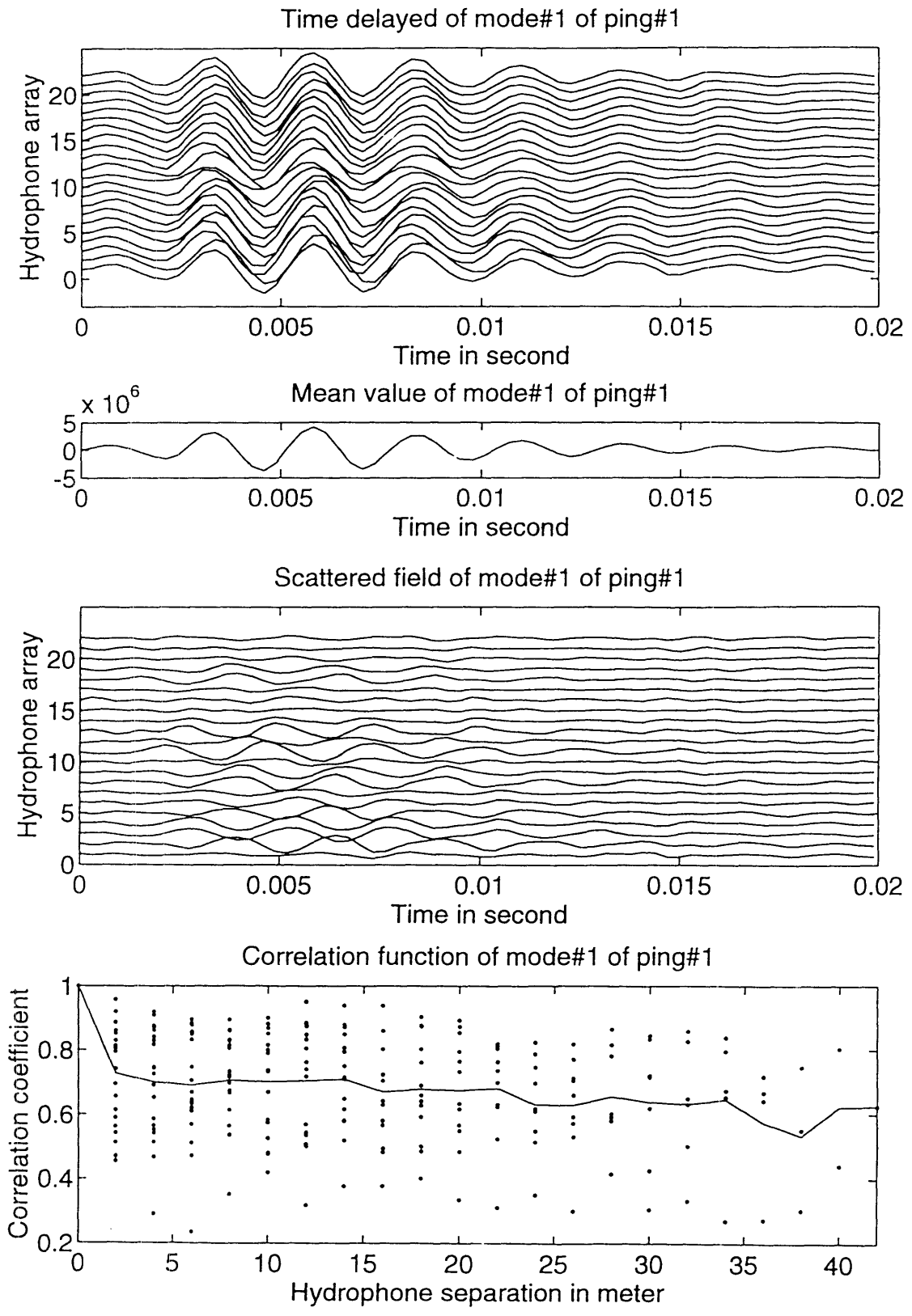


Figure 4.15. Total field, coherent field, scattered field and its correlation function of mode#1, ping#1

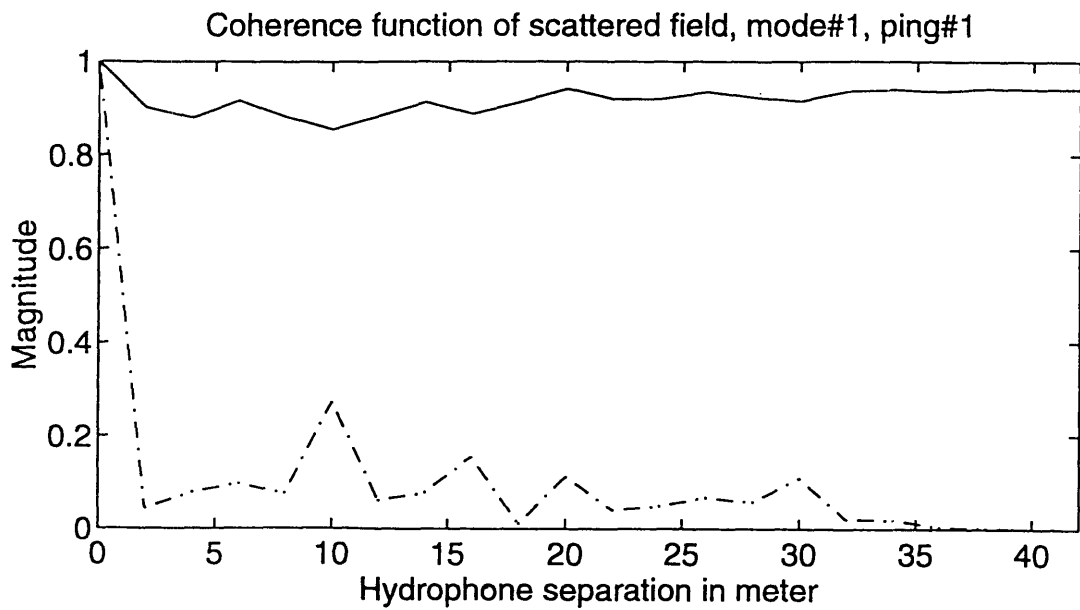
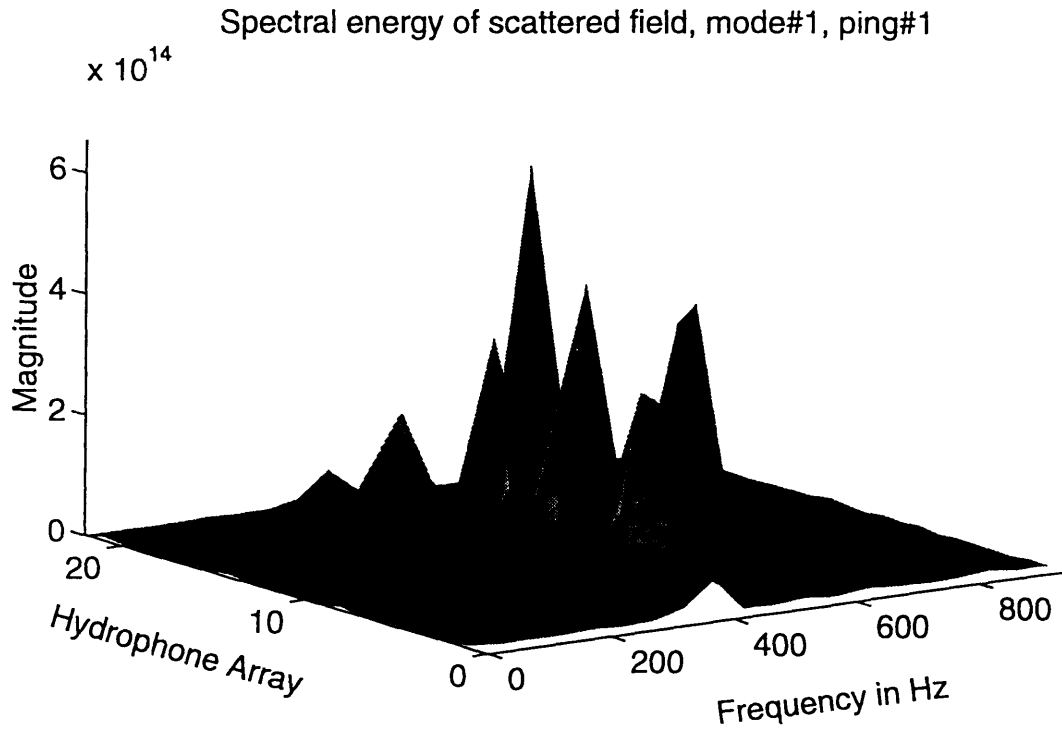


Figure 4.16a. Spectral energy of scattered field of mode#1, ping#1

Figure 4.16b. Coherence function of total field (solid) and scattered field (dash) of mode#1, ping#1

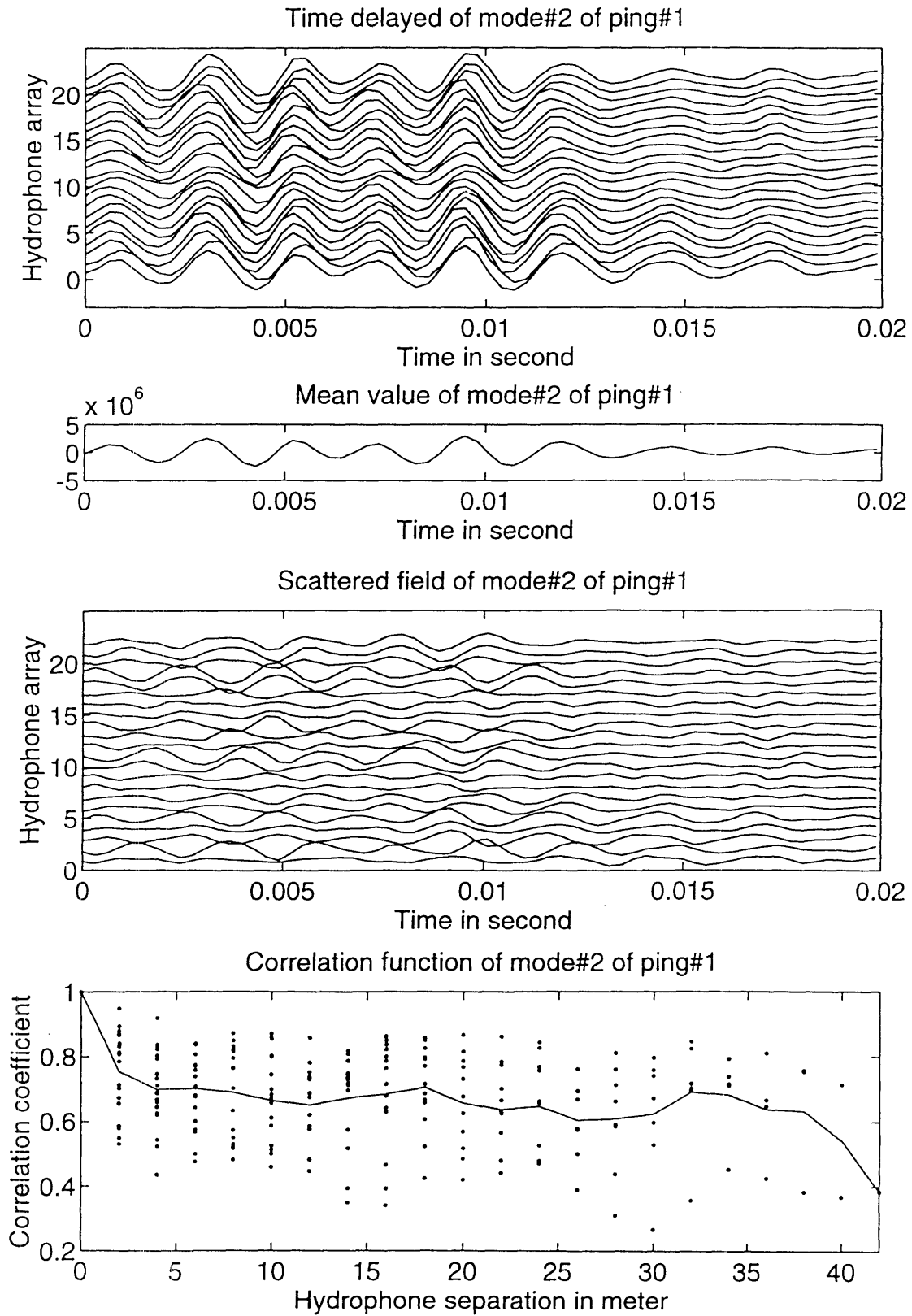


Figure 4.17. Total field, coherent field, scattered field and its correlation function of mode#2, ping#1

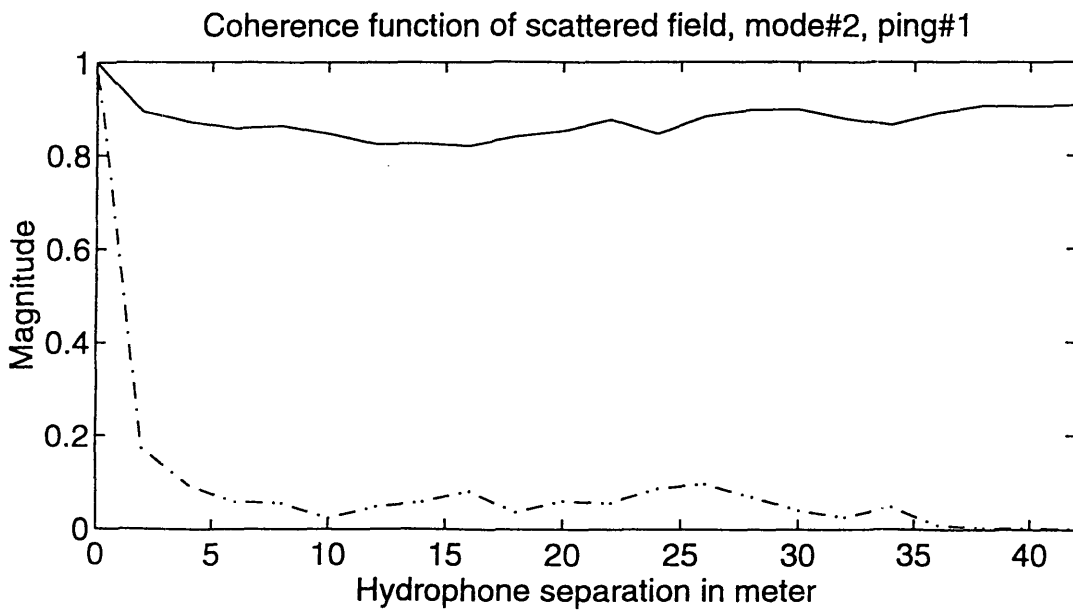
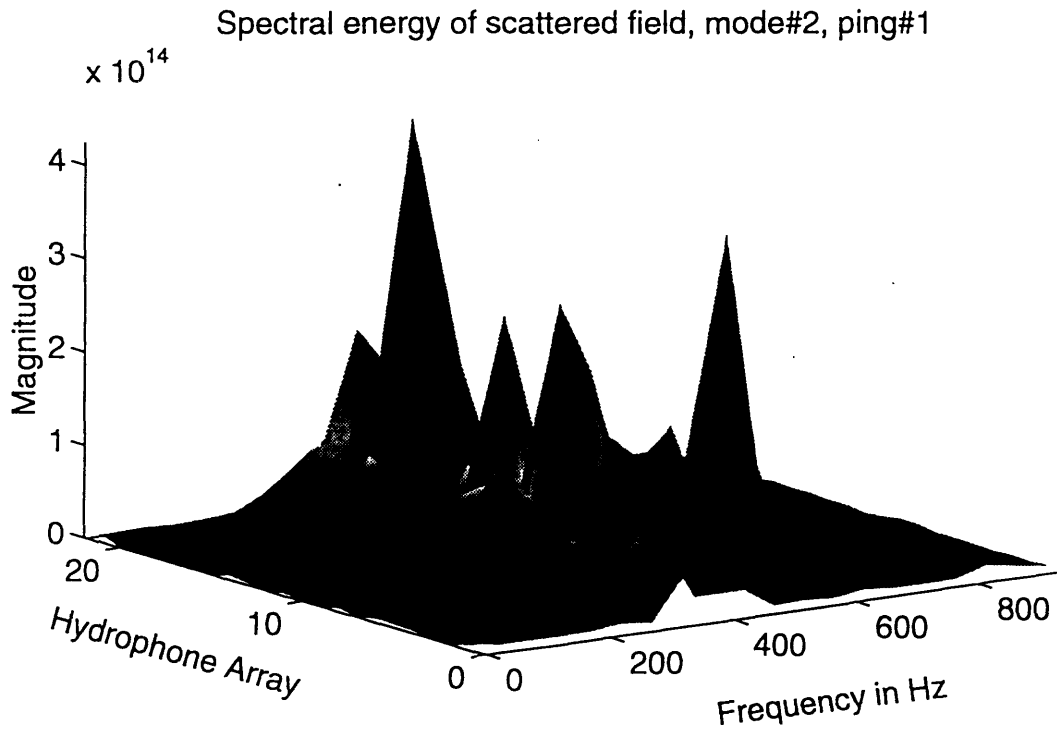


Figure 4.18a. Spectral energy of scattered field of mode#2, ping#1

Figure 4.18b. Coherence function of total field (solid) and scattered field (dash) of mode#2, ping#1

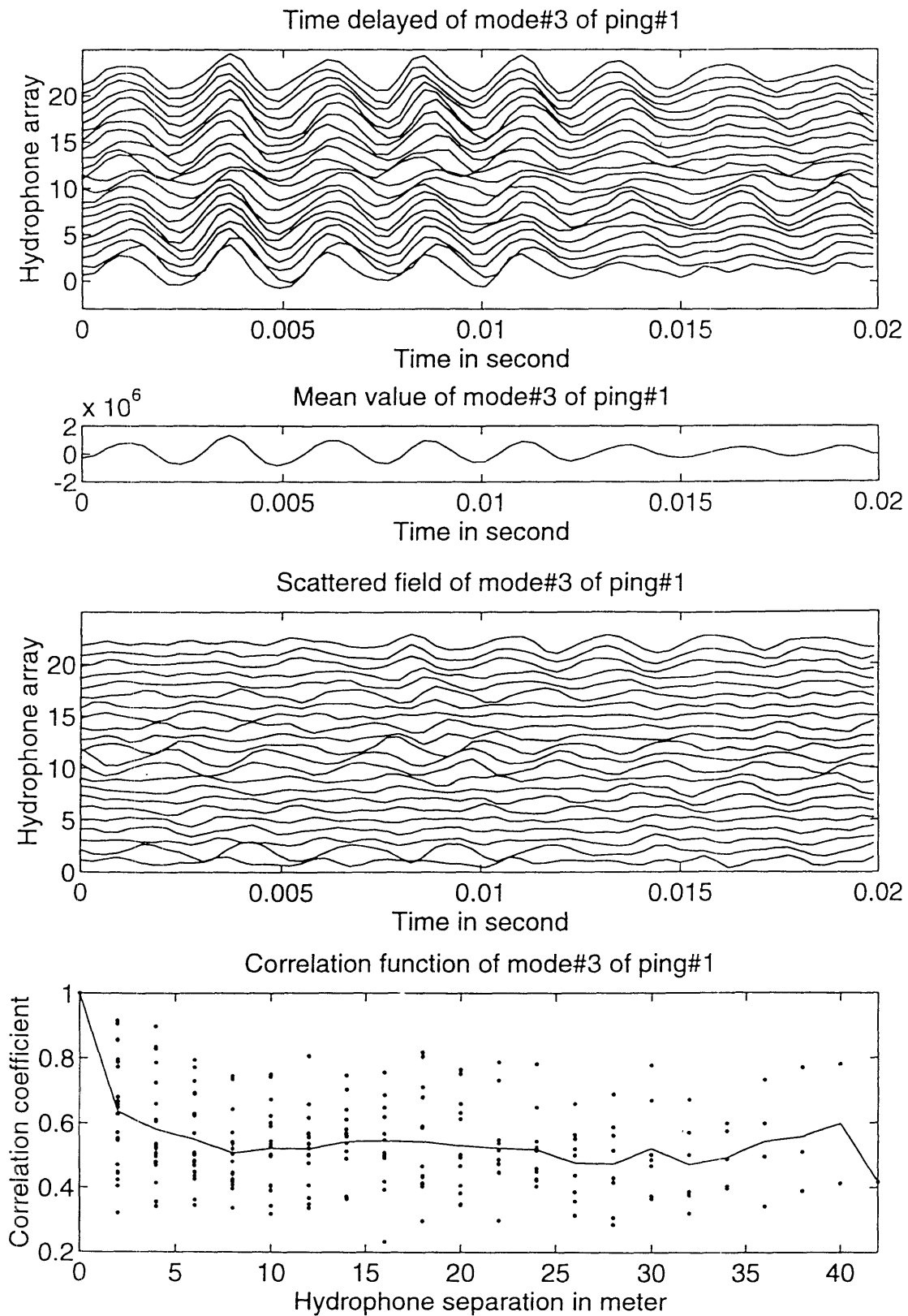


Figure 4.19. Total field, coherent field, scattered field and its correlation function of mode#3, ping#1

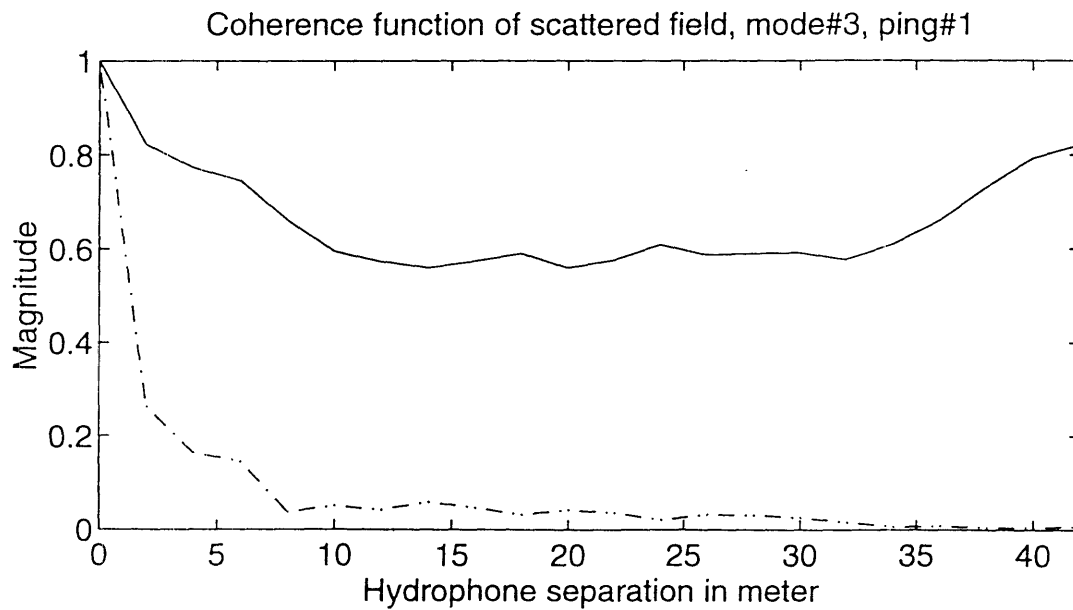
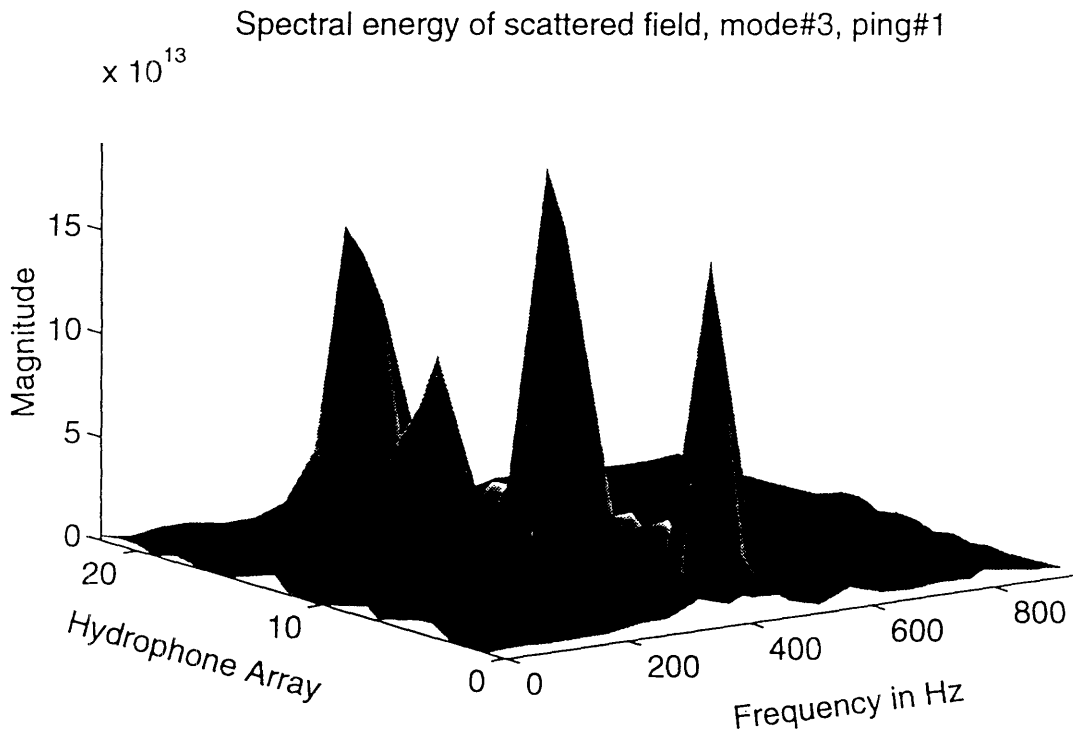


Figure 4.20a. Spectral energy of scattered field of mode#3, ping#1

Figure 4.20b. Coherence function of total field (solid) and scattered field (dash) of mode#3, ping#1

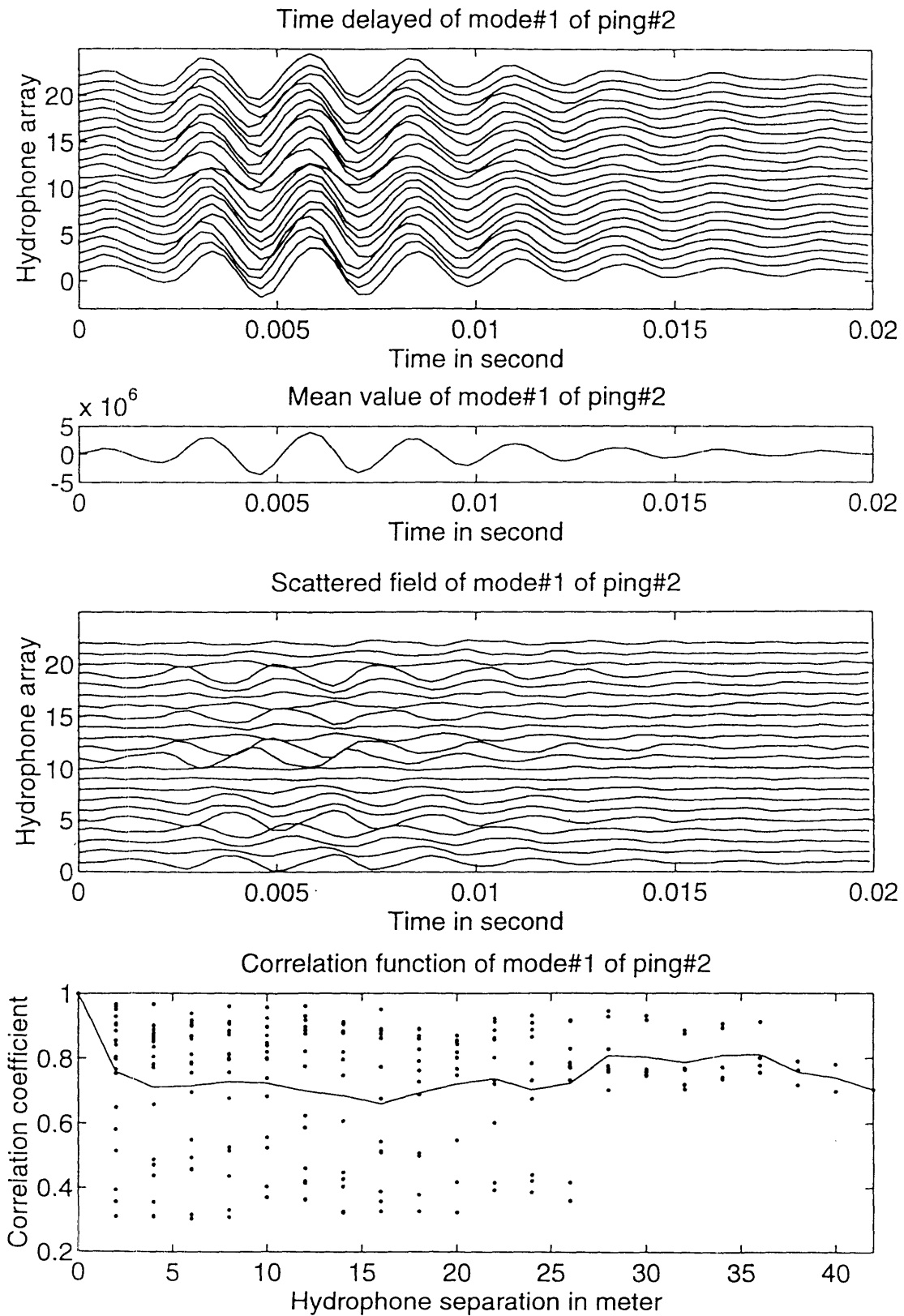


Figure 4.21. Total field, coherent field, scattered field and its correlation function of mode#1, ping#2

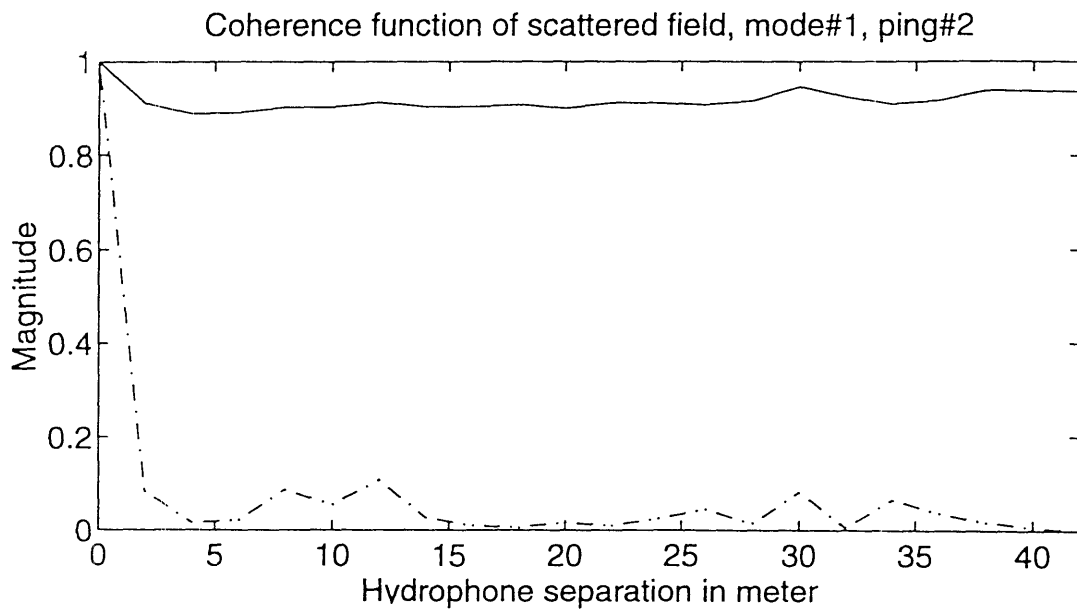
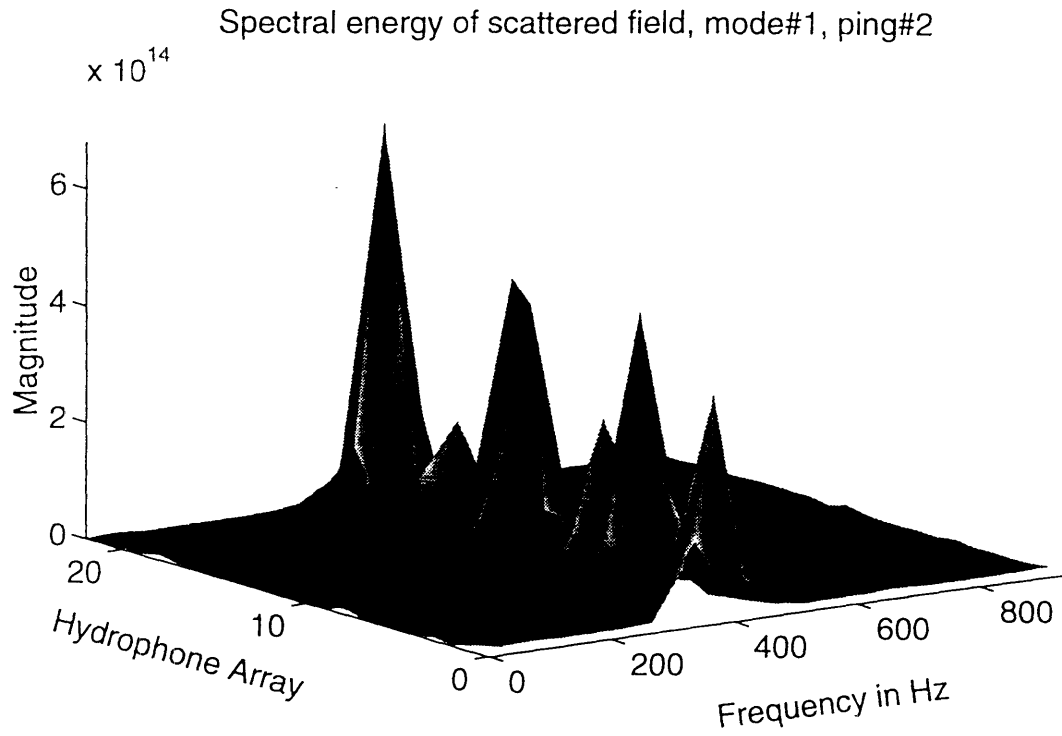


Figure 4.22a. Spectral energy of scattered field of mode#1, ping#2

Figure 4.22b. Coherence function of total field (solid) and scattered field (dash) of mode#1, ping#2

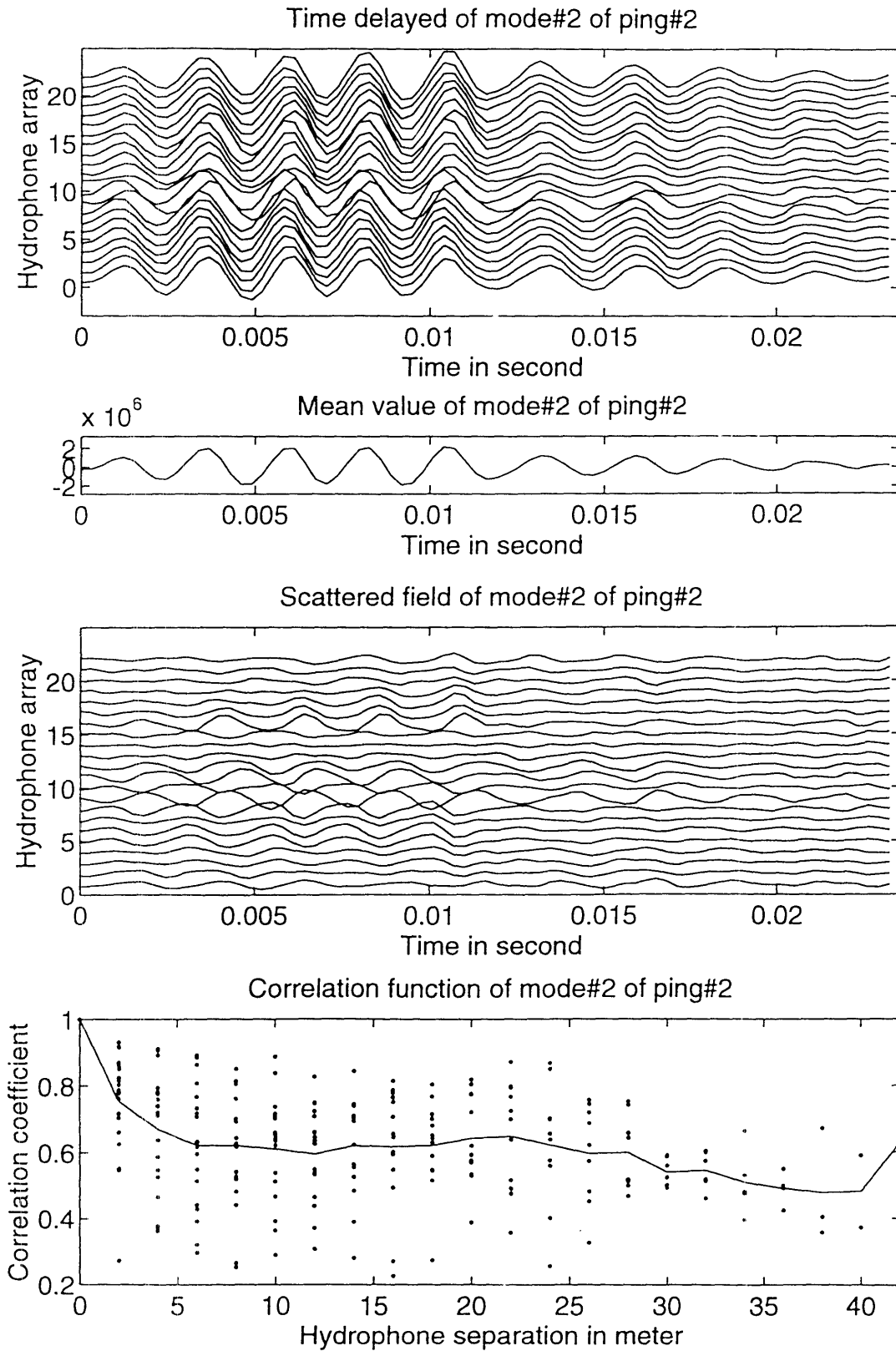


Figure 4.23. Total field, coherent field, scattered field and its correlation function of mode#2, ping#2

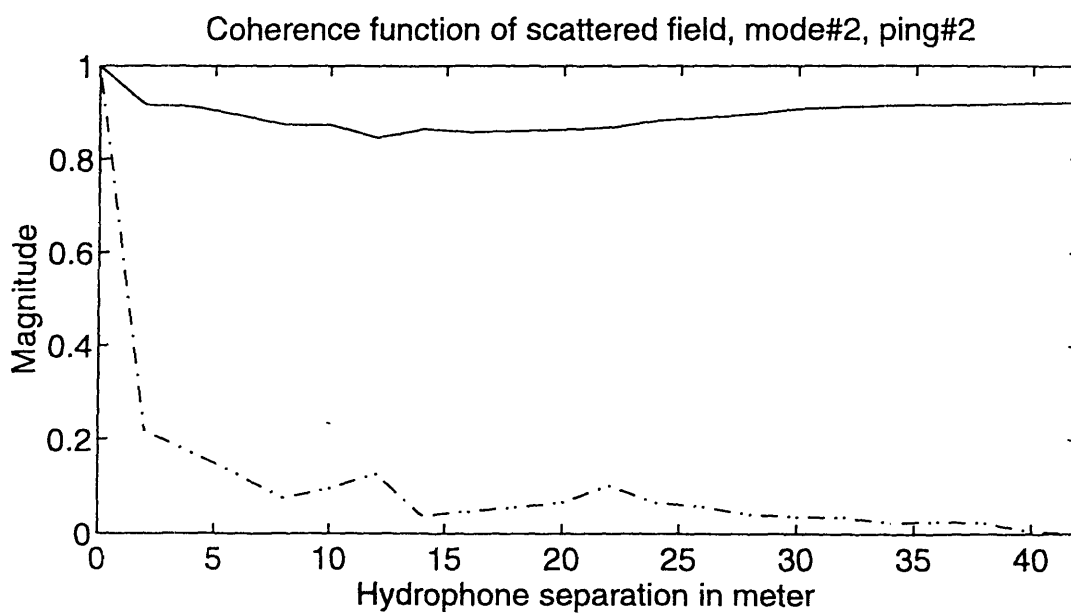
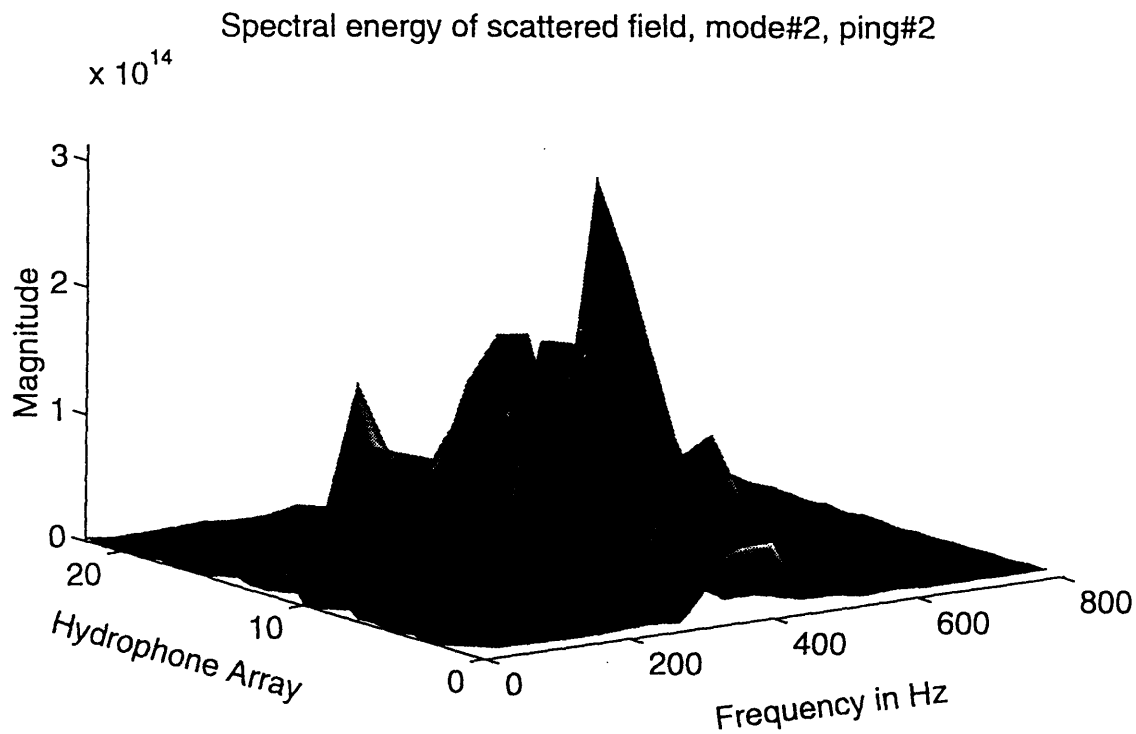


Figure 4.24a. Spectral energy of scattered field of mode#2, ping#2

Figure 4.24b. Coherence function of total field (solid) and scattered field (dash) of mode#2, ping#2

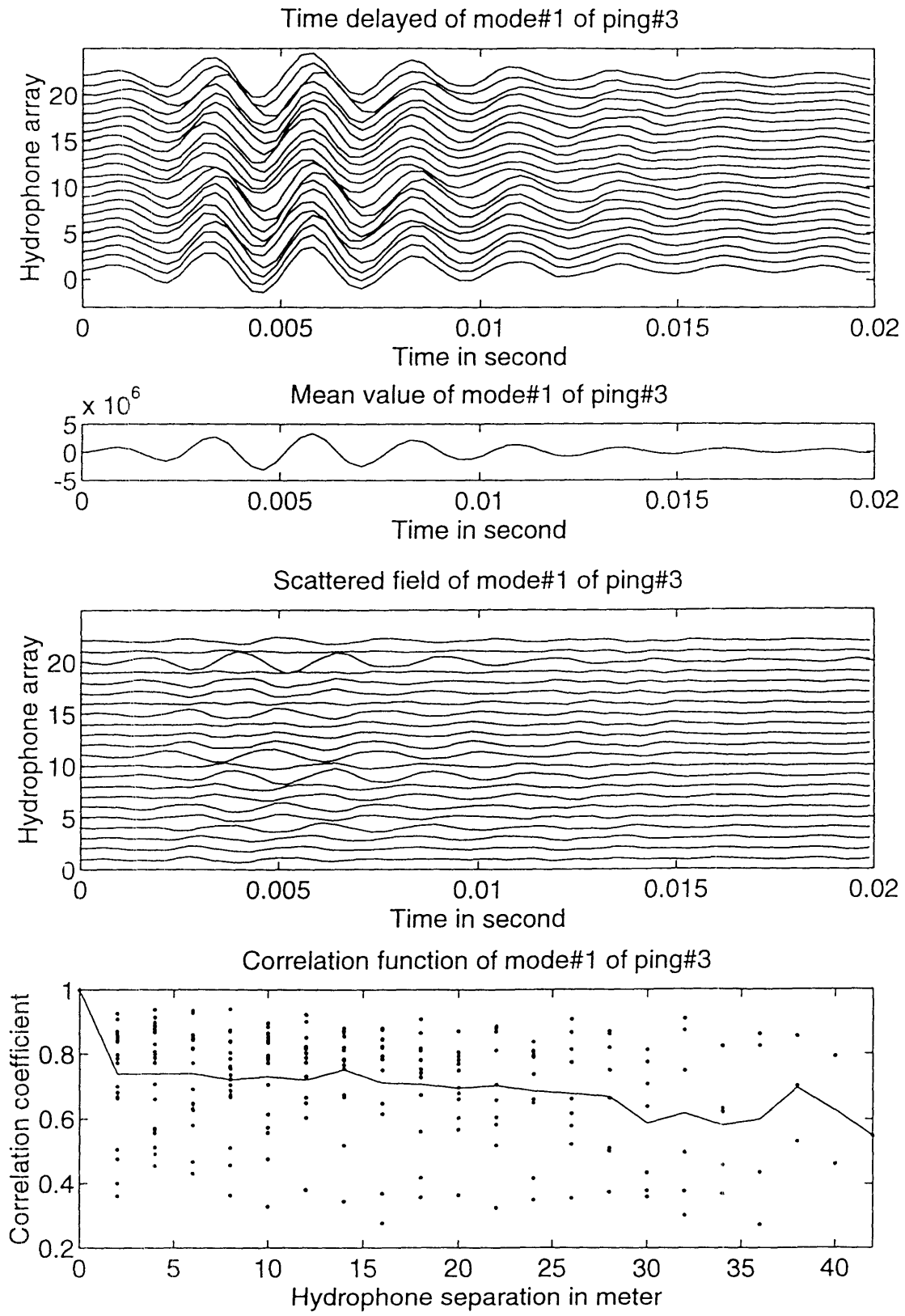


Figure 4.25. Total field, coherent field, scattered field and its correlation function of mode#1, ping#3

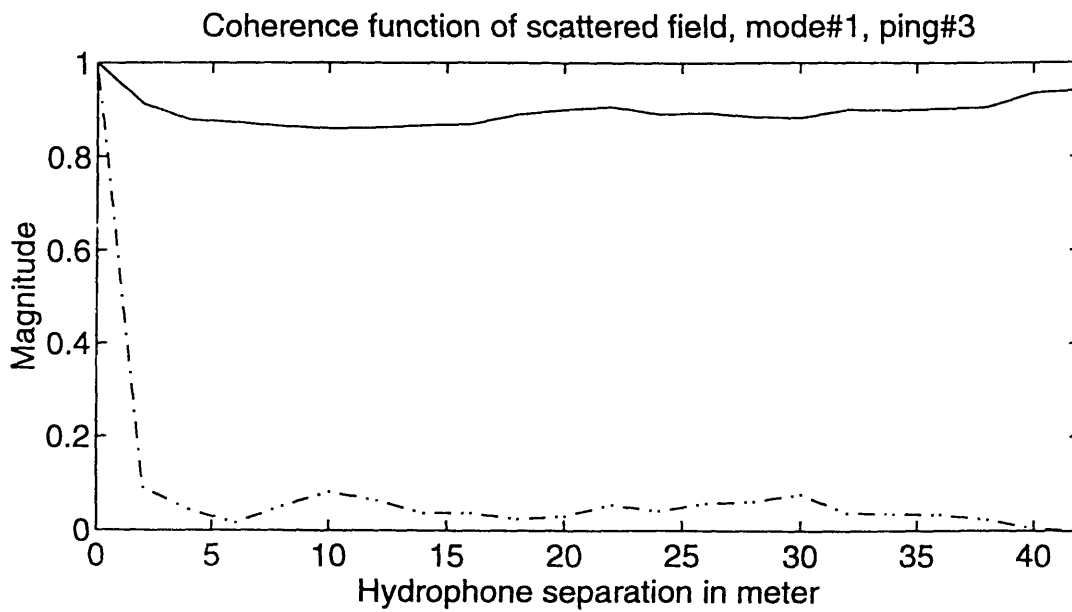
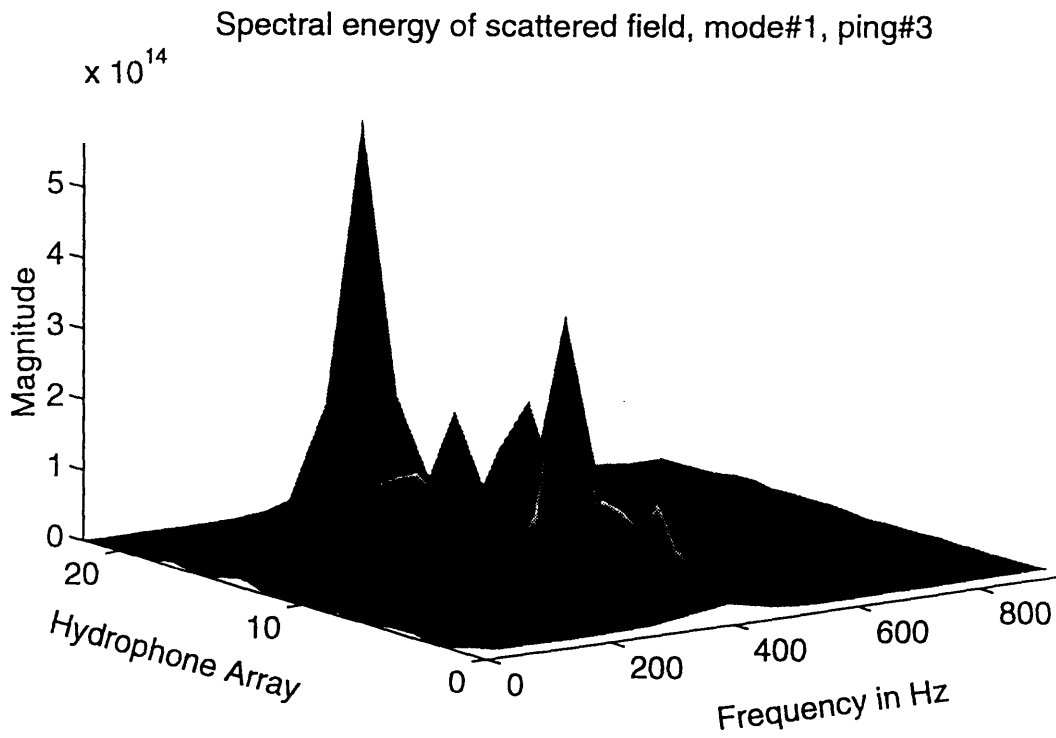


Figure 4.26a. Spectral energy of scattered field of mode#1, ping#3

Figure 4.26b. Coherence function of total field (solid) and scattered field (dash) of mode#1, ping#3

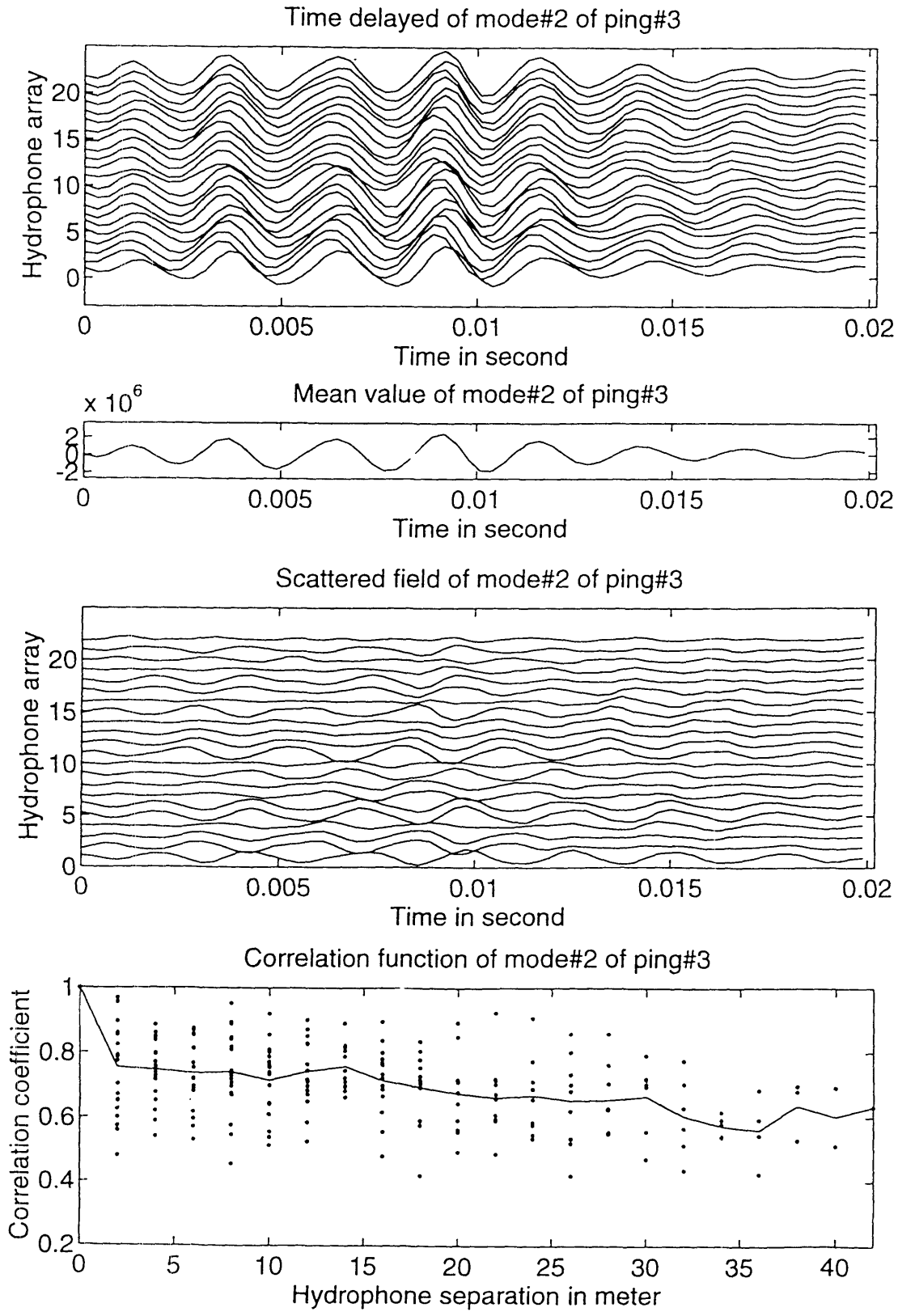


Figure 4.27. Total field, coherent field, scattered field and its correlation function of mode#2, ping#3

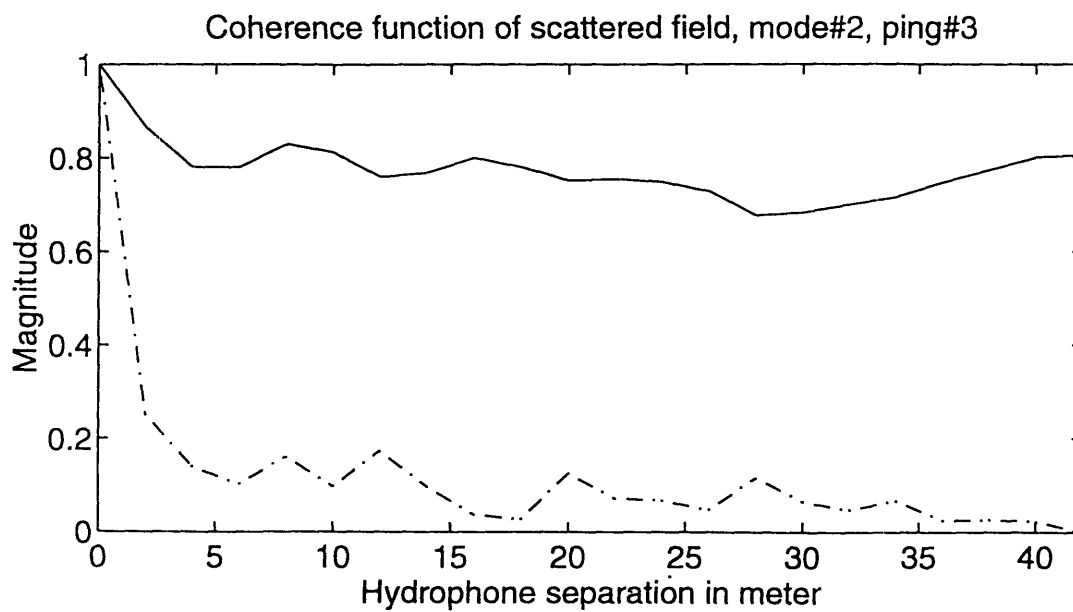
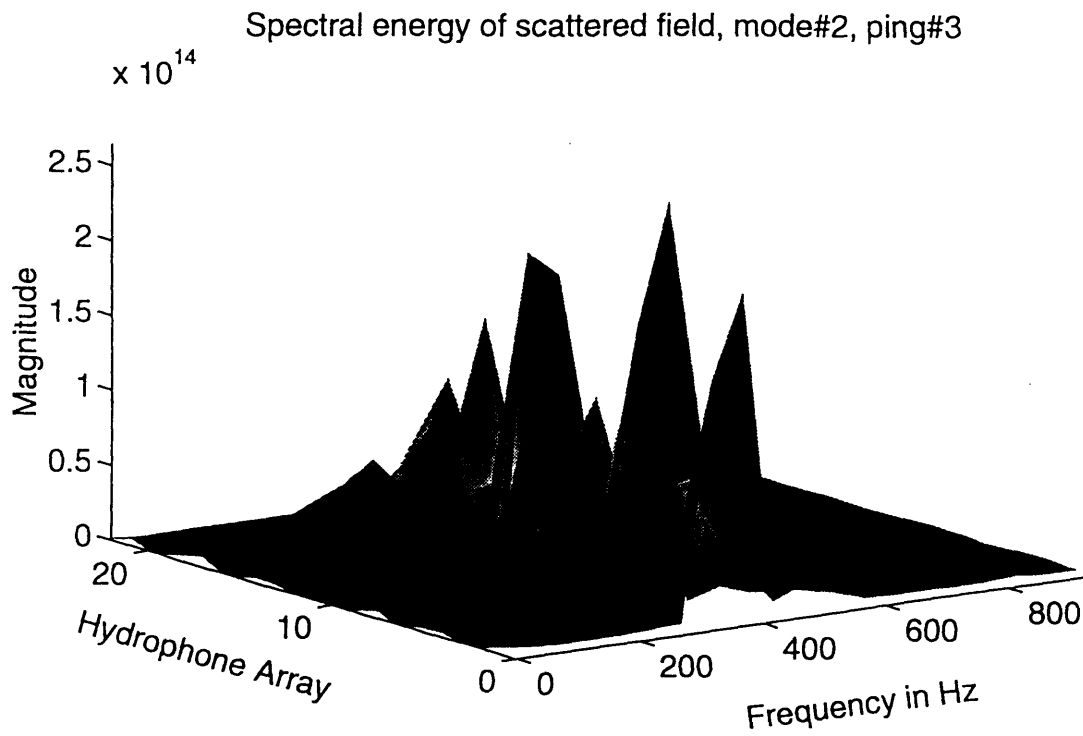


Figure 4.28a. Spectral energy of scattered field of mode#2, ping#3

Figure 4.28b. Coherence function of total field (solid) and scattered field (dash) of mode#2, ping#3

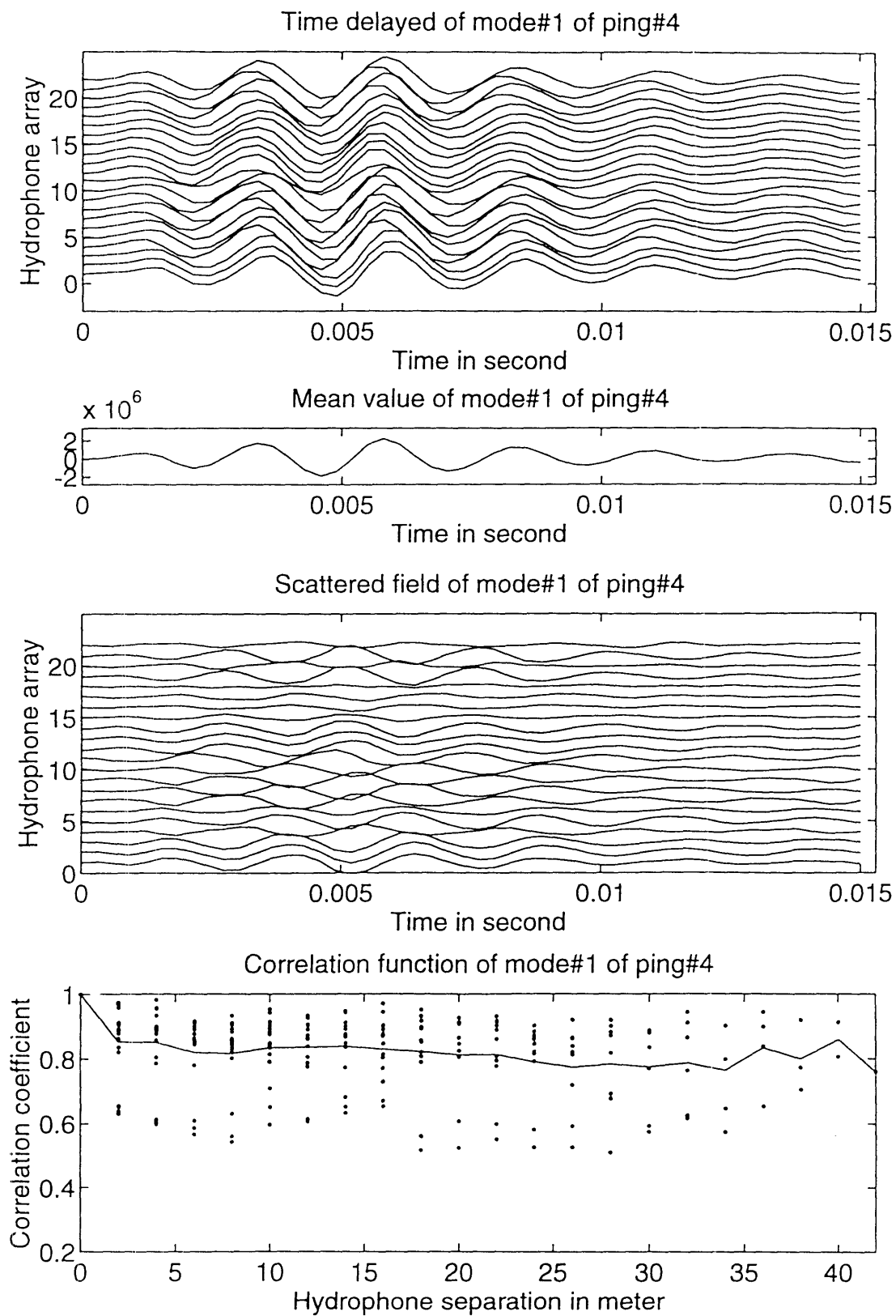


Figure 4.29. Total field, coherent field, scattered field and its correlation function of mode#1, ping#4

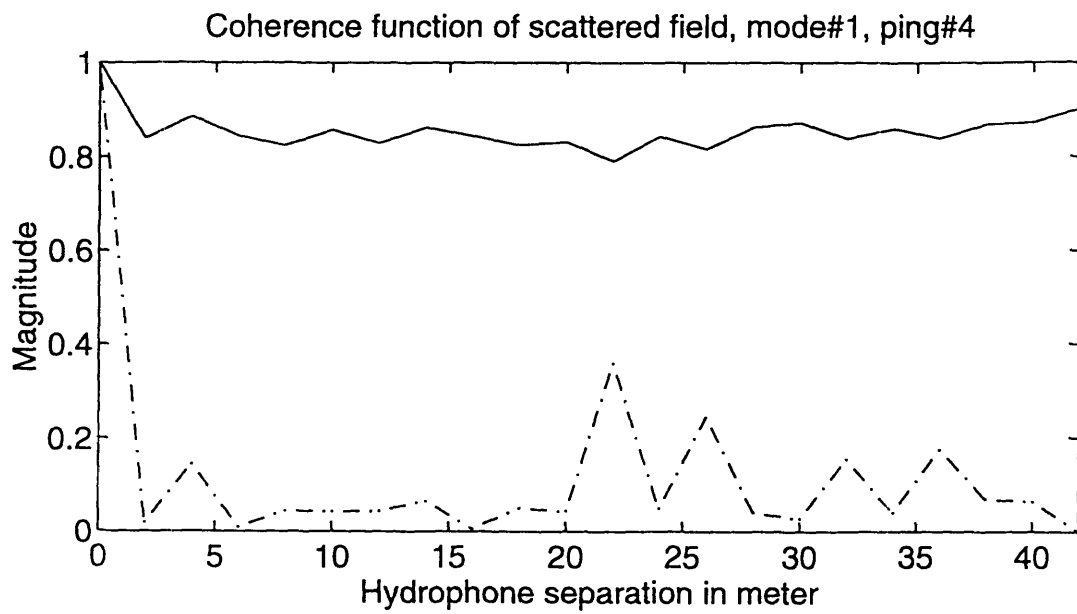
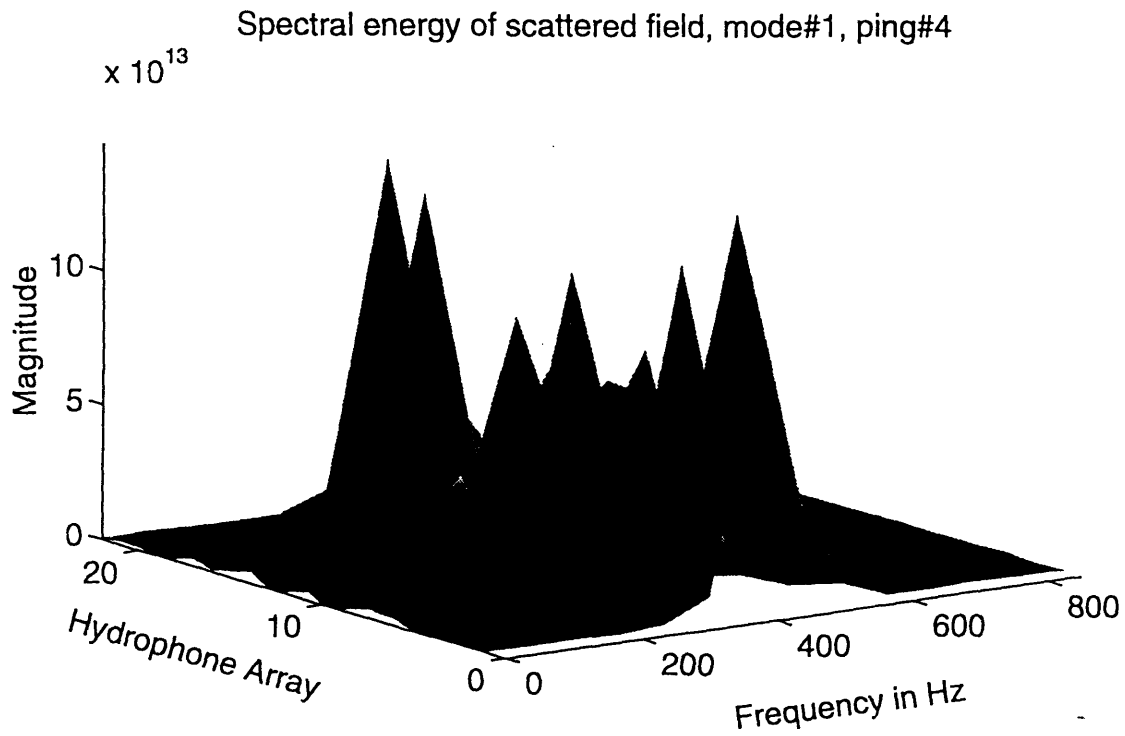


Figure 4.30a. Spectral energy of scattered field of mode#1, ping#4

Figure 4.30b. Coherence function of total field (solid) and scattered field (dash) of mode#1, ping#4

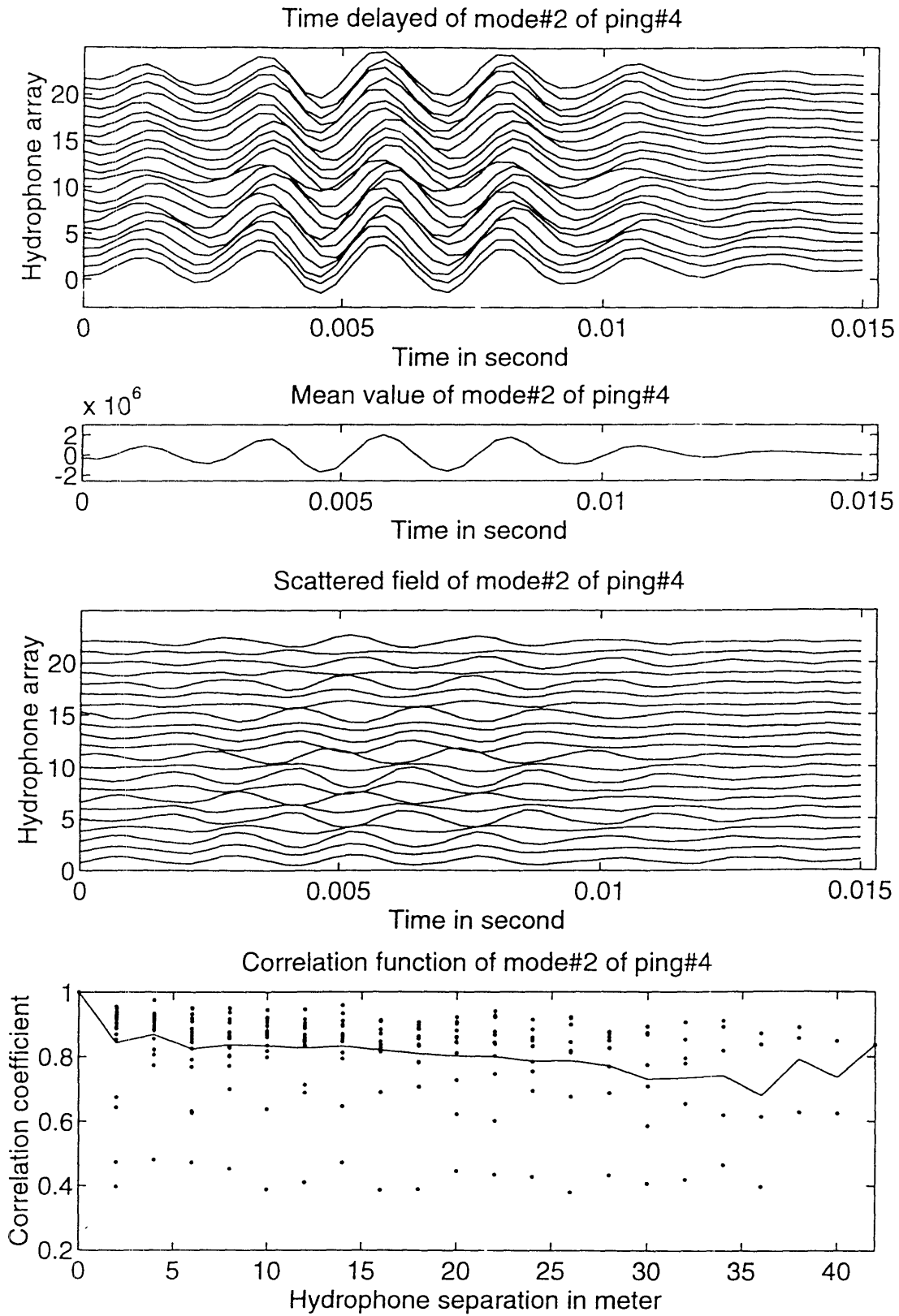


Figure 4.31. Total field, coherent field, scattered field and its correlation function of mode#2, ping#4

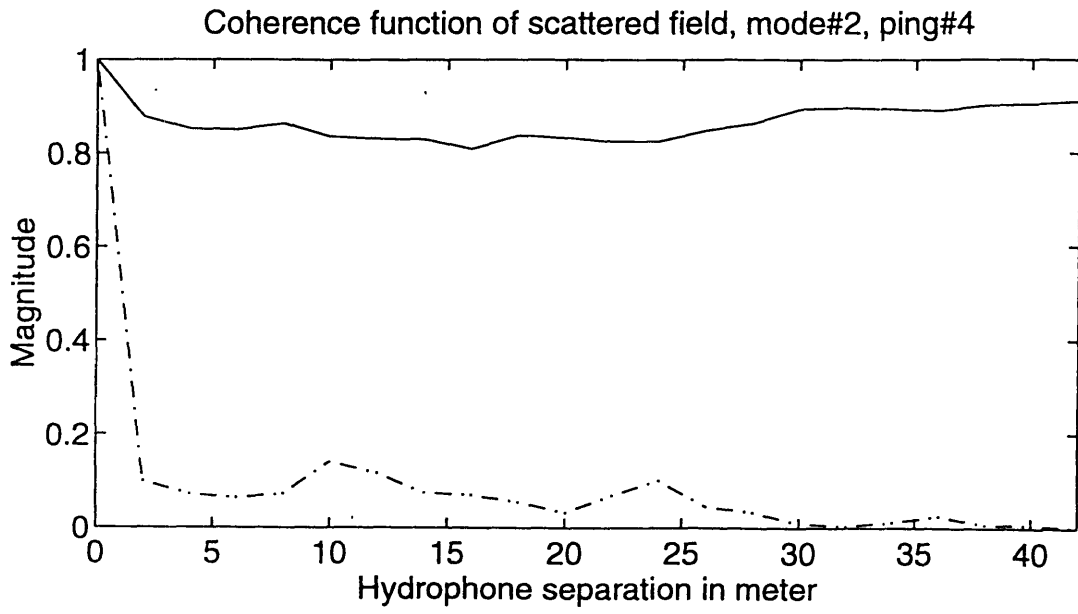
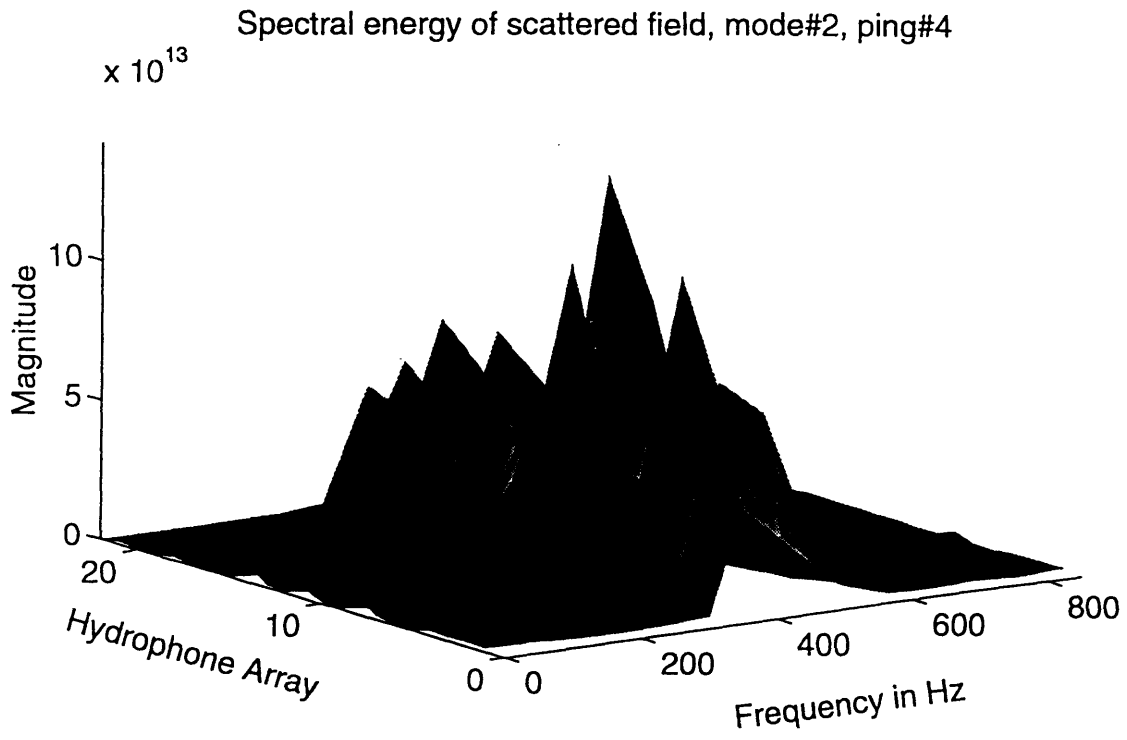


Figure 4.32a. Spectral energy of scattered field of mode#2, ping#4

Figure 4.32b. Coherence function of total field (solid) and scattered field (dash) of mode#2, ping#4

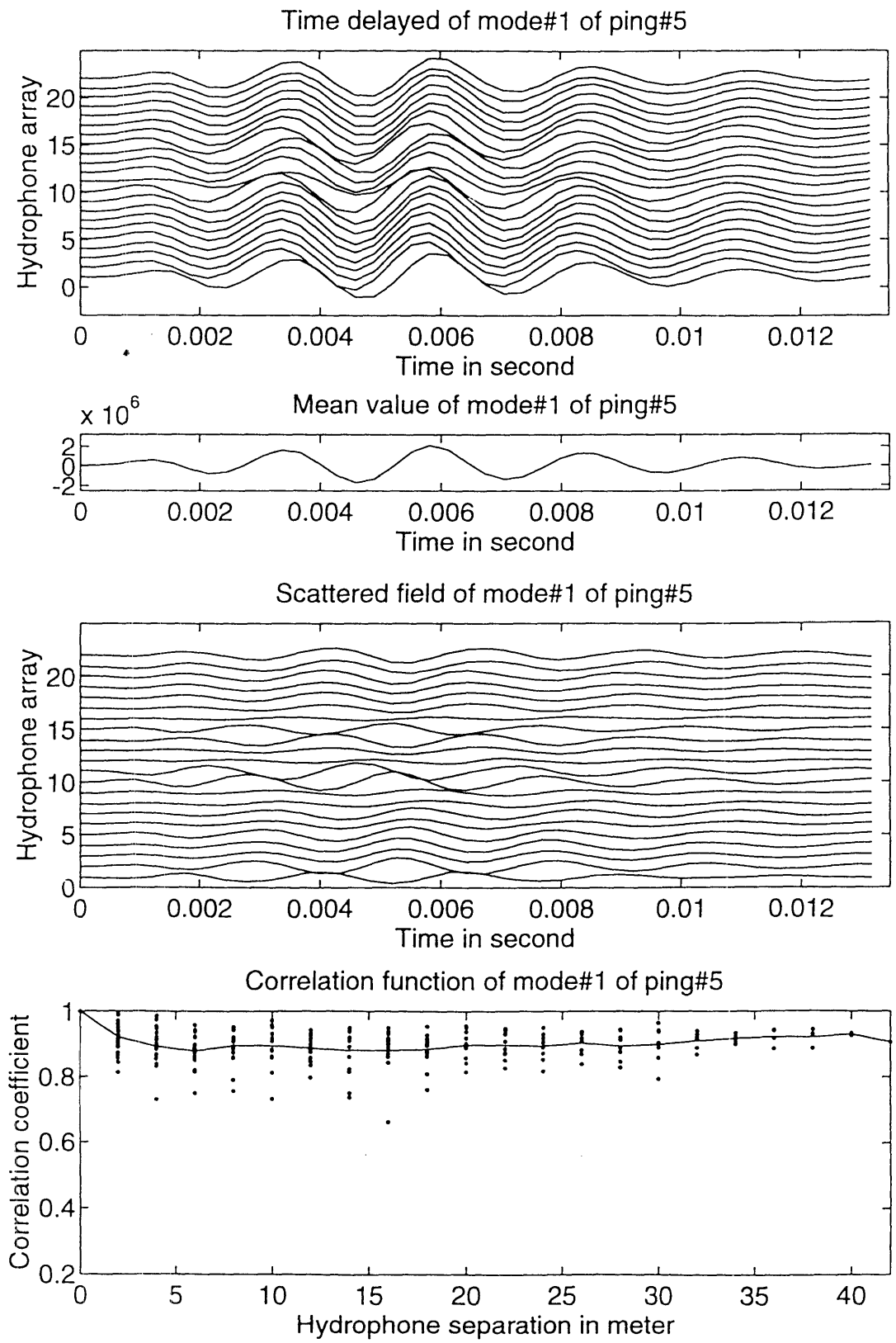


Figure 4.33. Total field, coherent field, scattered field and its correlation function of mode#1, ping#5

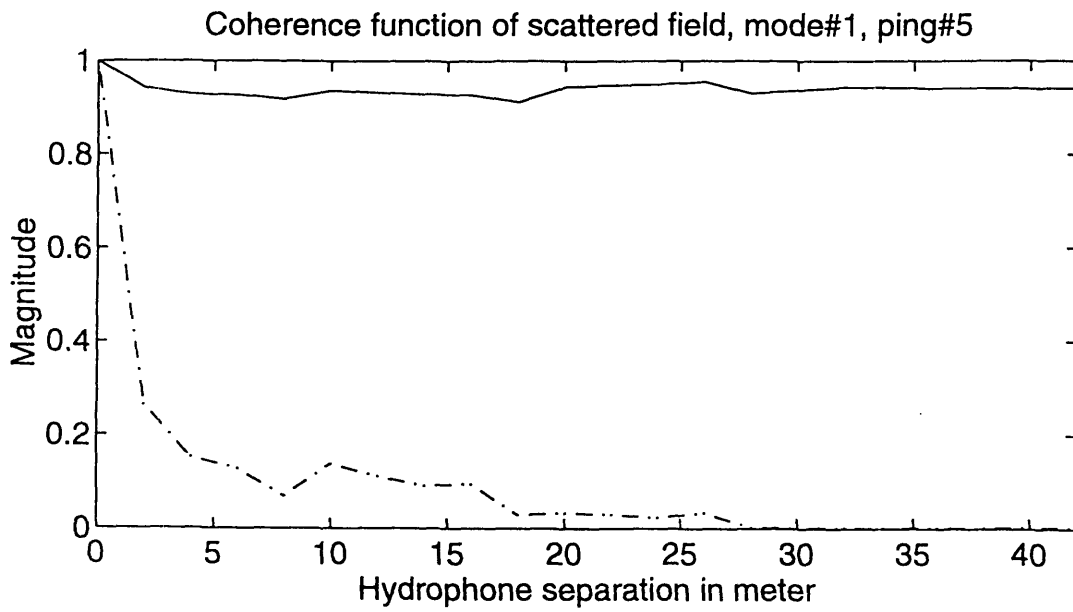
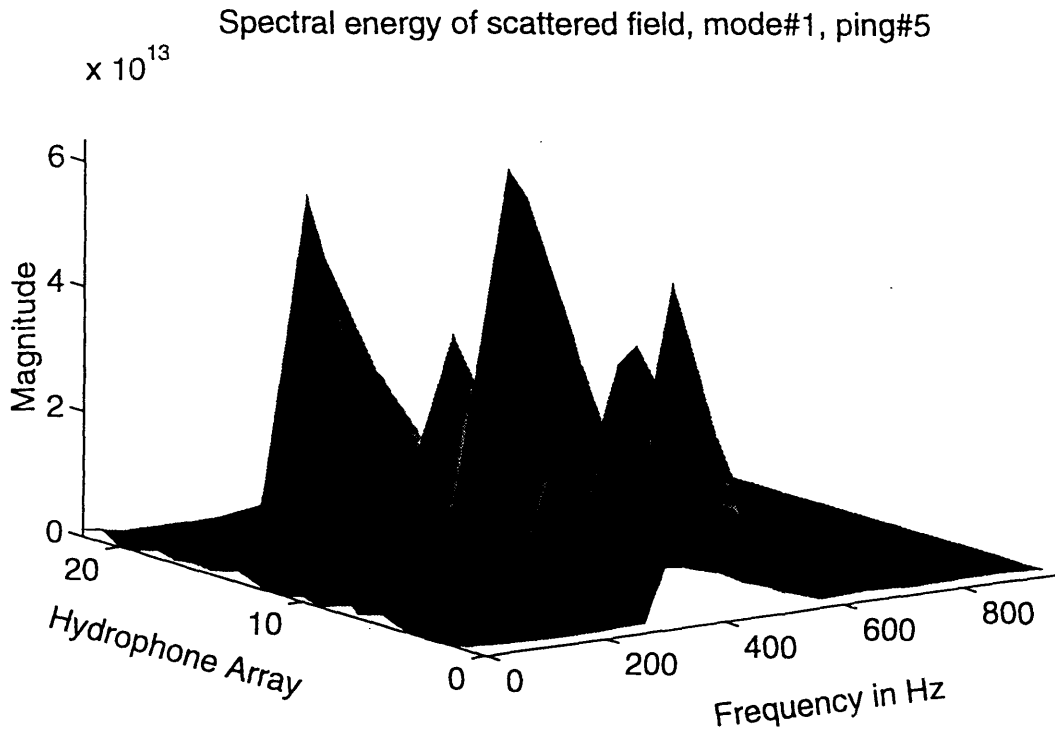


Figure 4.34a. Spectral energy of scattered field of mode#1, ping#5

Figure 4.34b. Coherence function of total field (solid) and scattered field (dash) of mode#1, ping#5

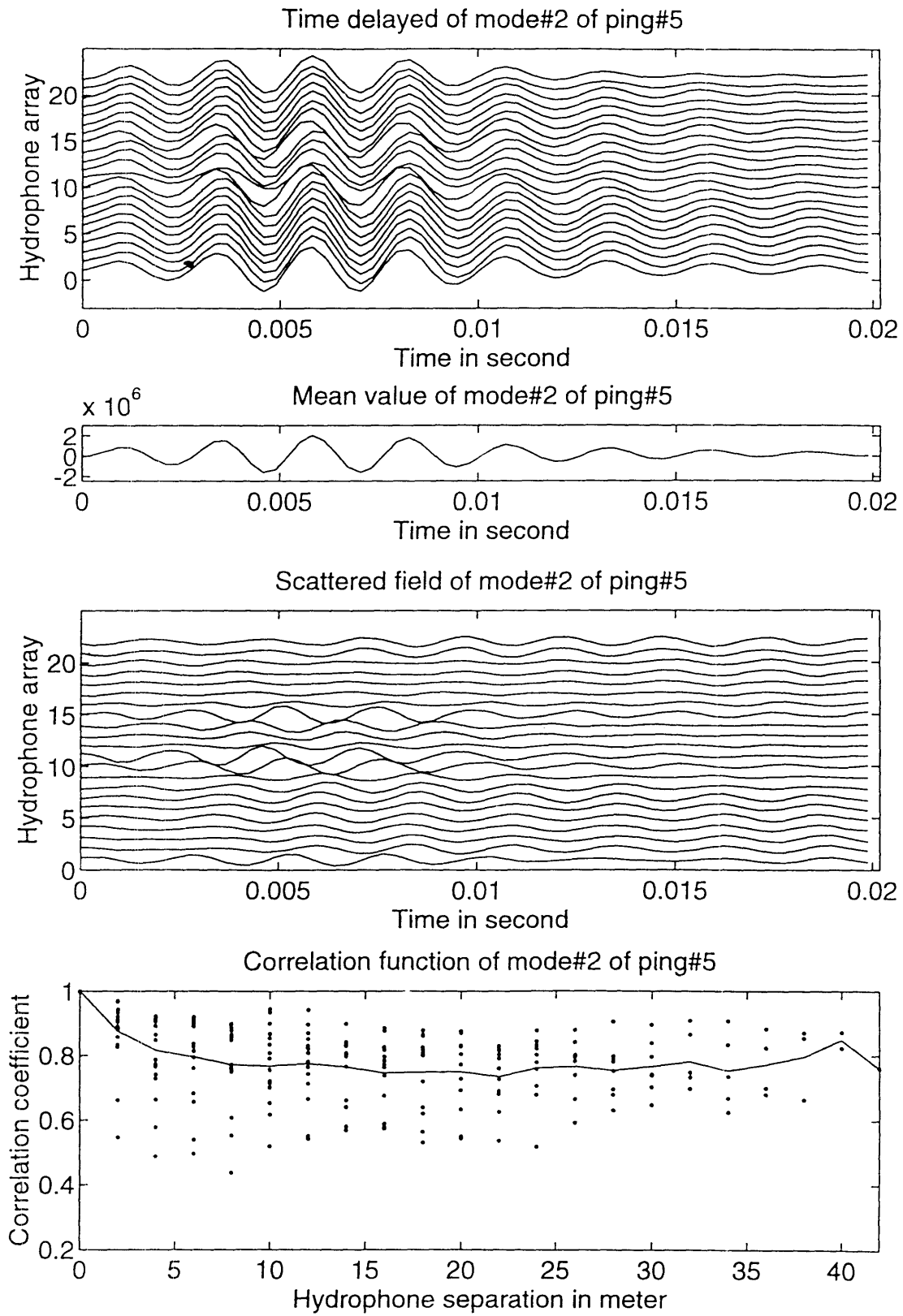


Figure 4.35. Total field, coherent field, scattered field and its correlation function of mode#2, ping#5

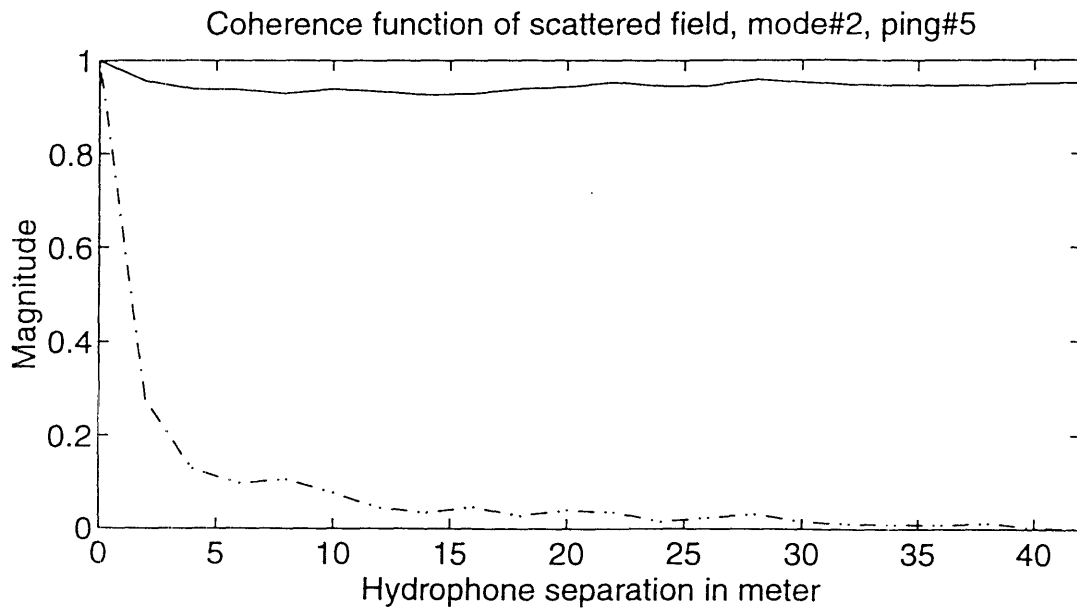
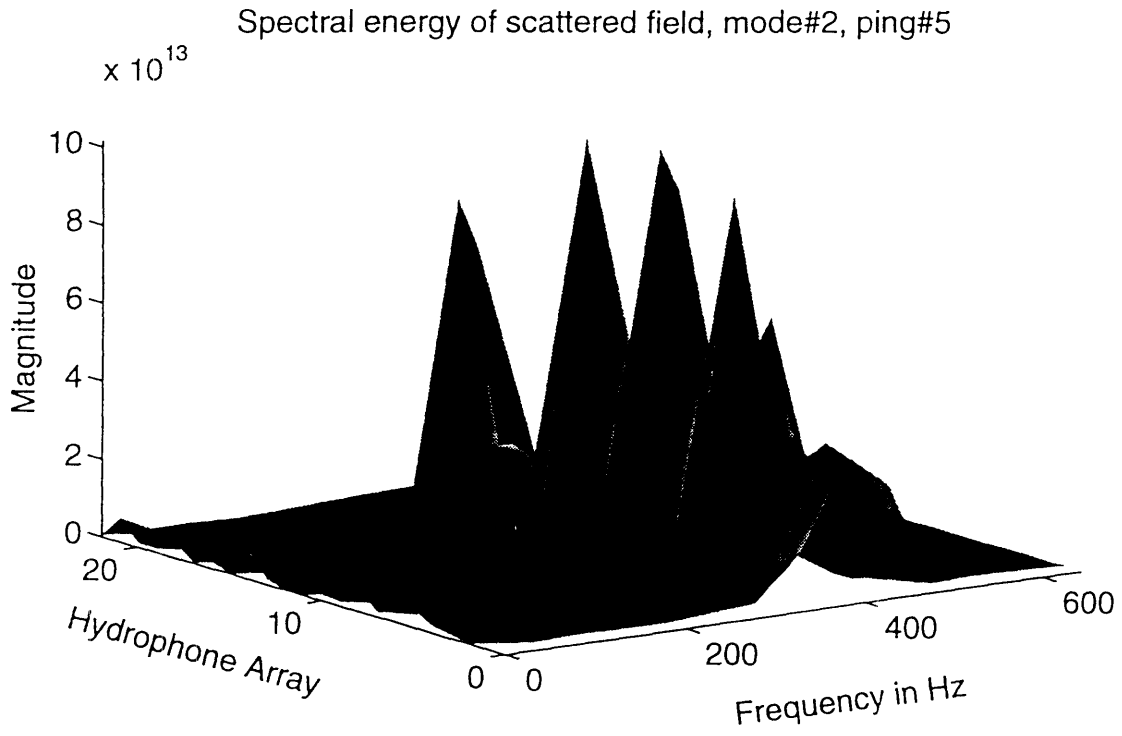


Figure 4.36a. Spectral energy of scattered field of mode#2, ping#5

Figure 4.36b. Coherence function of total field (solid) and scattered field (dash) of mode#2, ping#5

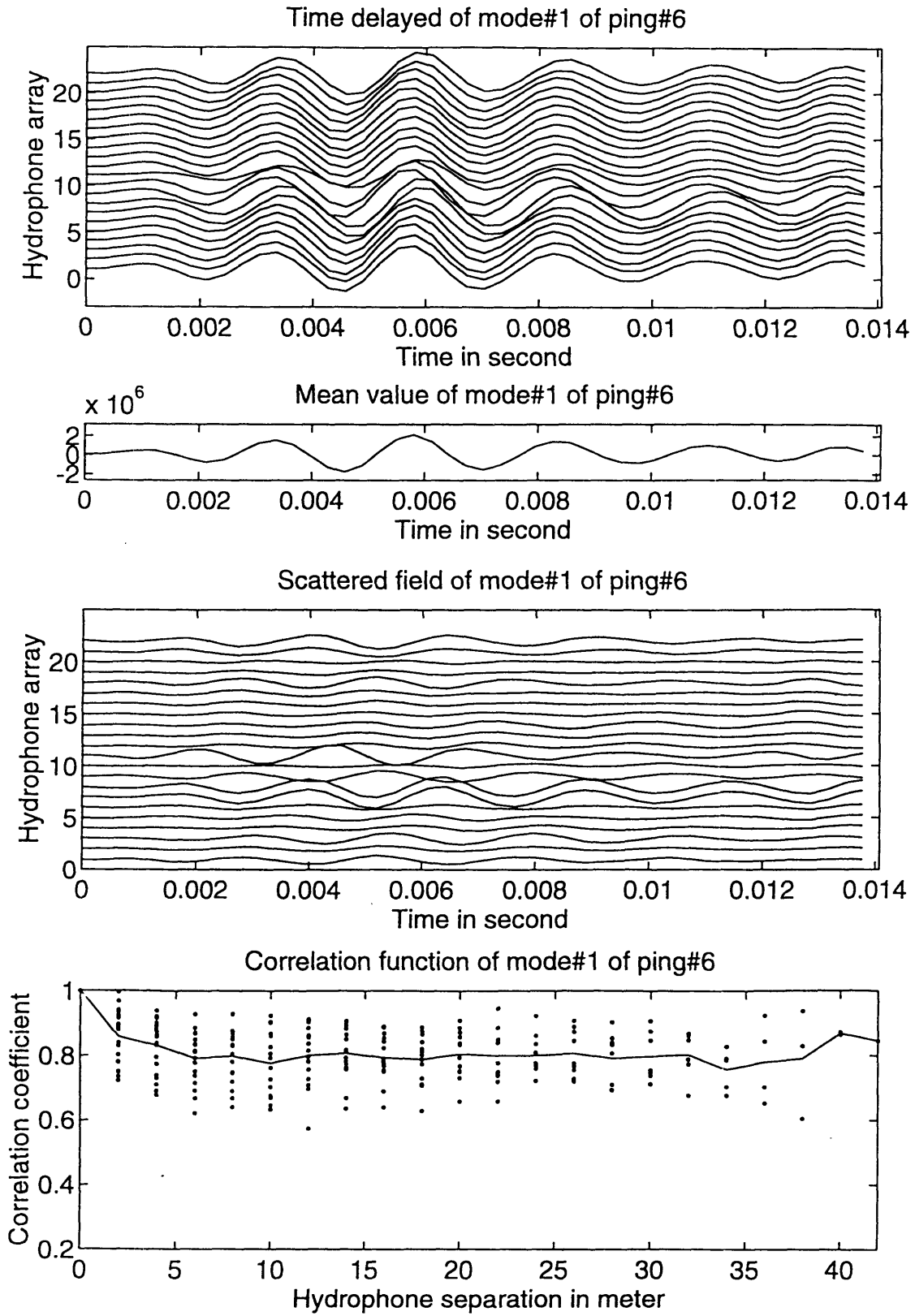


Figure 4.37. Total field, coherent field, scattered field and its correlation function of mode#1, ping#6

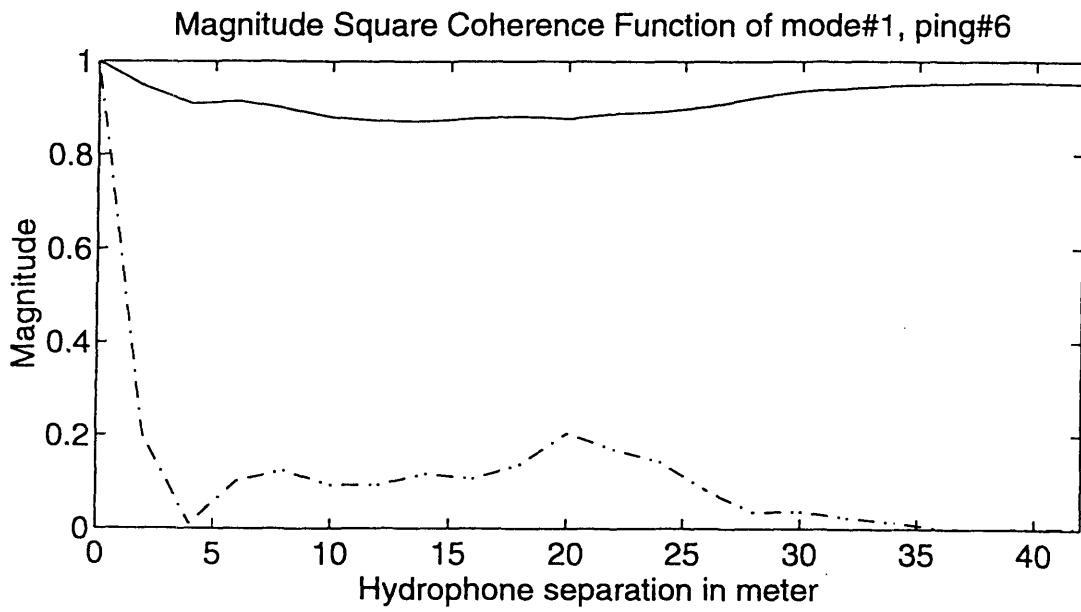
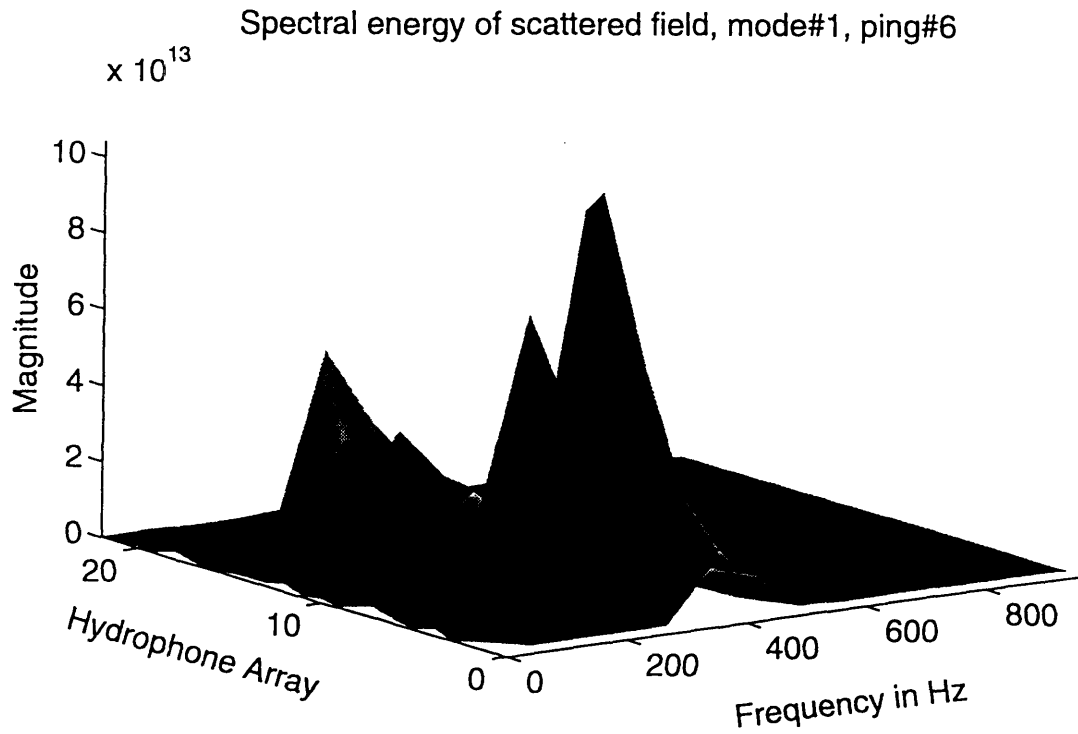


Figure 4.38a. Spectral energy of scattered field of mode#1, ping#6

Figure 4.38b. Coherence function of total field (solid) and scattered field (dash) of mode#1, ping#6

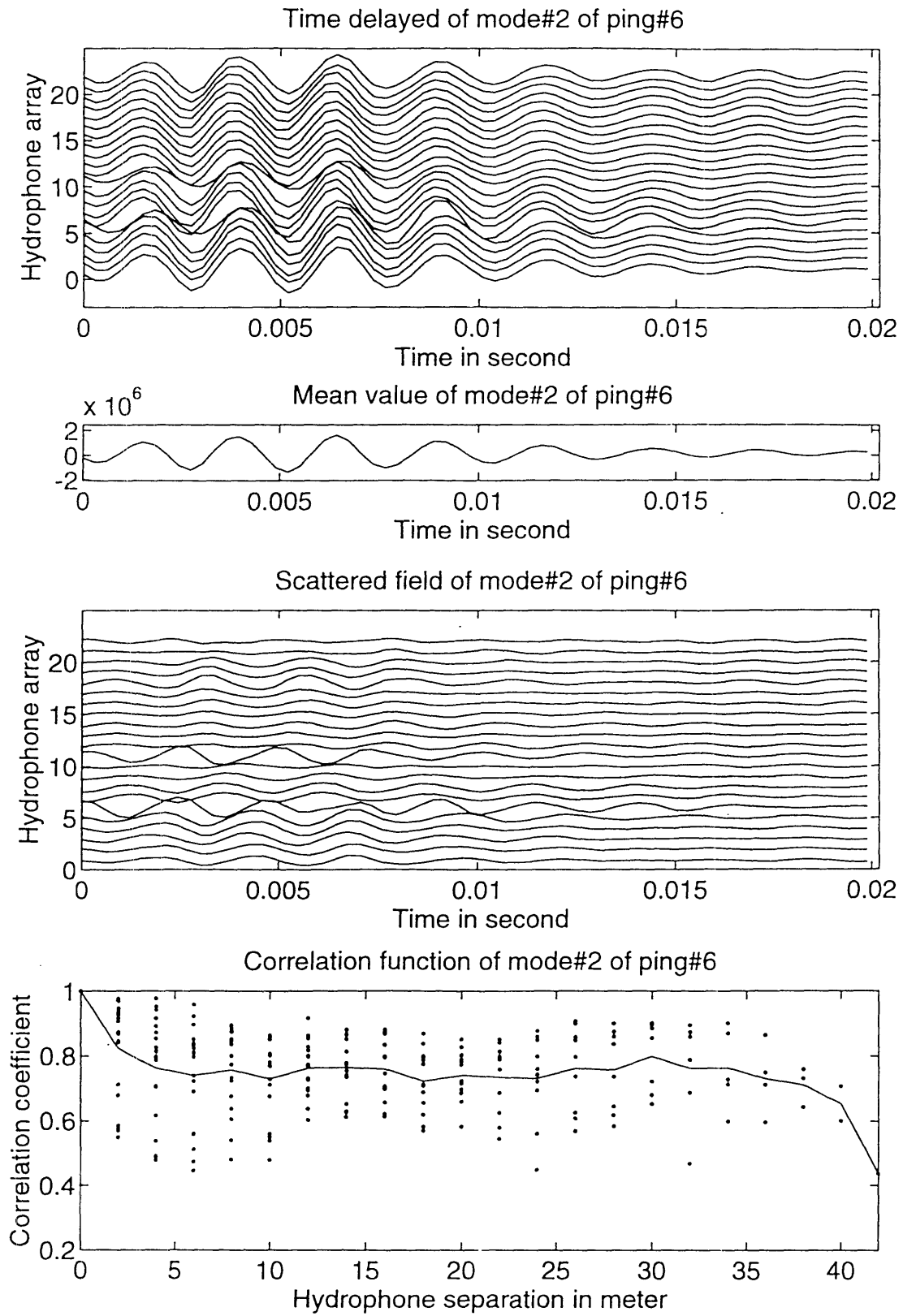


Figure 4.39. Total field, coherent field, scattered field and its correlation function of mode#2, ping#6

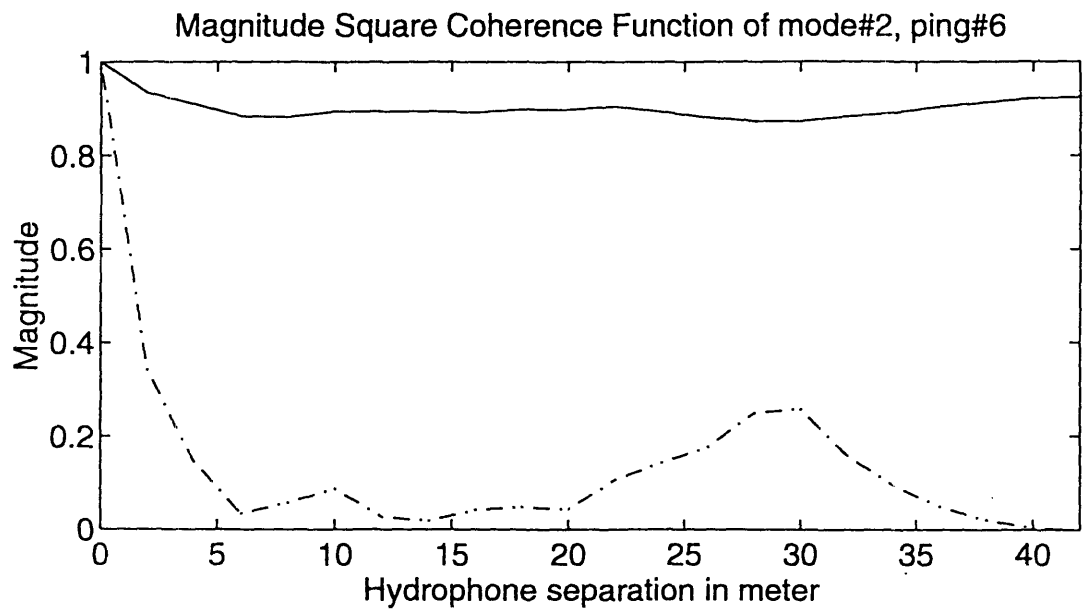
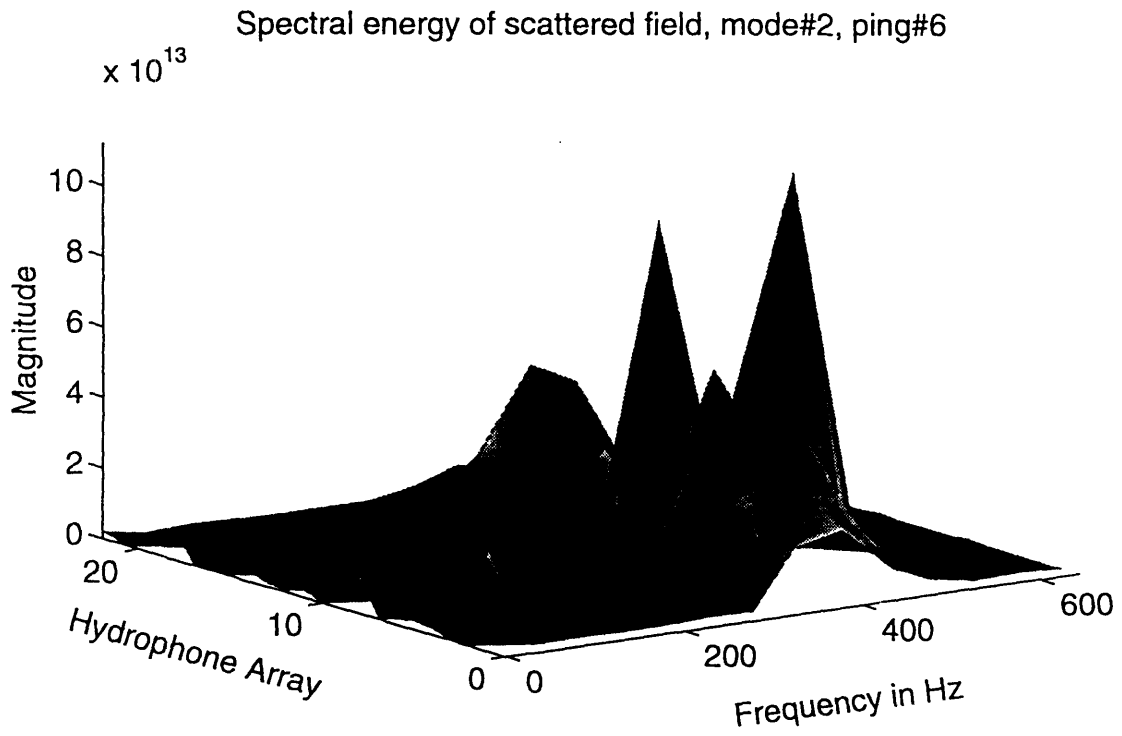


Figure 4.40a. Spectral energy of scattered field of mode#2, ping#6

Figure 4.40b. Coherence function of total field (solid) and scattered field (dash) of mode#2, ping#6

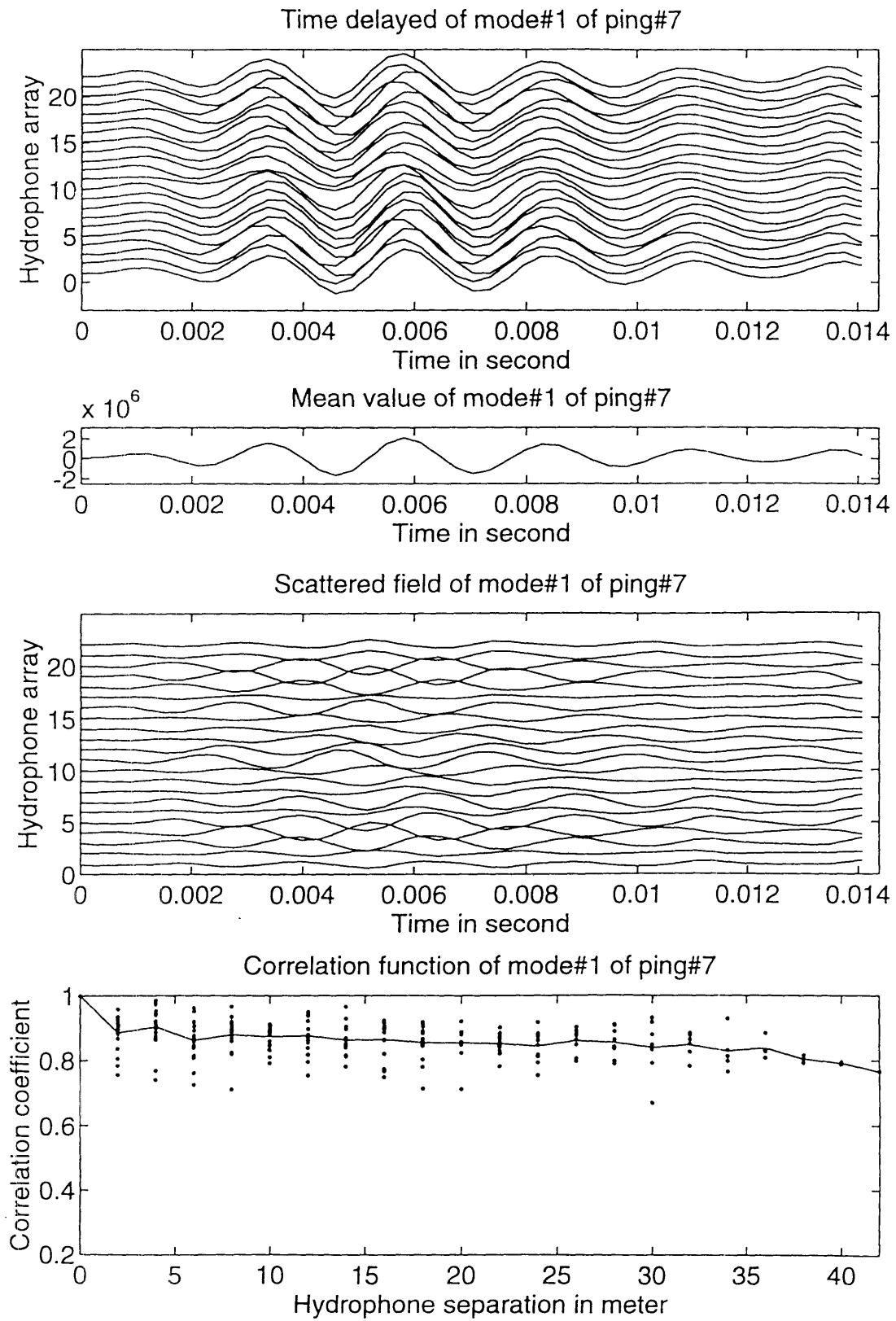


Figure 4.41. Total field, coherent field, scattered field and its correlation function of mode#1, ping#7

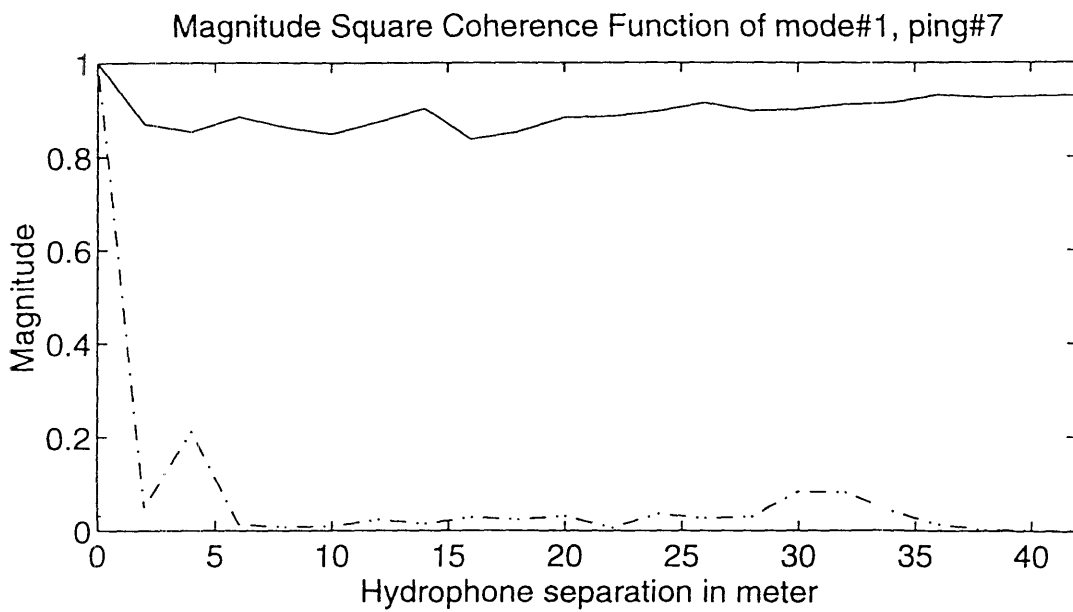
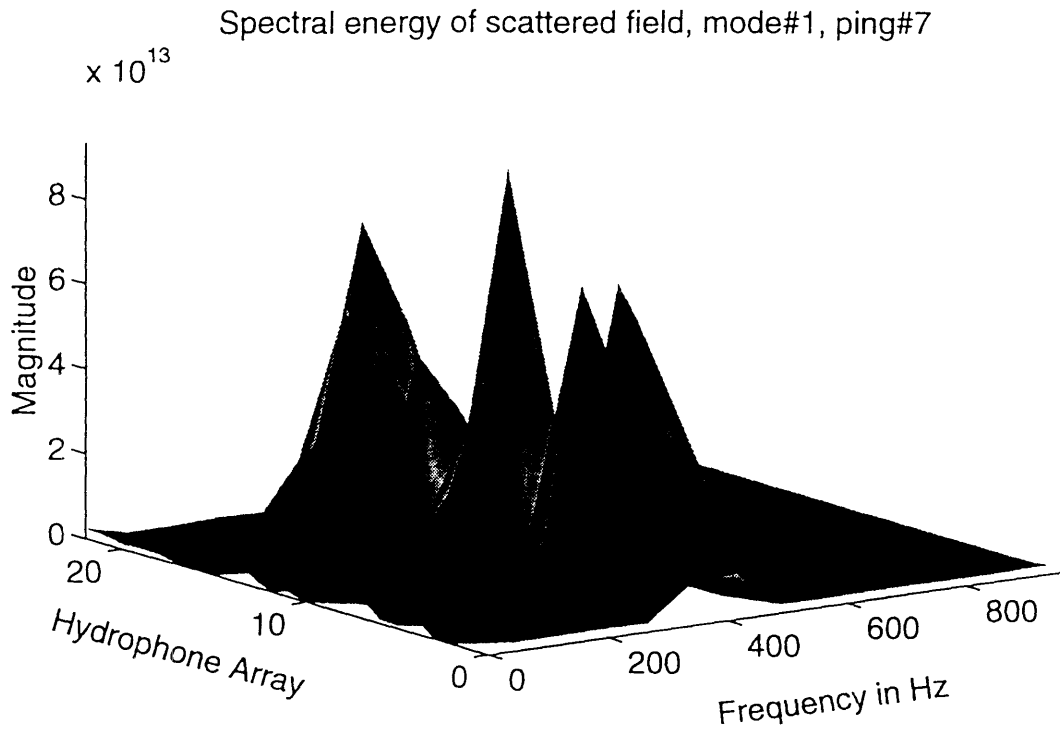


Figure 4.42a. Spectral energy of scattered field of mode#1, ping#7

Figure 4.42b. Coherence function of total field (solid) and scattered field (dash) of mode#1, ping#7

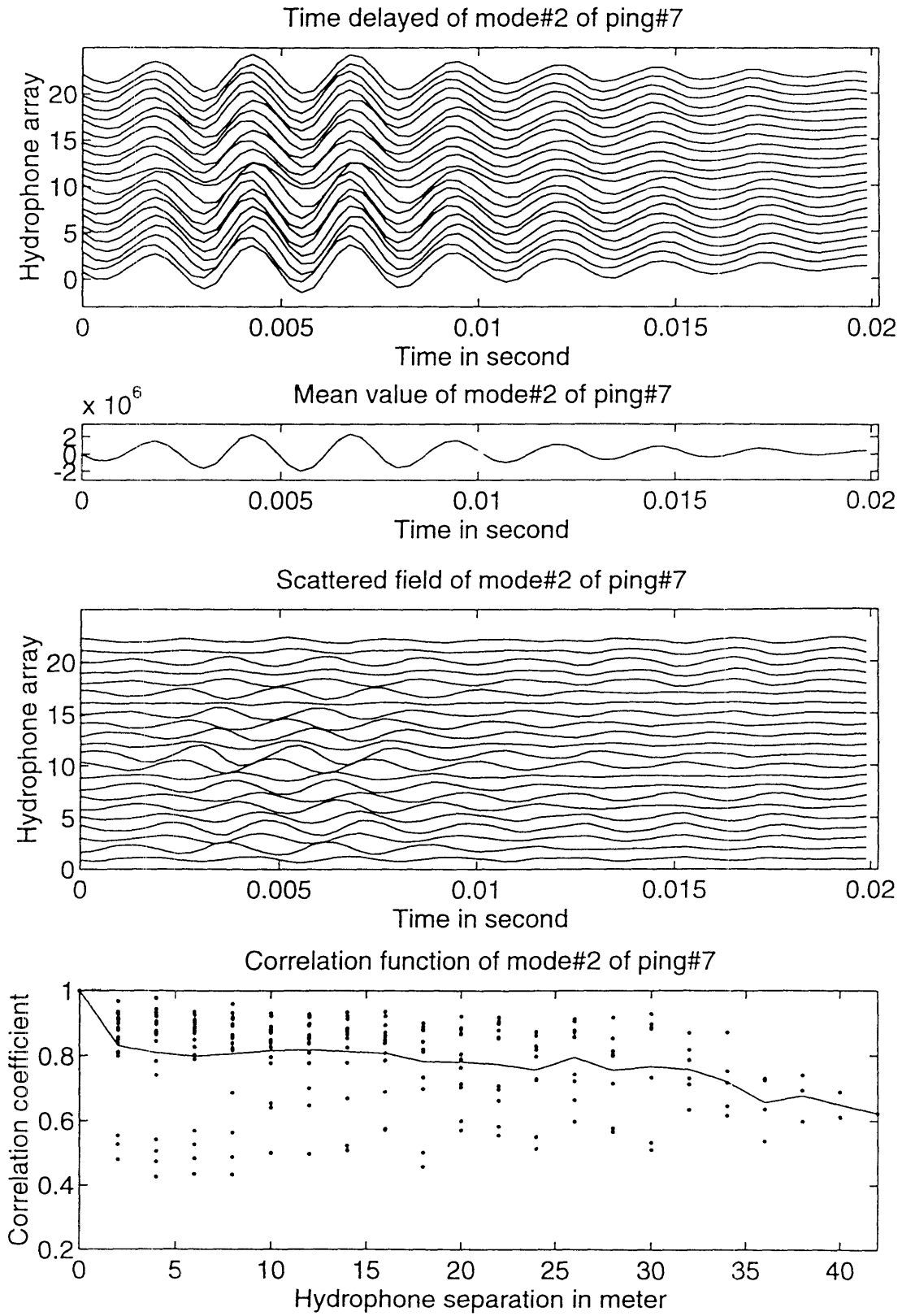


Figure 4.43. Total field, coherent field, scattered field and its correlation function of mode#2, ping#7

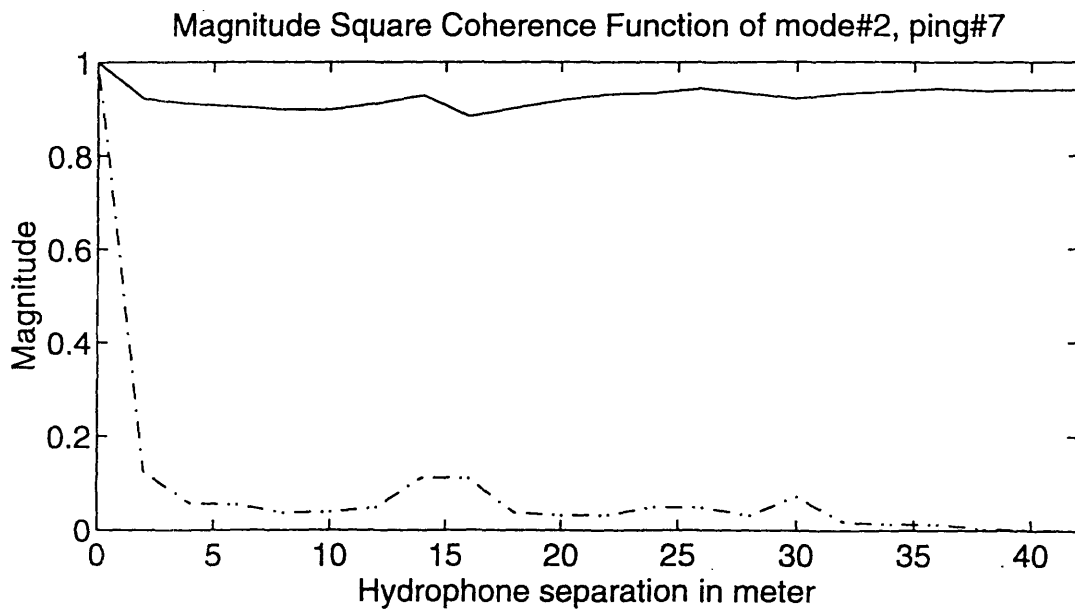
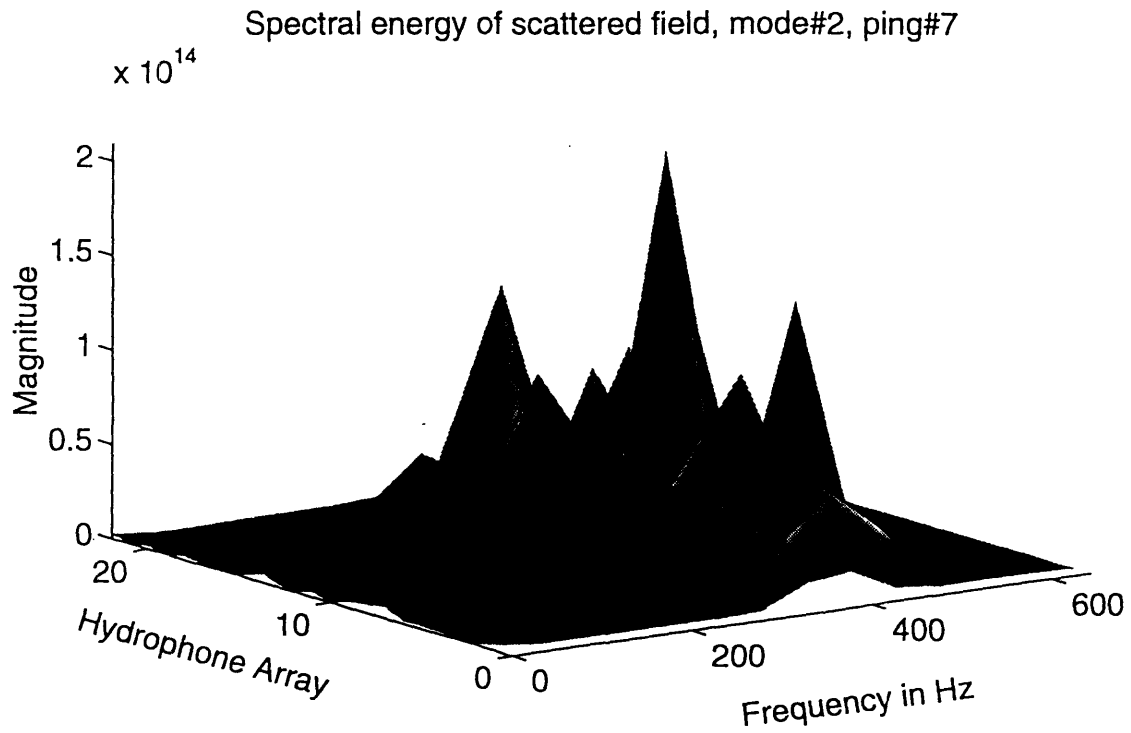


Figure 4.44a. Spectral energy of scattered field of mode#2, ping#7

Figure 4.44b. Coherence function of total field (solid) and scattered field (dash) of mode#2, ping#7

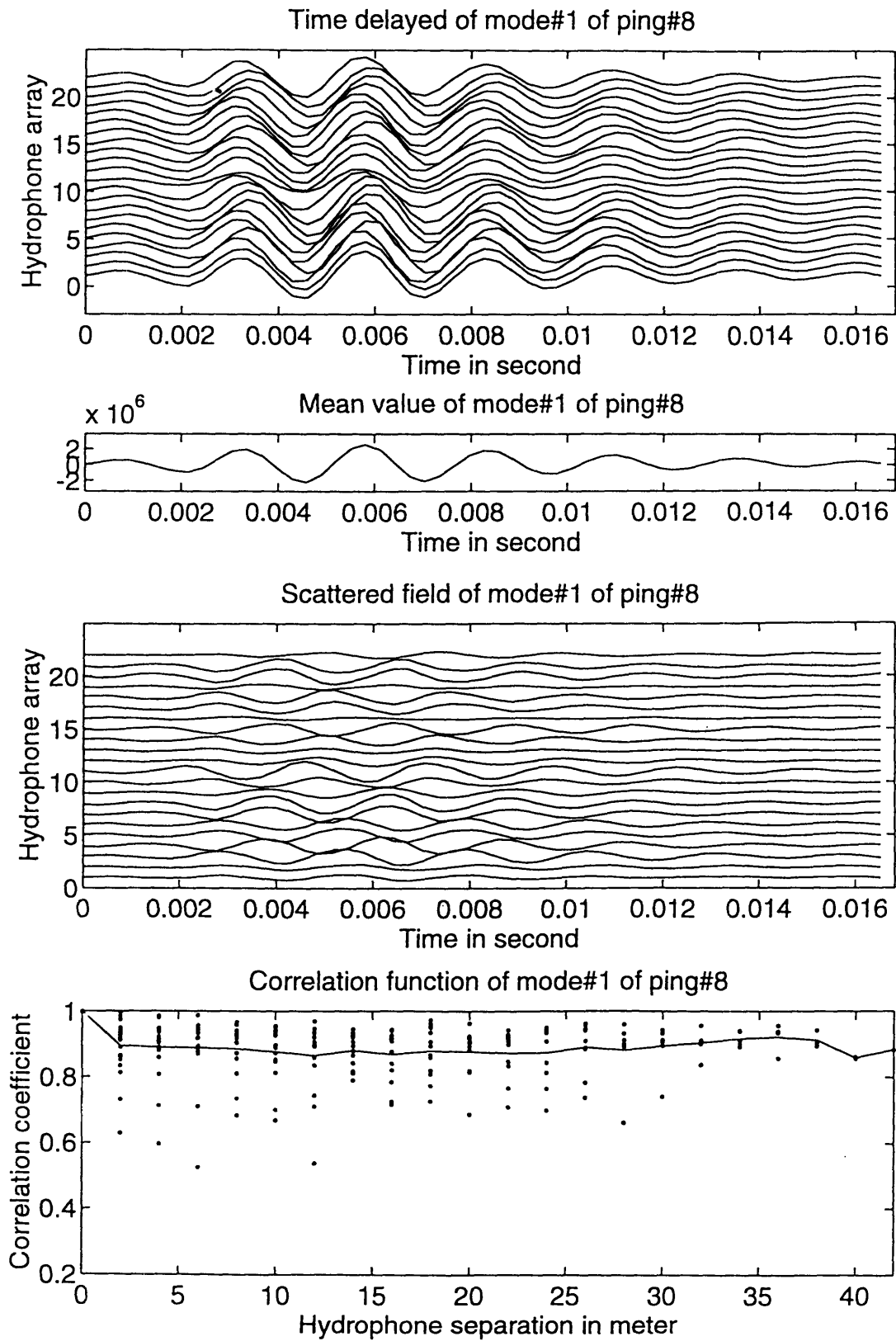


Figure 4.45. Total field, coherent field, scattered field and its correlation function of mode#1, ping#8

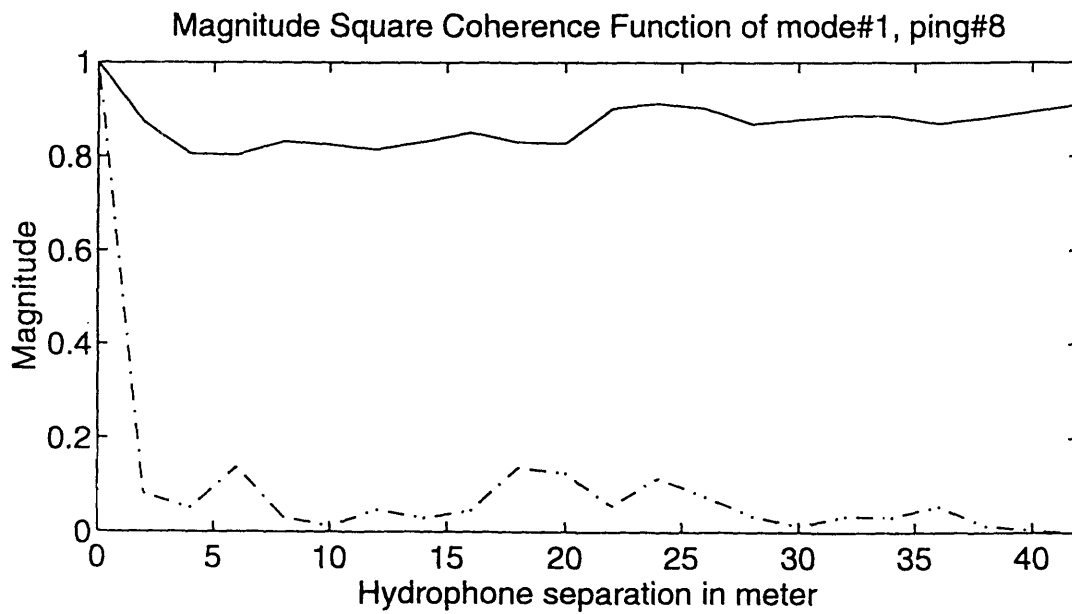
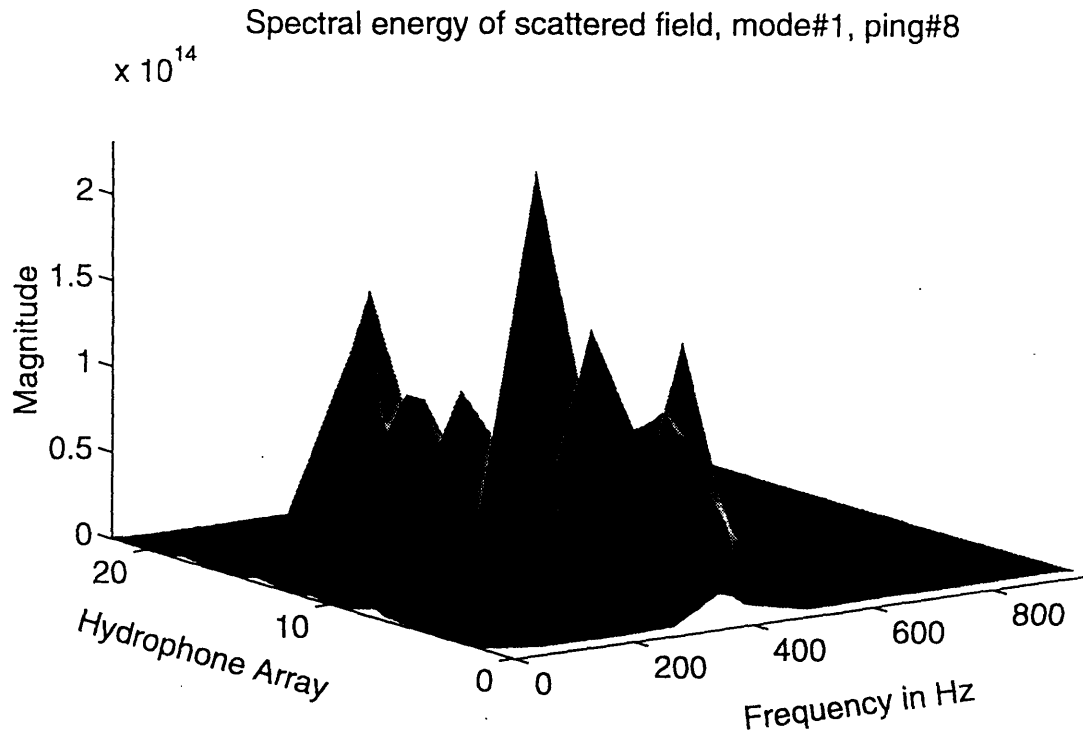


Figure 4.46a. Spectral energy of scattered field of mode#1, ping#8

Figure 4.46b. Coherence function of total field (solid) and scattered field (dash) of mode#1, ping#8

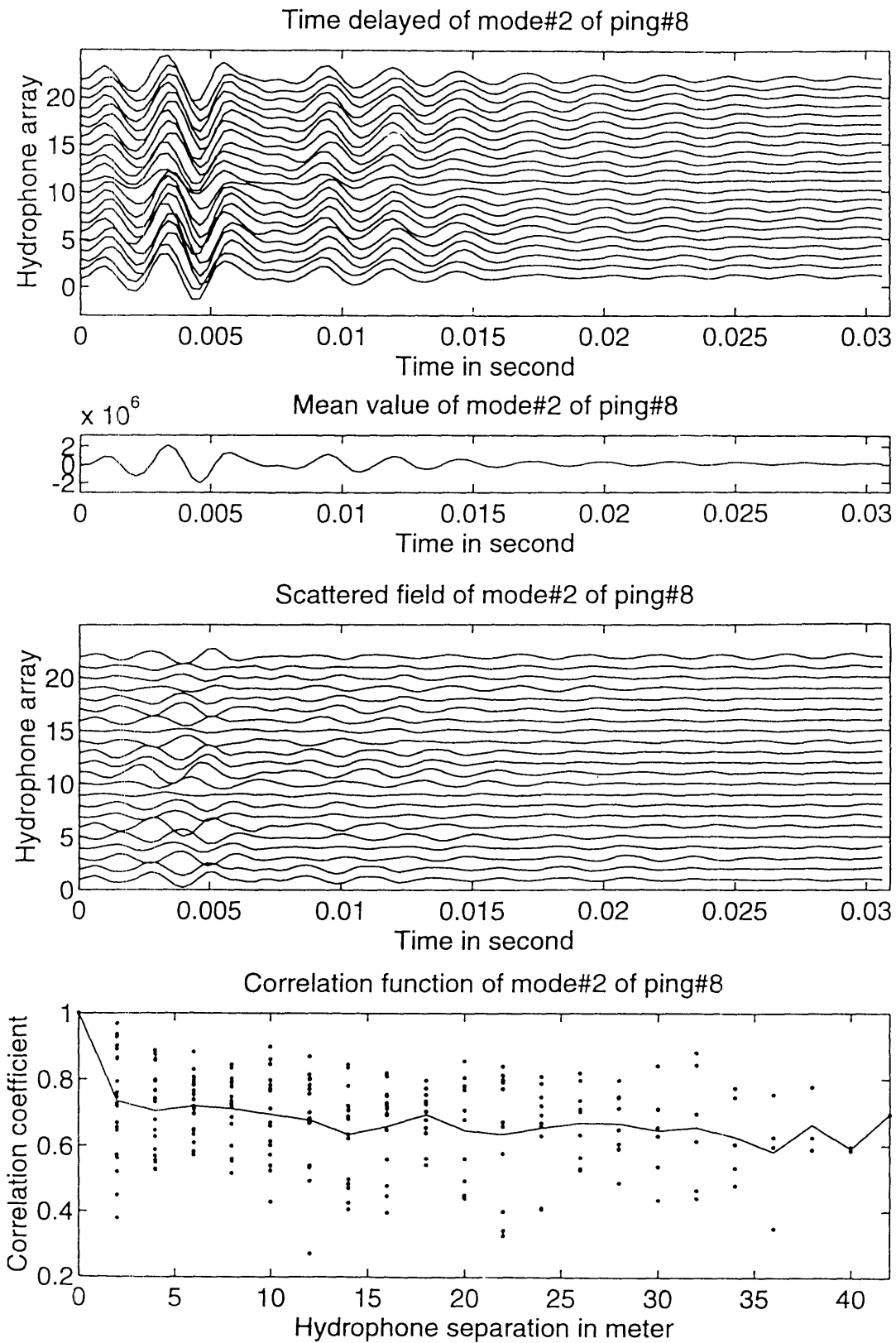


Figure 4.47. Total field, coherent field, scattered field and its correlation function of mode#2, ping#8

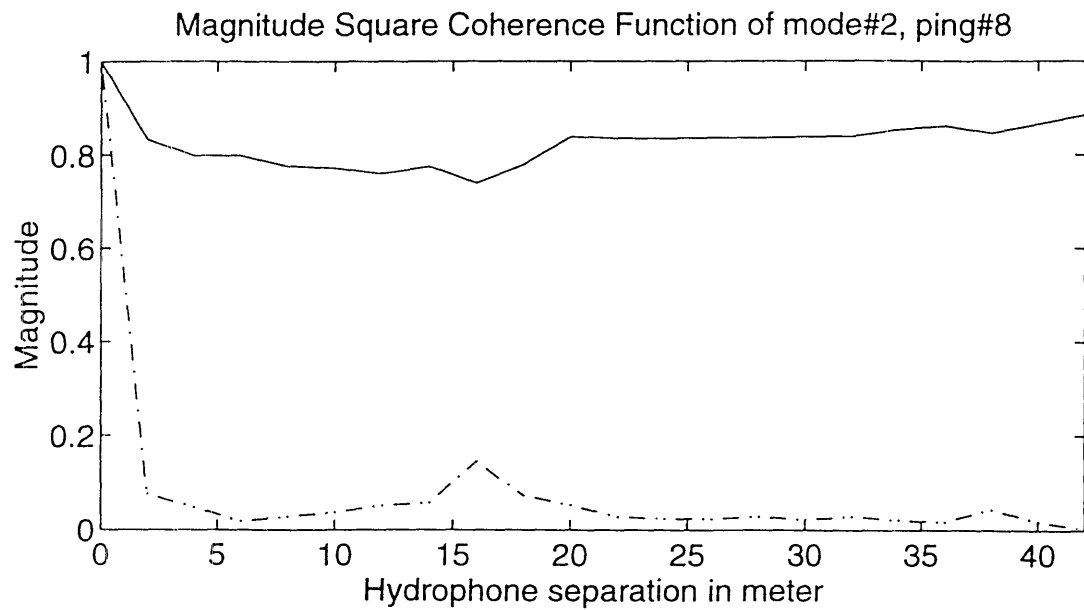
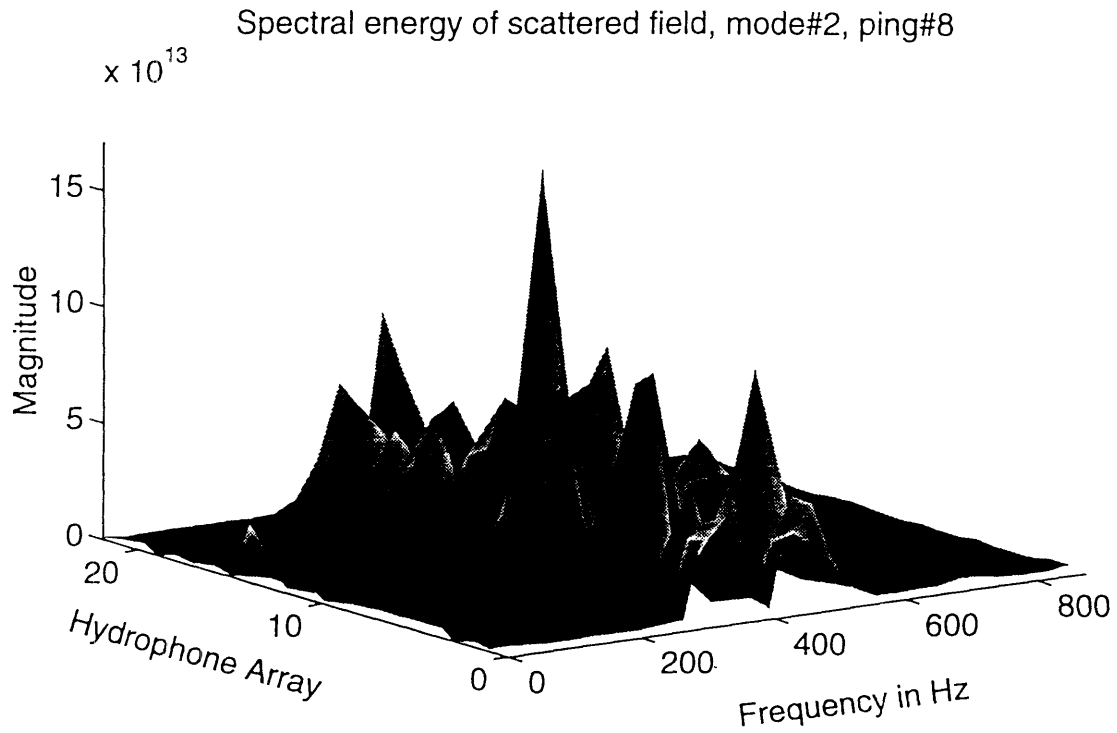


Figure 4.48a. Spectral energy of scattered field of mode#2, ping#8

Figure 4.48b. Coherence function of total field (solid) and scattered field (dash) of mode#2, ping#8

CHAPTER 5.

CONCLUSIONS AND RECOMMENDATIONS

FOR FUTURE RESEARCH

5.1. Conclusions

Ocean bottom scattering in shallow water environment is very complicated problem. This thesis presents experimental analysis of some aspects of the bottom scattering problem. The total field can be written as a composite of mean field or coherence field and residual field or scattered field. We put emphasis on the spatial coherence of the scattered field using correlation and coherence function and its relation to the rough bottom scattering. We have some conclusions :

1. Since the tone burst of the signal generated by flextentional transducer was unknown a synthetic source was built based on the theoretical flextentional characteristic ($Q=5$) and has given a good approximation.
2. Because the global positioning system (GPS) has given significant error during the cruise, the sources and receiver array position and

orientation was determined using an acoustics inversion method. The result showed that the receiver array position should be moved 150m to the north and 120m to the east from the position given in cruise report; on the other hand, the bearing should be 158° instead of 338° or 292° as stated in the cruise report. The receiver array bearing angle was (180°) different, it seems due to the reference choice which one was hydrophone#1 and hydrophone#24.

3. Conventionally, bottom scattering research has concentrated on modeling and/or measuring the scattered intensities. However, the scattering intensities only describe the amount of energy being scattered; it can not provide information on how the scattered field is spatially related[68]. Spatial correlation function of scattered field carries the information of the statistical properties of the bottom scatterer. Therefore by calculating the correlation function we can relate the bottom roughness. The mean correlation coefficient was found to be around 0.9 to 0.65 from 2m to 42m hydrophone separation, which means the amplitude and phase between hydrophones are closely related, or the bottom roughness was very small.
4. Detailed study of the spatial coherence uses coherence function. By calculating the magnitude square complex coherence function(MSC) for both total field and scattered field we can relate the rough

bottom properties. The MSC for the total field is around 0.9, while the MSC of the scattered field varies from 0.15 to 0.0 for 2m to 42m hydrophone separation. These results suggest that the scattering from the bottom mostly toward coherent (specular) angle or the bottom roughness was very small.

5.2. Recommendations for future research.

We recommend the following future research :

1. Since this thesis emphasizes on the experimental analysis of scattering from rough bottom boundary in shallow water environment, we recommend comparing the spatial coherence using the correlation function and coherence function based on the theoretical approach.
2. The correlation and coherence coefficient of the scattered field has been calculated, it is better if we determine also the directionality of the scattering field.
3. Analyze the mode coupling and energy transfer between modes due to scattering from the rough bottom boundary.
4. Derive the scattering theory from rough bottom which includes elastic bottom boundaries.

BIBLIOGRAPHY

- [1]. McDaniel, S.T., "*A small slope theory of rough surface scattering*", J. Acoust. Soc. Am., 95(4), 1994.
- [2]. Essen, H.H., "*Scattering from a rough sedimental seafloor containing shear and layering*", J. Acoust. Soc. Am., 95(30), 1994.
- [3]. Haralabus, G. et.al., "*Source localization in an uncertain acoustic scattering environment*", J. Acoust. Soc. Am., 94(6), 1993.
- [4]. Ivanova, K. and Broschat, S.L., "*The method of the local parabolic approximation for rough surface scattering*", J. Acoust. Soc. Am., 94(4), 1993.
- [5]. Fawcett, J.A., "*An efficient three-dimensional boundary integral equation method for solving azimuthally symmetric scattering problems in the oceanic waveguide*", J. Acoust. Soc. Am., 94(4), 1993.
- [6]. Wild., M. and Joyce, R., "*Three-demensional modelling of narrow-band pulse spreading using normal modes*", J. Acoust. Soc. Am., 94(4), 1993.
- [7]. Cederberg, R.J., Siegmann, W.L., Jacobson, M.J., and Carey, W.M., "*Predictability of acoustic intensity and horizontal wave numbers in shallow water at low frequencies using parabolic approximations*", J. Acoust. Soc. Am., 94(2), 1993.
- [8]. Dowling, D.R., and Jackson, D.R., "*Coherence of acoustic scattering from a dynamic rough surface*", J. Acoust. Soc. Am., 93(6), 1993.
- [9]. Rogers, A.K., Yamamoto, T. and Carey, W., "*Experimental investigation of sediment effect on acoustic wave*

- propagation in the shallow*", J. Acoust. Soc. Am., 93(4), 1993.
- [10]. Lu, I., Chen, H. and Voltz, P., "A matched-mode processing technique for localizing a transient source in the time domain", J. Acoust. Soc. Am., 93(3), 1993.
- [11]. Robbins, A.J. "Exact solutions of the Helmholtz equation for plane wave propagation in a medium with variable density and sound speed", J. Acoust. Soc. Am., 93(3), 1993.
- [12]. Goalwin, P.W., "A stationary phase approach to the calculation of the correlation of the acoustic field scattered from a two-dimensional random sea surface", J. Acoust. Soc. Am., 93(1), 1993.
- [13]. Zhu, R. and Guan, D., "Spatial horizontal coherence of sound in shallow water", J. Acoust. Soc. Am., 92(2), 1992.
- [14]. Wang, Q., and Zhang, R., "Sound spatial correlation in shallow water", J. Acoust. Soc. Am., 92(2), 1992.
- [15]. LePage K., Schmidt, H., and Kuperman, W.A., "Experimental and theoretical analysis of spatial coherence on a horizontal array under the Arctic ice", Proceeding of European Conference on underwater acoustics, 1992.
- [16]. Kondapalli, P.S. and Shippy, D.J., "Analysis of acoustic scattering in fluids and solids by the method of fundamental solutions", J. Acoust. Soc. Am., 91(4), 1992.
- [17]. Collins, M.D. and Evans, R.B., "A two-way parabolic equation for acoustic backscattering in the ocean", J. Acoust. Soc. Am., 91(3), 1992.
- [18]. McDaniel, S. T., "Backscattering from rough interfaces and the parabolic approximation", J. Acoust. Soc. Am., 91(1), 1992.

- [19]. Milder, D.M., and Sharp, H. T., "*An improved formalism for rough-surface scattering. II. Numerical trials in three dimensions*", J. Acoust. Soc. Am., 91(5), 1992.
- [20]. Dawson, T.W. , "*Acoustic scattering in a three-dimensional oceanic wave guide using boundary integral equation methods*", J Acoust. Soc. Am., 90(5), 1991.
- [21]. Dougherty, M.E. "*Seismo/acoustic propagation through rough seafloor*", J. Acoust. Soc. Am., 90(5), 1991.
- [22]. Lynch, J.F. and Agrawal, Y.C. "*A model-dependent method for inverting vertical profiles of scattering to obtain particles size spectra in boundary layers*", Marine Geology, 99, 1991.
- [23]. Ellis, D. and Crowe D. V., "*Bistatic reverberation calculations using a three -dimensional scattering function*", J. Acoust. Soc. Am., 89(5), 1991.
- [24]. Milder, D.M. "*An improved formalism for wave scattering from rough surfaces*", J. Acoust. Soc. Am., 89(2), 1991.
- [25]. Berman, D.H., "*Simulations of rough interface scattering*", J. Acoust. Soc. Am., 89(2), 1991.
- [26]. Burns, D.R., and Stephen, R.A., "*Three-dimensional numerical modeling of geoacoustic scattering from seafloor topography*", 88(5), 1990.
- [27]. Fawcett, J.A. and Dawson, T.W. "*Fourier synthesis of three-dimensional scattering in a two-dimensional oceanic wave guide using boundary integral equation methods*", J. Acoust. Soc. Am., 88(4), 1990.
- [28]. Chen, J.S and Ishimaru, A., "*Numerical simulation of the second-order Kirchoff approximation from very rough surface and a study of backscattering enhancement*", J. Acoust. Soc. Am., 88(4), 1990.

- [29]. Berman, D.H., and Perkins, J.S. "*Rayleigh method for scattering from random and deterministic interfaces*", J. Acoust. Soc. Am., 88(2), 1990.
- [30]. Thorsos, E.I. "*Acoustic scattering from a "Pierson-Mokowitz" sea surface*", J. Acoust. Soc. Am. 88(1), 1990.
- [31]. Rolt, K.D., "*History of the flexensional electroacoustic transducer*", J. Acoust. Soc. Am., 87(3), 1990.
- [32]. Kuperman, W.A., and Schmidt, H. "*Self-consistent perturbation approach to rough surface scattering in stratified elastic media*", J. Acoust. Soc. Am, 86(4), 1989.
- [33]. Thorsos, E.I and Jackson, D.R., "*The validity of the perturbation approximation for rough surface scattering using a Gaussian roughness spectrum*", J. Acoust. Soc. Am., 86(1), 1989.
- [34]. Wetton, B. T., and Fawcett, J.A., "*Scattering from small three-dimensional irregularities in the ocean sea floor*", J. Acoust. Soc. Am., 85(4), 1989.
- [35]. Dacol, D.K, and Berman, D.H., "*Sound scattering from a randomly rough fluid-solid interface*", J. Acoust. Soc. Am, 84(1), 1988.
- [36]. Jackson ,D.R.; Winebrenner D.P. and Ishimaru, A., "*Comparison of perturbation theories for rough surface scattering*", J. Acoust. Soc. Am., 83(3), 1988.
- [37]. Thorsos, E.I. "*The validity of the Kirchoff approximation for rough surface scattering using a Gaussian roughness spectrum*", J. Acoust. Soc. Am., 83(1), 1988.
- [38]. McDaniel, S.T., "*Physical optics theory of scattering from ice canopy*", J. Acoust. Soc. Am. 82(6), 1987.

- [39] Lyons, A.P., Anderson, A.L, and Dwan, F.S. "*Acoustics scattering from the seafloor: Modelling and data comparison*", J. Acoust. Soc. Am., 95(5),1994.
- [40]. Kachoyan,B.J.and Macaskill C., "*Acoustic scattering from arbitrarily rough surface*", J. Acoust. Soc. Am. 82(5), 1987.
- [41]. Ogilvy, J.A. , "*Wave scattering from rough surfaces*", Rep. Prog. Phys. 50, 1987.
- [42]. Boehme,H, et. all, "*Acoustic backscattering at low grazing angles from the ocean bottom. Part I. Bottom Backscattering strength*", J. Acoust.Soc. Am., 77(3), 1985.
- [43]. Boehme,H, et. all, "*Acoustic backscattering at low grazing angles from the ocean bottom. Part II. Statistical characteristics of bottom backscatter at a shallow water site*", J. Acoust. Soc. Am. 77(3), 1985.
- [44]. Carter, G.C., "*Bias in magnitude-squared coherence estimation due to misalignment*", IEEE Trans. on Acoust, Speech, and Signal Proc., ASSP-28 (1), 1980.
- [45]. Smith Jr., P.W. "*Spatial coherence in multipath or multimodal channels*", J. Acoust. Soc. Am., 60(2), 1976.
- [46]. Carter, G.C., Knapp, C.H., and Nuttall, A.H., "*Estimation of the magnitude squared coherence function via overlapped fast Fourier transform processing*", IEEE Trans. on Audio and Electroacoustics, AU-21(4), 1973.
- [47]. Wille, P. and Thiele, R. "*Transverse horizontal coherence of explosive signals in shallow water*", J. Acoust. Soc. Am. 50(1), 1971.
- [48]. Gulin, E.P. and Malyshev, K.I., "*Spatial correlation of amplitude fluctuations of a continuous tone signal with reflection from ocean surface waves*", Soviet Physics-acoustics, 11(4), 1966.

- [49]. Jensen, F.B., Kuperman, W.A., Porter, MB, and Schmidt, H., Computational Ocean Acoustics, AIP Press, New York, 1994.
- [50]. Frisk, G.V., Ocean and seabed acoustics: A theory of wave propagation, Prentice Hall, New Jersey, 1994.
- [51]. Bendat, J.S., and Piersol, A.G., Engineering applications of correlation and spectral analysis, 2nd ed., John Willey & Sons Inc., New York, 1993.
- [52]. Garidel-Thoron, G. Backscattering distributions from smooth and rough bottom near the Mid-Atlantic Ridge., MS Thesis, MIT, 1993
- [53]. Schmidt, H. SAFARI: Seismo-acoustic fast field algorithm for range independent environment , User Guide, MIT, 1993
- [54]. Schmidt, H., OASES Version 1.6. Application and Upgrade notes, MIT, 1993
- [55]. LePage, K. Elastic scattering in oceanic wave guides, Ph.D. thesis, MIT, 1992.
- [56]. Liu, Jin-Yuan, Seismo-acoustic rough interface scattering of surface-generated ambient noise in a stratified ocean, Ph.D. thesis, MIT, 1992.
- [57]. Fricke, J.R. Acoustics scattering from elastic ice: finite difference solution, Ph.D.-thesis, WHOI-MIT, 1991.
- [58]. Etter, P.C. Underwater acoustic modeling -principles, techniques and application; Elsevier Applied Science, New York, 1991
- [59]. Ogilvy, J.A., Theory of wave scattering from random rough surfaces, Adam Hilger, New York, 1991.

- [60]. Miller, B.E. Observation and inversion of seismo-acoustics waves in a complex arctic ice environment, OE thesis, MIT, 1990.
- [61]. Bendat, J.S., and Piersol, A.G., Random data: Analysis and measurement Procedures, 2nd. ed., Willey-interscience, New York, 1986.
- [62]. Ziomek, L.J. Underwater acoustics, a linear system theory approach, Academic Press, New York, 1985
- [63]. Urick, R.J. Sound propagation in the sea, DARPA, Washington D.C. 1984.
- [64]. Bass, F.G. and Fuks I.M. Wave Scattering from statistically rough surfaces, Pergamon Press, New York, 1st Ed. 1979.
- [65]. Tencate, J. and Stern, M. "Brief report on experiment from 18 to 22 March 1993 Malloca Cruise".
- [66]. Max, M.D., and Michelozzi, E., "Shallow seafloor geology of the western Mallorca platform", Draft report.
- [67]. Anonymous, "Test plan overview R/V Alliance off the Balearic i islands, Mediterranean Sea March 1993".
- [68]. Tang D., Acoustic wave scattering from a random ocean bottom, Ph.D. Thesis, MIT, 1991.
- [69]. Gillette, G., "*Coupled modes in a waveguide with a range-dependent rigid basement*", J. Acoust. Soc. Am., 95(1), 1994.
- [70]. Anand, G.V. and George, M.K., "*Normal mode sound propagation in an ocean with random narrow-band surface waves*", J. Acoust. Soc. Am., 94(1), 1993.
- [71]. McDaniel, A.T. and McCammon, D.F., "*Mode coupling and the environmental sensitivity of shallow water propagation loss predictions*", J. Acoust. Soc. Am., 82(1), 1987.

- [72]. Evans, R.B., "*A coupled mode solution for acoustic propagation in a waveguide with stepwise depth variations of a penetrable bottom*", J. Acoust. Soc. Am., 74(1), 1983.
- [73]. Boyles, C.A., "*Coupled mode solution for a cylindrically symmetric oceanic waveguide with a range and depth dependent refractive index and a time varying rough sea surface*", J. Acoust. Soc. Am., 73(3), 1983.
- [74]. McDaniel, S.T., "*Mode coupling due to interaction with the seabed*", J. Acoustic. Soc. Am., 72(3), 1982.
- [75]. McDaniel, S.T., "*Comparison of coupled-mode theory with the small-waveheight approximation for sea-surface scattering*", J. Acoust. Soc. Am., 70(2), 1981.
- [76]. William Jr., A.O., "*Mode interactions in an isovelocity ocean of uniformly varying depth*", 67(1), 1980.
- [77]. Bellis, A. and Tappert, F.D., "*Coupled mode analysis of multiple rough surface scattering*", J. Acoust. Soc. Am., 66(3), 1979.
- [78]. Nagl, A.; Uberall, H.; Haug, A.J., and Zarur, G.L., "*Adiabatic mode theory of underwater sound propagation in a range-dependent environment*", J. Acoust. Soc. Am., 63(3), 1978.
- [79]. McDaniel, S.T., "*Mode conversation in shallow-water sound propagation*", J. Acoust. Soc. Am., 62(2), 1977.
- [80]. Kuperman, W.A. and Ingenito, F., "*Attenuation of the coherent component of sound propagating in shallow water with rough boundaries*", J. Acoust. Soc. Am., 61(5), 1977.
- [81]. Ingenito, F. and Wolf, S.N., "*Acoustic propagation in shallow water overlying a consolidated bottom*", J. Acoust. Soc. Am., 60(3), 1976.
- [82]. Kuperman, W.A., "*Coherent component of specular reflection and transmission at a randomly rough two-fluid interface*", J. Acoust. Soc. Am., 58(2), 1975.